



**Politecnico
di Torino**

Politecnico di Torino

Master's Degree Thesis
in Mechanical Engineering.
Academic year: 2020/2021

Numerical modelling of a Rotor-Bearing system for Machinery Condition Monitoring

Relatori:

Prof. Eugenio Brusa
Prof.ssa Cristiana Delprete

Candidato:

Luigi Ceruti

Index

1. Introduction	1
2. Bearing model	3
2.1 Assumptions of the model.....	4
2.2 Contact between bodies.....	4
2.3 Bearings of the model.....	11
2.4 Bearing forces	13
2.4.1 Evaluation of deflection in bearings.....	14
2.4.2 Evaluation of deflection in bearings with localized defects.....	16
3. Theory of a rotor with 4 degrees of freedom	23
3.1 Reference frame	24
3.2 Equation of the system with four degrees of freedom	25
3.2.1 Forces generated by the imperfection of the shaft	27
3.2.2 Forces generated by damping.....	30
4. Vibration Condition Monitoring	32
4.1 Sources of vibration in a rotor-bearing system	33
4.2 Characteristics of the signal in the time domain	34
4.3 Characteristics of the signal in the frequency domain	38
5. Rotor-Bearing model	44
5.1 Rotor-bearing system	45
5.2 Equations of the system	46
5.3 Implementation of the numerical model in MATLAB code	52
6. Numerical simulation and analysis of the system	59
6.1 Healthy bearings	59
6.1.1 Case with rigid shaft.....	63
6.1.2 Case with elastic shaft.....	67
6.2 Bearing damaged in the external ring.	70

6.2.1 Case with rigid shaft.....	70
6.1.2 Case with elastic shaft.....	73
6.3 Bearing damaged in the inner ring	75
6.3.1 Case with rigid shaft.....	76
6.3.2 Case with elastic shaft.....	78
6.4 Bearing with damaged rolling element	81
6.4.1 Case with rigid shaft.....	81
6.4.2 Case with elastic shaft.....	83
6.5 Eccentricity on the rotor	86
6.5.1 Case with rigid shaft.....	86
6.5.2 Case with elastic shaft.....	88
7. Conclusion and future development	92
Bibliography	94

1. Introduction

The real-time monitoring of rotors is used to speed up the identification of damage and allows to reduce the risk of failures. The detected vibration signal needs algorithms to be analysed and classified, moreover require an accurate placement of sensors. It is also possible to create a digital replica of the physical systems to simulate the behaviour of the machine and to carry out all the necessary tests. Vibration monitoring analysis offers lots of information about anomalies that could be present inside rotating machines. These usually generate inside bearings which are critical elements for the safety of the entire system. The work of this master's degree thesis focuses on the creation of an analytical-numerical model to describe the behaviour of a flexible rotor supported by rolling elements bearings. This model can be adopted to perform two kind of monitoring activities: "in-monitoring", where a continuous identification of the operating conditions is performed on the bearing itself, to detects the possible presence of defects inside the component through the dynamic firm of the system, and "out-monitoring", as an indirect measurement, which allows to identify the defects affecting one part of the machine and to determine the dynamic signature of the entire system. In this work the model is studied considering the presence of different types of localized defects, that can be located inside the bearings: on the inner ring, on the outer ring and on the rolling elements. The mains parameters of the system and the defects are described with an analytical approach, to obtain a Digital Twin of the real system where the goal is to identify and classify damages through the monitoring activity. It is then studied how the vibrations, produced by bearings, affects the behaviour of the rotor. The simulation is obtained through a complete analysis of the contact between bodies, and the acceleration signal, produced by the vibration of the system, is studied in different locations on the shaft. The dynamic analysis of the signals is performed considering the presence of each defect separately, and obtaining the particular features of the vibration signal, both in the time and frequency domain. The work starts describing the bearing model created by Giorio in [2]: the assumptions of the model are summarised, and the theory of radial ball and roller bearings is reported defining the relation force-deformation of the contacts. Finally, it is reported the equations describing the bearing forces of the model also considering the presence of localized defect on the different components. Then it is reported the theory of a rotor with 4-dof describing the typical forces that act on the rotor and obtaining the equations of motion. The work continues describing

the statistical parameters useful for the analysis in the time domain of vibration signal and the characteristic frequencies of the bearing useful for the analysis in the frequency domain together with the main steps that characterize the envelope analysis technique. In Chapter 5 is then described the rotor-bearing system adopted in the simulation, combining the theory of the 4-dof rotor with the bearing model. After the definition of the equations, they are solved in a MATLAB code that is able to simulate the system considering also the presence of defects on its components. The results obtained by the numerical simulations are then reported and discussed for all the different studied cases (presence of localized defect on the outer ring, inner ring or rolling element of a bearing, and the presence of eccentricity on the rotor).

2. Bearing model

Bearings play an essential role in all rotating machines, allowing the rotational motion of the shaft with respect to a fixed structure supporting the system. An incorrect behaviour of these components, caused by a rupture of one of their constituent elements may lead to the failure of the entire machine. Bearings are subjected to dynamic loads that from the machine are transmitted through the components of rolling element bearings. Any defect in the bearing's components increases vibration levels significantly and should be identified on time to avoid failure of the machine. The individuation of these defects plays an essential role for quality inspection and condition monitoring of bearings [1].

In this work bearings are modelled following the thesis of Giorio [2] where the effect of localized defects on the vibrational response of a radial, ball or cylindrical roller bearing is analysed. The bearing model, visible in fig. 2.1, highlights the three main elements of the system: inner raceway, outer raceway, and spheres.

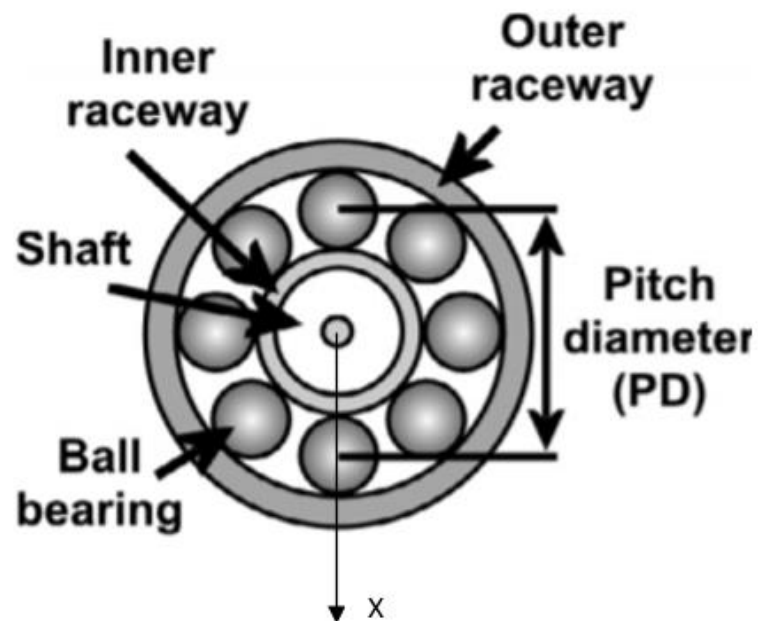


Figure 2.1: Main components of the bearing model [3].

2.1 Assumptions of the model

In [2] bearings are modelled with the following assumptions: the outer ring is considered fixed, integral with the stator casing, which is considered solid with respect to the foundations. The inner ring of the bearing is bounded to the rotor's shaft and has two translational degrees of freedom (X, Y). The motion is due to the stiffness of the rolling elements. The radial displacement, indeed, results from the deformation of the rolling elements on the raceways under the action of the radial force F_r . The deformation of the track is neglected while only the deformation of the rolling elements is considered. The angular velocity Ω of the shaft is considered constant and it is defined a priori. The rolling elements can be spheres or cylindrical rollers that are hypothesized as equally distributed in the circumferential direction, neglecting the variations in distance between them during operation. The effect caused by the sliding of the rolling elements on the two tracks during contact is also neglected, and the interaction that occurs between rolling elements and tracks is pure rolling. At the initial time t_1 the position of the rolling element $i = 1$ is vertical with respect to the centre of the bearing. Furthermore, each rolling element is considered as massless with a linear stiffness coefficient and a damping coefficient as it has already been studied in other works of literature [4,5,6,7]. The losses due to the viscosity of the lubricant inside the bearing are considered depending on the damping coefficient c_b that has a range of values depending on the linear stiffness K_{lin} that will be analysed in Paragraph 2.4.

2.2 Contact between bodies

The ideal behaviour of two elastic bodies in contact has been solved by Hertz under the following hypotheses [8, 9, 10]:

- The deformable bodies in contact are linear elastic isotropic material, that is they obey Hooke's law.
- Small deformations when compared with the geometric dimensions of the bodies in contact.
- Shear stresses in the contact area are negligible.
- The contact area is very small compared with the size of the bodies; in particular, the semi-major axis of the elliptical contact area, a , must be small when compared with the minimal curvature of the bodies on contact:

$$a \ll \min \{ \rho_I, \rho_{II} \}$$

- The bodies have a smooth surface and the effect of friction in the contact is neglected.

It is necessary to introduce a parameter that indicate the curvature of a body, which is related to his radius. Following the reference planes of fig 2.2 it is possible to write the curvatures of the two bodies in their contact points:

$$\rho_{i,1} = \frac{1}{r_{i,1}} \quad \rho_{i,2} = \frac{1}{r_{i,2}}$$

Where “*i*” indicate the considered body.

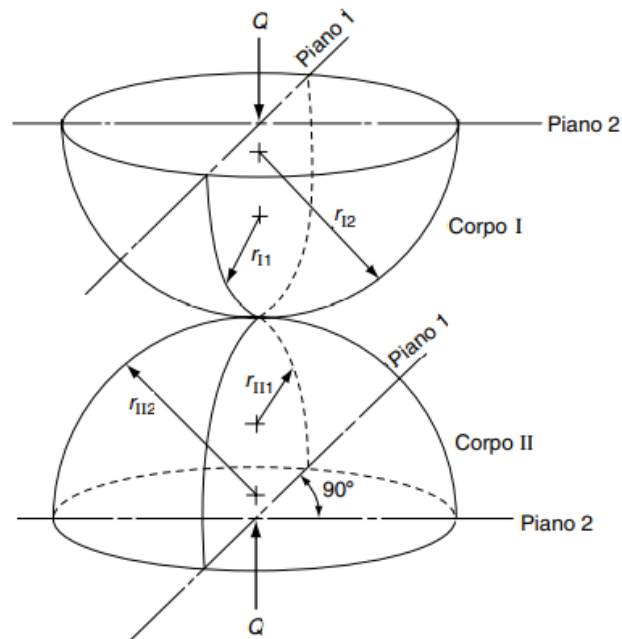


Figure 2.2: Definition of the radii of curvature for two bodies in their contact points [11].

It is now possible to evaluate the following parameters:

Curvature sum:

$$\sum \rho = \frac{1}{r_{I,1}} + \frac{1}{r_{I,2}} + \frac{1}{r_{II,1}} + \frac{1}{r_{II,2}}$$

Curvature difference:

$$F_{\rho} = \frac{(\rho_{I,1} - \rho_{I,2}) + (\rho_{II,1} - \rho_{II,2})}{\sum \rho}$$

Indicating with δ the relative displacement between the bodies in contact, with a major semiaxis and with b the minor ones, the formulas useful for the calculation are shown below [11]:

$$a = a^* \left[\frac{3Q}{2 \sum \rho} \left(\frac{1 - \nu_I^2}{E_I} + \frac{1 - \nu_{II}^2}{E_{II}} \right) \right]^{\frac{1}{3}}$$

$$b = b^* \left[\frac{3Q}{2 \sum \rho} \left(\frac{1 - \nu_I^2}{E_I} + \frac{1 - \nu_{II}^2}{E_{II}} \right) \right]^{\frac{1}{3}}$$

$$\delta = \delta^* \left[\frac{3Q}{2 \sum \rho} \left(\frac{1 - \nu_I^2}{E_I} + \frac{1 - \nu_{II}^2}{E_{II}} \right) \right]^{\frac{1}{3}} \frac{\sum \rho}{2}$$

Where ν is the indicate the Poisson's coefficient, E is the Young's modulus and Q is the value of the perpendicular force applied.

In [11] is explained the theoretical treatment of solving the problem and are reported the values of quantities (a^*, b^*, δ^*) in tabular form or in the form of diagrams, in function of the curvatures differences $F(\rho)$. In the case of steel bodies, formulas are reported in literature [6,9, 11], where it is evaluated the contact area and the relative displacement using values of $\nu = 0.3$, $E = 206 \times 10^3$ MPa for both bodies.

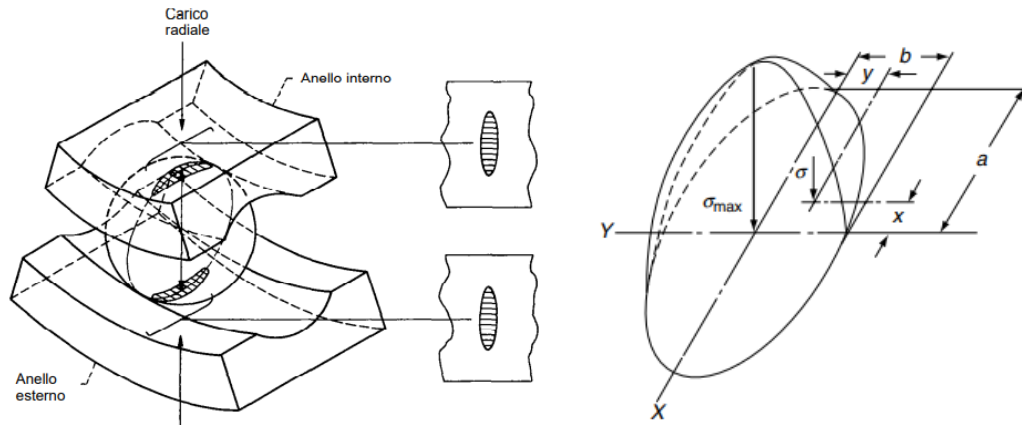


Figure 2.3: Contact area between a spherical rolling element and the two raceways of the radial bearing [12].

In the case of cylinders, the bodies in contact are considered as two ideal cylinders with same length L . In this case parameter a loses his meaning, and only b will be considered, with the modified formula:

$$b = \left[\frac{4Q}{\pi L \sum \rho} \left(\frac{1 - \nu_I^2}{E_I} + \frac{1 - \nu_{II}^2}{E_{II}} \right) \right]^{\frac{1}{2}}$$

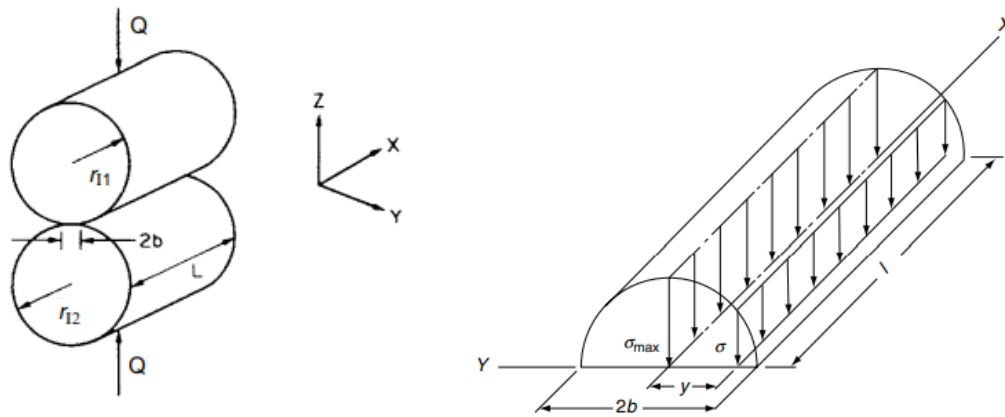


Figure 2.4: Linear contact between two ideal cylinders of equal length (left). Contact area showing the contact pressure trend (right) [13].

In [2] are reported different way to describe the relative displacement δ of parallel cylinders in contact under the action of a perpendicular force Q described in detail in [8,10,14,15]. In this work it will be used the formula presented by Palmgren et al. [14], as it has already been used extensively in the scientific literature:

$$\delta = 3,84 \times 10^{-5} \frac{Q^{0.9}}{L^{0.8}}$$

As shown in [11], the rotational speed of rolling elements is not so high, and centrifugal forces can be neglected because of the low inertia of the bodies. Furthermore, frictions and torque on each rolling element is neglected because their effect is not relevant compared with the other loads. The deformation of each rolling element δ is linked to the load Q throw the following relations:

Case of cylinder:

$$Q = K \delta^{\frac{3}{2}}$$

Case of sphere:

$$Q = K \delta^{\frac{10}{9}}$$

Where K which is the equivalent contact stiffness, is obtained with the following expression:

Case of cylinder-track:

$$K = \left[\frac{L^{0.8}}{3,84 \times 10^{-5}} \right]^{\frac{10}{9}}$$

Case of sphere-track:

$$K = \left\{ \frac{1}{\delta^* \left[\frac{3Q}{2 \sum \rho} \left(\frac{1 - \nu_1^2}{E_1} + \frac{1 - \nu_{II}^2}{E_{II}} \right) \right]^{\frac{1}{3}} \frac{\sum \rho}{2}} \right\}^{\frac{3}{2}}$$

These formulas describe the relation between force and deformation that occurs, in a contact point between two bodies. In bearings, rolling elements have two contact points, one with the inner race and one with the outer. The total displacement between the two raceways in the radial direction can be expressed with the sum of, the approach of the rolling element with the inner race δ_i and the approach of the rolling element with the outer race δ_o :

$$\delta_n = \delta_o + \delta_i$$

It can be also found an equivalent stiffness K for the two contacts. It is evaluated by the formulas for the series coupling of two springs. The Stiffness of the inner K_i and outer K_o contacts can be evaluated with the previous formulas depending on the geometry of the rolling element, and are both necessary to find out the equivalent stiffness with the following formula:

$$K = \left[\frac{1}{\left(\frac{1}{K_i} \right)^{\frac{1}{n}} + \left(\frac{1}{K_o} \right)^{\frac{1}{n}}} \right]^n$$

Now it is possible to write the expression between the force and deformation, on a system composed by a rolling element between two raceways:

$$Q = K\delta_n^n$$

Respect to fig. 2.5 at each rolling element corresponds an angular displacement φ from the vertical position. Calling δ_φ the radial deformation of the rolling element in that position, it can be evaluated as:

$$\delta_\varphi = \delta_r \cos(\varphi) - \frac{1}{2}g$$

Where δ_r is the displacement between the inner and outer race in the vertical direction as it is shown in fig. 2.5, while g is the clearance ($g > 0$) or interference ($g < 0$).

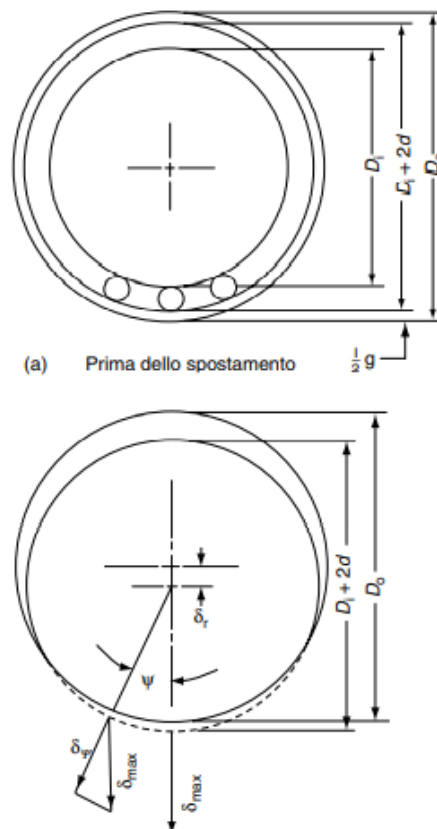


Figure 2.5: Displacement of the inner ring of a bearing [74].

Furthermore, it is possible to write the radial displacement in function of the maximum radial displacement δ_{\max} :

$$\delta_{\varphi} = \delta_{\max} \left[1 - \frac{1}{2\varepsilon} (1 - \cos\varphi) \right]$$

Where ε depends on δ_r with the following relation:

$$\varepsilon = \frac{1}{2} \left(1 - \frac{g}{2\delta_r} \right)$$

The external load Fr , applied on the inner ring, distributes on the rolling elements. Assuming Fr applied in the vertical direction, for the balance of the inner ring of the bearing, the sum of the vertical components of the forces acting on each rolling element must equal the applied load.

$$Fr = \sum_{\varphi=-\varphi_{\max}}^{\varphi_{\max}} Q_{\varphi} \cos\varphi$$

Where Q_{φ} is the radial load applied on the body in the angular position φ which multiplied by $\cos\varphi$ is projected along the vertical direction. While φ_{\max} indicates the maximum angle in which rolling bodies are loaded. It depends on the clearance g and on the displacement of the inner ring δ_r following the equation:

$$\varphi_{\max} = \arccos\left(\frac{g}{2\delta_r}\right)$$

It is also possible to express the radial load Q_{φ} as a function of δ_r :

$$\frac{Q_{\varphi}}{Q_{\max}} = \left(\frac{\delta_{\varphi}}{\delta_{\max}} \right)^n$$

$$Q_{\varphi} = Q_{\max} \left[1 - \frac{1}{2\varepsilon} (1 - \cos\varphi) \right]^n$$

It is finally possible to write the relation between the external force Fr and the displacement of the inner ring of the bearing δ_r which is present in the definition of ε . Given a value of δ_r it is possible to find the correspondent force Fr .

$$Fr = Q_{max} \sum_{\varphi=-\varphi_{max}}^{\varphi_{max}} \left[1 - \frac{1}{2\varepsilon} (1 - \cos\varphi) \right]^n \cos\varphi$$

In the above equation the relation between the force and the displacement is obtained in a discrete way because of the finite number n of rolling elements present in the bearing, each one with its stiffness. To write the same relation in an integral form it is possible to distribute the stiffness along the load zone, in a continuous form, introducing the load distribution factor $J_r(\varepsilon)$ [11,16].

$$J_r = \frac{1}{\pi} \int_{-\varphi_{max}}^{\varphi_{max}} \left[1 - \frac{1}{2\varepsilon} (1 - \cos\varphi) \right]^n \cos\varphi d\varphi$$

2.3 Bearings of the model

In this work the bearings implemented in the model are the same used in the thesis of Giorio [2] (Single row deep groove ball bearing type 6305). Data of this bearing are available online from the SKF website [17]. The geometry of the bearing is reported in Tab. 2.1 with all the necessary factors to evaluate the relation Force-deformation $Fr(\delta_r)$ such as diameters of rings and balls, number of rolling elements and the value of clearance.

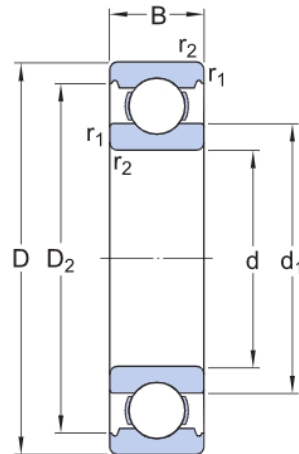


Figure 2.6: Geometry of the bearing [17].

Table 2.1: Geometric properties of deep groove ball bearing 6305.

Bearing	Geometry
Inner ring diameter d_1	32.1 mm
Outer ring diameter D_2	54.67 mm
Bore diameter d	25 mm
Diameter of rolling element d_r	11.274 mm
Number of rolling element N	7
Contact angle (assumed)	0°
Clearance g	22.57×10^{-3} mm

In fig. 2.7 the relationship between the two possible ways to evaluate the radial force is compared: discrete and continuous approach. With discrete approach it is possible to obtain the value of the radial force for values of the radial displacement, which agree with the continuous method:

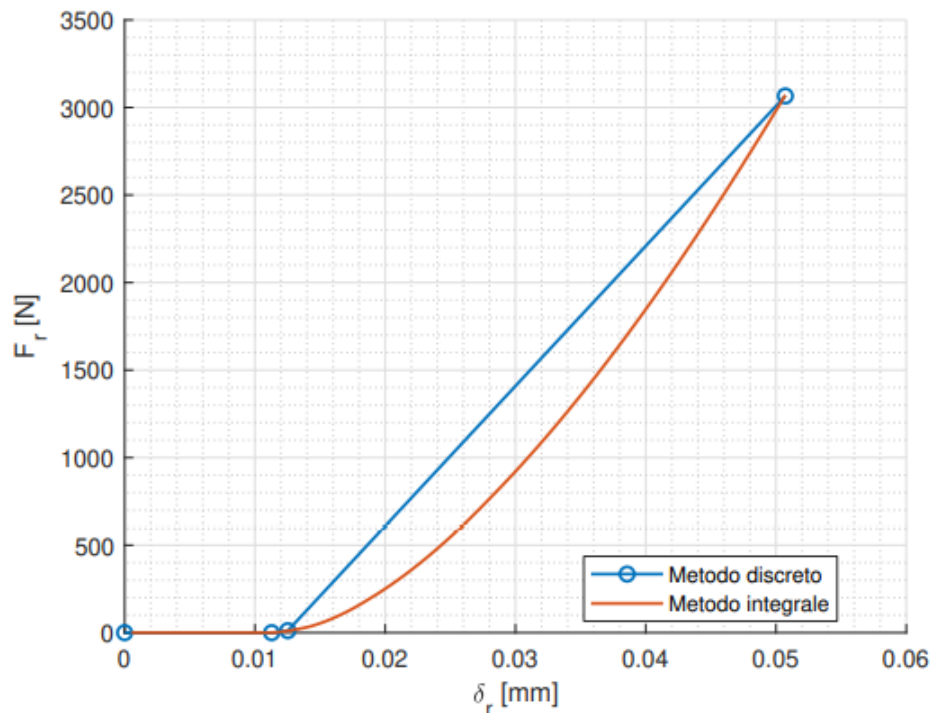


Figure 2.7: Comparison of the results obtained with the discrete and continuous method for the calculation of the bond $F_r - \delta_r$ of a radial bearing [2].

The equivalent linearized stiffness can be defined as [15]:

$$K_{lin} = \frac{dF_r}{d\delta_r}$$

This value of stiffness depends on the load as in the following graph:

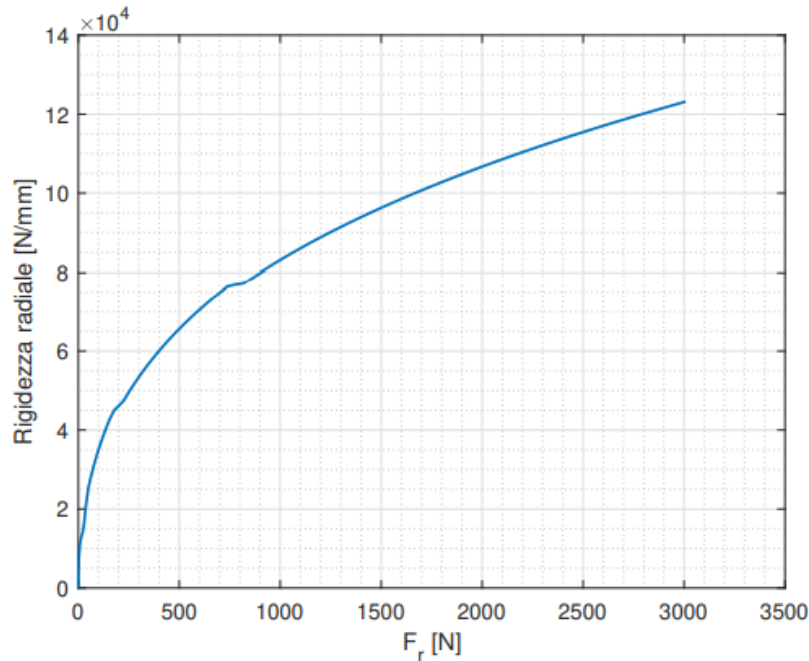


Figure 2.8: Equivalent linearized stiffness for a 6305 radial bearing in function of δ_r [2].

In this work the value of stiffness is implemented in parametric form, and a tentative value of $K_{lin} = 10 \times 10^4 \frac{\text{N}}{\text{mm}}$ is used to validate the model.

2.4 Bearing forces

Applying a load F_r on the inner ring of a bearing, generates a deflection of the rolling elements. In this work bearings are modelled as in fig. 2.9 where each rolling element is represented as a system composed by a spring and a damper in parallel. The deformation of balls creates a reaction force that depend on the relative displacement δ_r between the two rings and from its velocity $\dot{\delta}_r$.

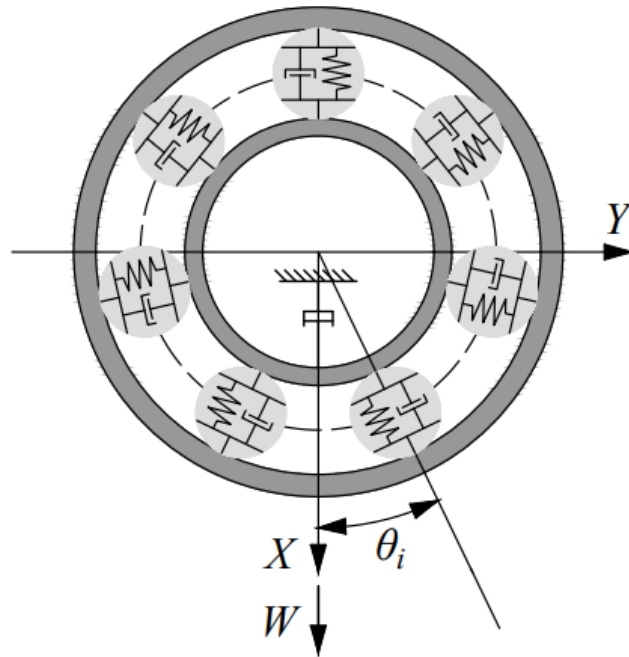


Figure 2.9: Model of the bearing system adopted, with the chosen reference frame XY and the generic rotation of the inner ring θ_i [2].

2.4.1 Evaluation of deflection in bearings

To analyse the deformation of each rolling element is necessary to introduce the angular coordinate θ that indicate the rotation of a body from the vertical position. Defining the initial position of the body, its rotation θ can be expressed in function of time t . Knowing the angular velocity of the inner ring ω it is possible to write the velocity of the cage ω_c

$$\omega_c = 2\pi FTF$$

in which FTF indicates the “Fundamental Train Frequency” and can be calculated as

$$FTF = \frac{f_s}{2} \left(1 - \frac{d}{D} \cos \alpha \right)$$

Where d and D , are respectively the diameter of the rolling body and the mean diameter of the bearing, f_s is the rotational frequency of the shaft and α is the contact angle that is equal to 0 in a radial, spherical, or cylindrical, roller bearing.

It is now possible to derive the angular position of each rolling element i shown also graphically in fig 2.10:

$$\theta_i = \frac{2\pi}{N}i + \omega_c t$$

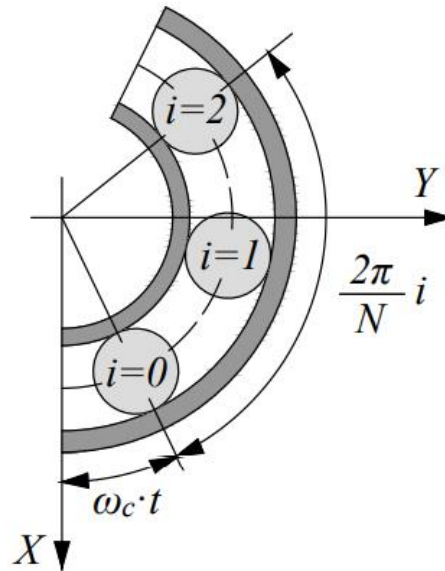


Figure 2.10: Angular position of the rolling element i [2].

The deflection of each ball can be expressed in function of the angle θ_i :

$$\delta_i = x \cos\theta_i + y \sin\theta_i - \frac{g}{2}$$

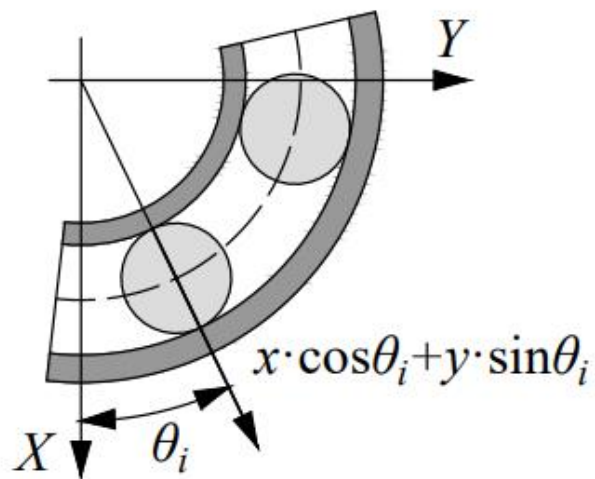


Figure 2.11: Radial displacement of the i -th rolling element at time t , due to the translation of the bearing inner ring [2].

If δ_i results positive, it means that the body is subjected to load, while if it is negative, it means that the body and the raceway are not in contact, and no force is developed. The velocity of deflection of each body can instead be written deriving the displacement δ_i :

$$\dot{\delta}_i = \dot{x} \cos\theta_i + \dot{y} \sin\theta_i$$

Elastic force depends on the displacement δ_i and is proportional to the K_{lin} obtained in chapter 2.3. Damping force instead is proportional to the damping coefficient c_b coming from the losses due to the viscosity of the lubricant inside the bearing. Its range values depend on the linear stiffness as it was described by Kong et al. [19] according to which the values vary in the range:

$$0.25 \times 10^{-5} K_{lin} \ll c_b \ll 2.5 \times 10^{-5} K_{lin}$$

2.4.2 Evaluation of deflection in bearings with localized defects

Defects on bearings can be of different type. They can be divided in two main categories, distributed and localized defect:

- Distributed defect, include abrasive wear of surfaces, surface roughness, ripple and misalignment defect, errors of production such as oversize raceways or rolling elements [20,21].
- Localized defects typically indicate defects due to the fatigue phenomenon. Rolling element surface fatigue is characterized by pitting and spalling that leaves craters on the surfaces. Pitting originates on the surface and occurs where surface dents or scratches are present. It initiates as a crack and propagates as shallow craters. Spalling is subsurface originated instead and occurs when microcracks originate below the surface in correspondence of material inhomogeneities and propagates toward the surface. Spalling leaves deeper cavities with respect to pitting [20,22,23].

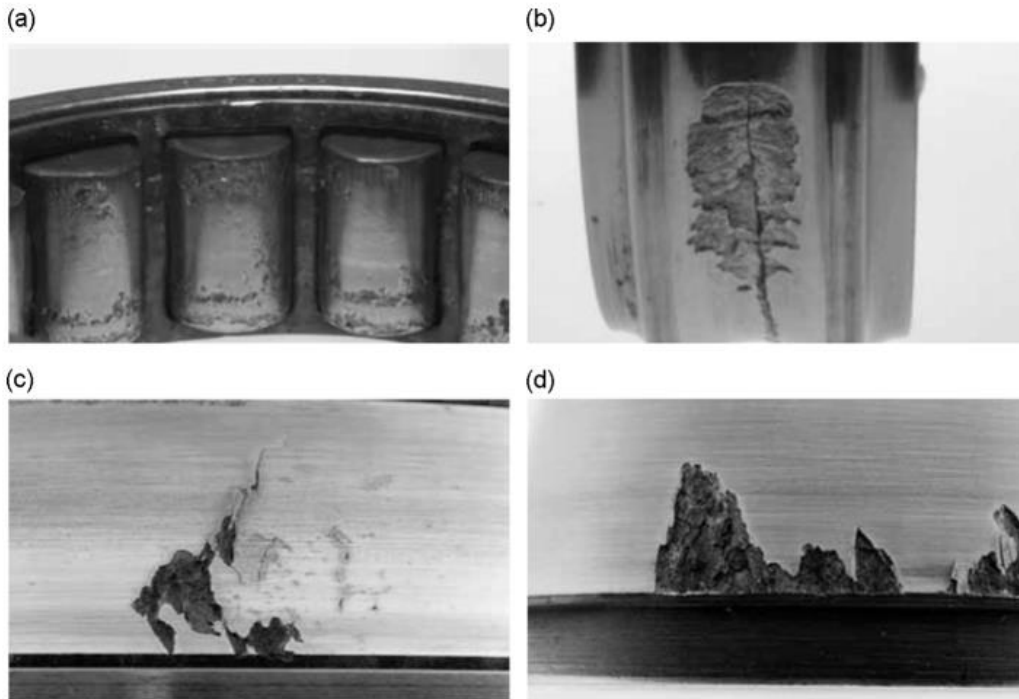


Figure 2.12: Fatigue effect on various elements of a bearing: (a) localized defect on the rolling elements, (b) flaking area in the inner raceway, (c) flaking area in the outer raceway, (d) flaking area in the outer raceway [22].

When rolling element enters in the zone with the localized crack, it undergoes to an impulsive contact force which cyclically consumes the edges of the defect, increasing the dimension of the crack that could transform into an extended defect [22].

In this work, in order to simulate a possible defect present in a component of the bearing (inner ring, outer ring or rolling element), the defect itself is modelled as in [2] as a part of a sine wave (instead of using a periodically repeating pulse function). Defects are modelled as a local variation of radial displacement of the rolling bodies that are in the same zone of the defect. In [18] is defined the angular extension φ_j of a j -error.

$$\varphi_j = ff_j \frac{H_j 2\pi}{\pi D_{i/o}}$$

Where ff_j indicates the relationship between the length of the defect and the maximum height H_j and D_i, D_o alternatively indicates the diameter of the inner or outer race, depending on which of the two is damaged. It is so possible to derive the radial displacement variation of the rolling element in the defect zone. This value is important because it modifies the force of the bearing that depend on the deformation of the rolling elements.

$$\Delta\delta_j = -H_j \sin \left[\frac{\pi}{\varphi_j} (\theta_t - \theta_{init}) \right]$$

Where θ_{init} indicate the angle of the defect at time 0, while θ_t depend on the position of the defect.

β_{ij} is an index adopted to understand if the rolling element i is in the crack position. Its values are:

$$\beta_{ij} = \begin{cases} 1 & \text{if the rolling element is in the crack zone} \\ 0 & \text{if not} \end{cases}$$

The radial deformation δ_i described in the previous chapter is therefore modified by the presence of localized defects as follows:

$$\delta_i = x \cos\theta_i + y \sin\theta_i - \frac{g}{2} - \sum_{j=1}^{jmax} \beta_{ij} \Delta\delta_j$$

Where the value $\Delta\delta_j$ depend on the position of the crack because it changes the definition of θ_t :

- Outer ring

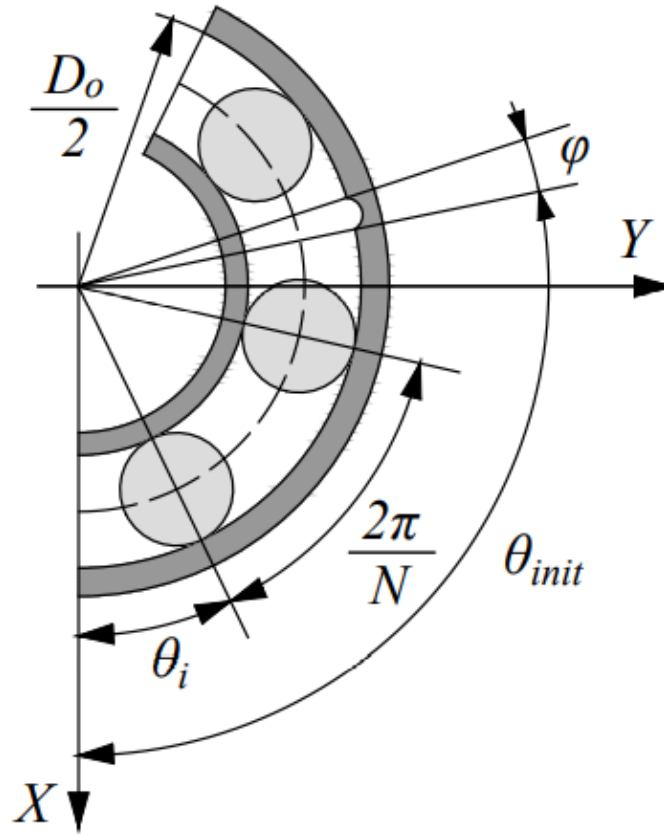


Figure 2.13: Parameters for the implementation of a localized defect on the outer track [2].

The value of θ_t is expressed as:

$$\theta_t = \frac{2\pi}{N}i + \omega_c t$$

Where N is the number of rolling elements, ω_c is the rotation of the cage, i indicate the rolling element and t is time.

Parameter β_{ij} is equal to 1 if:

$$\alpha_j \leq \theta_i \leq \alpha_j + \varphi_j$$

Where α_j indicate the position of the defect and is equal to θ_{init} because the outer ring is considered as fixed. While φ_j is the defect's angle.

- Inner ring

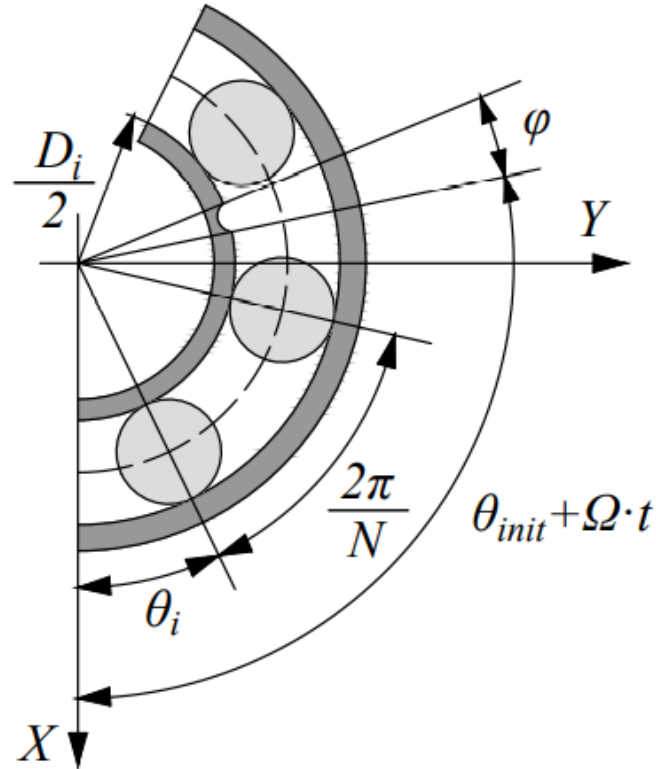


Figure 2.14: Parameters for the implementation of a localized defect on the inner track [2].

The inner ring rotates at the angular speed Ω and the equation of θ_t is modified as:

$$\theta_t = \frac{2\pi}{N}i + (\omega_c - \Omega) t$$

Where N is the number of rolling elements, ω_c is the rotation of the cage, i indicate the rolling element and t is time.

Parameter β_{ij} is equal to 1 if:

$$\alpha_j \leq \theta_i \leq \alpha_j + \varphi_j$$

Where α_j indicate the position of the defect. In this case the inner ring rotates with the defect so:

$$\alpha_j = \theta_{init} + \Omega(t - t_1)$$

- Rolling body

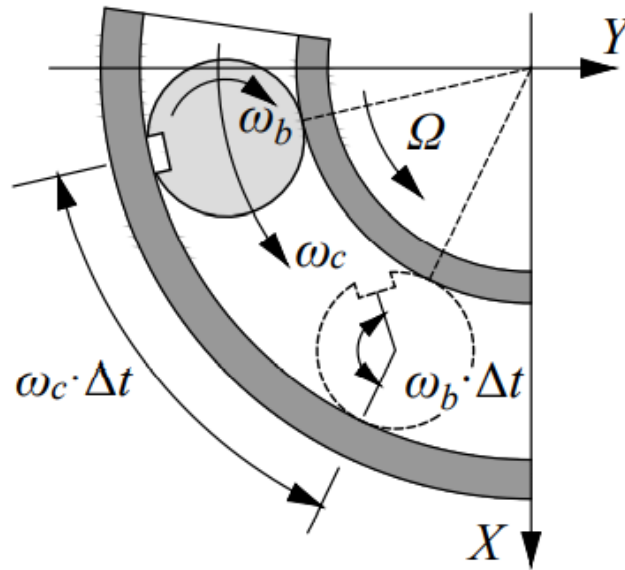


Figure 2.15: Parameters for the implementation of a localized defect on the rolling element [2].

The radial displacement of the rolling element is modified of the quantity $\Delta\delta_j$ when the localized defect lies along the radial direction between the centre of the rolling body and rotation axis. When the defect is on the rolling element the displacement $\Delta\delta_j$ is considered constant along all the angle φ_j . This condition occurs when:

$$\omega_b t - \vartheta_{init} = 0, \pi$$

Where ϑ_{init} is the angle from the vertical direction at t_1 , ω_b is the spin speed of the body and t is the time. Parameter β_{ij} is equal to 1 if $i = j$ since the defect on a particular rolling element i only affects that one body.

Defined the deflection δ_j for each case, it is possible to write the equation of the elastic force as in Chapter 2.2, considering the presence of localized defects also:

$$Q_{ei} = \begin{cases} 0 & \text{if } \delta_i \leq 0 \\ K\delta_i^n & \text{if } \delta_i > 0 \end{cases}$$

Furthermore, losses inside bearings generate a damping force that depends on the velocity $\dot{\delta}_i$ and on the damping factor c_b already described in previous chapter:

$$Q_{di} = \begin{cases} 0 & \text{if } \delta_i \leq 0 \\ c_b \dot{\delta}_i & \text{if } \delta_i > 0 \end{cases}$$

These equations can be written in the two coordinates X, Y as:

$$F_{eY} = \sum_{i=1}^N Q_{ei} \cos \theta_i = \sum_{i=1}^N \{K \delta_i \cos \theta_i\}$$

$$F_{eX} = \sum_{i=1}^N Q_{ei} \sin \theta_i = \sum_{i=1}^N \{K \delta_i \sin \theta_i\}$$

$$F_{dY} = \sum_{i=1}^N Q_{di} \cos \theta_i = \sum_{i=1}^N \{c_b \dot{\delta}_i \cos \theta_i\}$$

$$F_{dX} = \sum_{i=1}^N Q_{di} \sin \theta_i = \sum_{i=1}^N \{c_b \dot{\delta}_i \sin \theta_i\}$$

The sum of the elastic force and damping force in each direction are the bearing's forces that can be wrote in the vector F_b :

$$F_b = \begin{Bmatrix} F_{eX} + F_{dX} \\ F_{eY} + F_{dY} \end{Bmatrix}$$

3. Theory of a rotor with 4 degrees of freedom

“Rotor dynamic is that branch of systems dynamics dealing with mechanical devices in which at least one part, usually defined as rotor, rotates with significant angular momentum, the parts of the machine that do not rotate are generally referred to with the general definition of stator” [24].

In this chapter the theory of a rotor with four degrees of freedom is reported by reference mainly to the work of Genta [24]. In fig. 3.1 are represented three different model that can be used to describe a rotor with four degrees of freedom. They represent a rotor that spins on two bearings which are considered rigid fig. 3.1(a) or compliant fig. 3.1(b, c). The rotor is considered as a rigid body, outlined as a disc, fixed to a massless shaft that can be rigid fig. 3.2(b) or compliant fig. 3.2(a, c). In the Jeffcott rotor theory, the rotor is considered as a point mass without account for its moments of inertia. Unlike that theory, to study the phenomena that influence the dynamic behaviour of rotors, such as the gyroscopic effects, it is necessary to introduce the principal moments of inertia about the rotation axis J_p and the transversal moment of inertia J_t about any axis in the rotation plane. Values of moments of inertia depend on the geometry of the rotor: if J_p is higher than J_t the body can be seen as a disc, otherwise with $J_t > J_p$ the body is usually referred to as a long rotor. In the limiting case with $J_t = J_p$ the ellipsoid of inertia degenerate into a sphere. This system has six degrees of freedom, but it is possible to uncouple axial, flexural, and torsional behaviour. Indeed, for the study of the flexural behaviour with the hypothesis of constant speed and under wide simplifying assumptions, it can be modelled with 4 coordinates. The goal of this chapter is to obtain the equations that describe the motion of the rotor and the procedure to write them follows the theory described by Genta in [24].

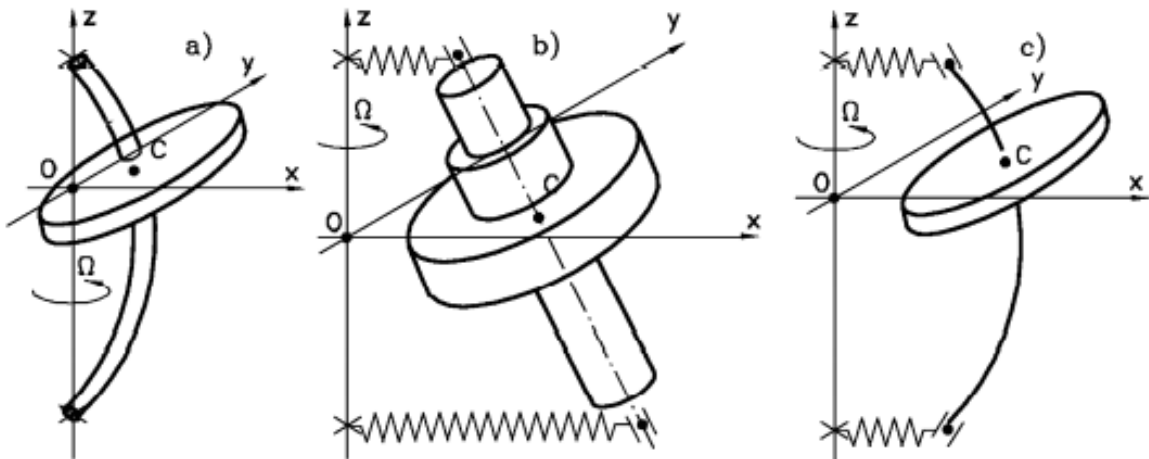


Figure 3.1: Scheme of a Rotor with four degrees of freedom. (a) Compliant shaft on rigid bearing. (b) Rigid rotor on compliant bearings. (c) Both bearings and shaft are compliant [24].

3.1 Reference frame

To describe the motion of the rotor it is defined a reference system. Point C indicates the point on the shaft where it is located the rigid disc with its mass and moments of inertia. The frame used in this work is in accordance with the one of [24]:

- O-XYZ is the fixed frame that has its origin in point O and the Z-axis coincides with the rotor's rotation axis.
- O-ΞHZ is the rotating frame in which O is the origin and axes Ξ and H rotate in the XY-plane with angular velocity Ω , during constant speed operation. Z-axis coincides, as the previous frame, with the rotation axis of the rotor.
- C-X'Y'Z' is the frame that has its origin in C, with all the axes that remain parallel with those of frame OXYZ.
- C-xyz also has the origin in point C, but its z-axis is the same of the rotation axis of the rigid disc in its deformed position. It is obtained from the X'Y'Z'-frame rotating about the X'-axis until Y' is parallel to the rotation plane. That angle is called $\phi_{x'}$ and Y' became y. Then from the new configuration, the frame is rotated of the angle ϕ_y around the new y-axis until X' will lie on the rotation plane. After these two rotations the new z-axis correspond apart from χ error to the symmetry axis of the rotor.
- C-ξηz is the frame obtained rotating C-xyz frame of the rotation angle θ of the rotor that in case of constant spin-speed is equal to Ωt .

- Frame P-123 is obtained from C- $\xi\eta z$ frame considering the effect of unbalance χ that will be described in 3.2. In the new reference system, the principal axis of inertia, corresponding to the polar moment of inertia of the rotor J_p , lies in a plane parallel to ξz -plane.

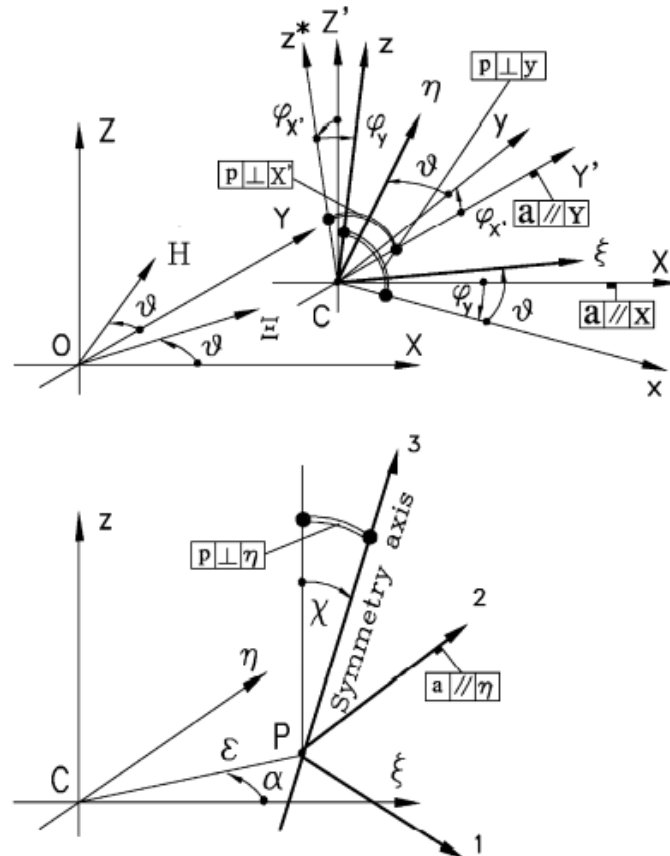


Figure 3.2: Reference frames of a 4-dof rotor with. Letter in boxes indicate respectively axis and plane [24].

3. 2 Equation of the system with four degrees of freedom

Several simplifications are needed to obtain and correctly describe a linearized model. The rotation axis of the rotor in its undeformed configuration is considered equal with the barycentric principal axes of inertia. This condition is true if the rotor is considered

perfectly balanced and this is only an approximation. Indeed, in many cases, the unbalance can be considered small. Displacements and velocities can be assumed small, excluding the rotation angle and the angular velocity about the spin axis, that can be considered as imposed by the driving system, as described in many works in literature. Following these considerations, the equations of the centre of the rotor C are obtained with the Lagrange approach:

considering the uncoupling between axial, flexural and torsional movement and with the small displacement assumptions, point P, which indicates the centre of mass of the disc, will move on the same xy-plane. Firstly, the position of point P is found and integrated to obtain the velocity. then through kinetic and potential energy, the Lagrange equations are obtained. To study the flexural behaviour, four degrees of freedom are enough if spin speed is considered as constant. The forces on point C are produced by the shaft, which is considered elastic. Assuming the behaviour of the shaft as linear, reaction forces of the shaft depend to its stiffness matrix. Matrix, respect to the two planes K_{xz}, K_{yz} , are similar. Considering the axial symmetry of the shaft they can be written as:

$$K_{yz} = \begin{bmatrix} K_{11} & -K_{12} \\ -K_{21} & K_{22} \end{bmatrix} \quad K_{xz} = \begin{bmatrix} K_{11} & K_{12} \\ K_{21} & K_{22} \end{bmatrix}$$

Values of K can be obtained inverting the compliance matrix:

$$K = B^{-1} = \begin{bmatrix} \beta_{11} & -\beta_{12} \\ -\beta_{21} & \beta_{22} \end{bmatrix}^{-1}$$

Where the values β is the coefficients of influence of the system and each element are obtained as: β_{11} is equal to the displacement of C with a unit force applied on it. β_{21}, β_{12} indicates the rotation of C caused by a unit force and β_{22} is the rotation produced by a unit torque.

The resultant equations, written with the four generalized coordinates ($X, Y, \varphi_{x'}, \varphi_y$) are obtained, considering the force of the shaft as the only force acting on C, without external forces:

$$\begin{cases} m\ddot{X} + K_{11}X + K_{12}\varphi_y = 0 \\ m\ddot{Y} + K_{11}Y - K_{12}\varphi_{x'} = 0 \\ J_t\ddot{\varphi}_{x'} + J_p\Omega\dot{\varphi}_y - K_{12}Y - K_{22}\varphi_{x'} = 0 \\ J_t\ddot{\varphi}_y - J_p\Omega\dot{\varphi}_{x'} + K_{12}X + K_{22}\varphi_y = 0 \end{cases}$$

3.2.1 Forces generated by the imperfection of the shaft

The motion of point C is influenced also by the imperfection of the shaft that can be of different types:

- *Shaft bow* in fig. 3.3, happens when the shaft in its undeflected configuration is slightly bent. The angular misalignment χ_b of the shaft is defined as the tangent to the deflected configuration when no forces are applied to it. Point O' in fig. 3.3 indicates the new centre of the shaft C considering bow b . The direction of deformation is usually different from the eccentricity ε and the bow with the angular misalignment lie in a plane that differ from the ξz -plane of angles α_b and β_b . In complex coordinates the force can be described as:

$$f_{bow} = K \begin{Bmatrix} b e^{i\alpha_b} e^{i\omega t} \\ \chi_b e^{i\beta_b} \end{Bmatrix} e^{i\Omega t}$$

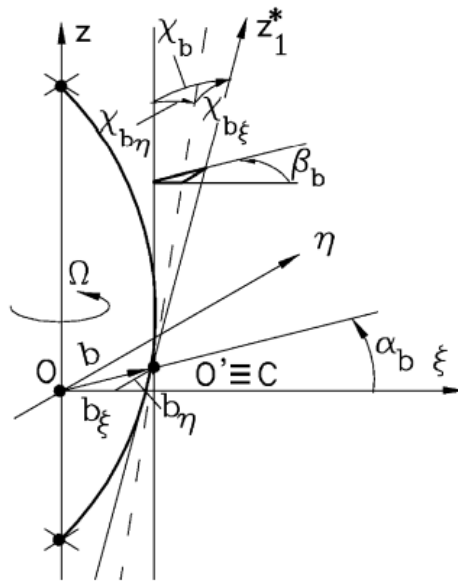


Figure 3.3: Undeflected configuration of the shaft considering the presence of shaft-bow [24].

- *Static and couple unbalance* are caused by two errors of the shaft: the centre of gravity of the rotor is moved from the axis of a distance ε , and the axis of symmetry of the rigid body does not coincide exactly with the rotation axis but differs of a small angular error χ . Static unbalances lie in a plane parallel to $\xi\eta$ -

plane and lead the couple unbalance of a phase angle α as shown in fig. 3.2. These errors of the rotor introduce the two whirling modes in fig. 3.4 if the translational degrees of freedom are elastically uncoupled from the rotational ones [26,27,28]. Translational motion occurs with the axis of the rotor parallel to itself and is called cylindrical whirling, rotational motion occurs about the centre of mass and is called conical whirling.

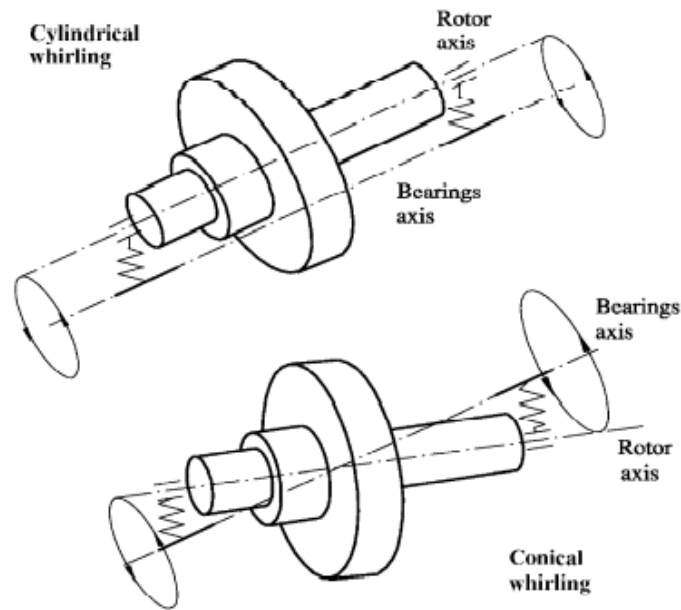


Figure 3.4: Cylindrical and conical whirling produced by static and couple unbalance of the rotor [24].

The vector of the force and moment, in complex coordinate, caused by unbalance then becomes:

$$f_{unb} = \left\{ \begin{array}{l} m\epsilon e^{i\alpha} \\ \chi(U_t - J_p)e^{i\beta} \end{array} \right\}$$

The following differential equations, written for the point C of the model, are obtained considering static and couple unbalance as generalized forces, and neglecting the effect of shaft bow.

$$\begin{cases} m\ddot{X} + K_{11}X + K_{12}\varphi_y = m\varepsilon\Omega^2 \cos(\Omega t + \alpha) \\ m\ddot{Y} + K_{11}Y - K_{12}\varphi_{x'} = m\varepsilon\Omega^2 \sin(\Omega t + \alpha) \\ J_t\ddot{\varphi}_{x'} + J_p\Omega\dot{\varphi}_y - K_{12}Y - K_{22}\varphi_{x'} = -\chi\Omega^2(J_t - J_p)\sin(\Omega t + \beta) \\ J_t\ddot{\varphi}_y - J_p\Omega\dot{\varphi}_{x'} + K_{12}X + K_{22}\varphi_y = \chi\Omega^2(J_t - J_p)\cos(\Omega t + \beta) \end{cases}$$

That can be also written in matrix form as:

$$\begin{bmatrix} m & 0 & 0 & 0 \\ 0 & J_t & 0 & 0 \\ 0 & 0 & m & 0 \\ 0 & 0 & 0 & J_t \end{bmatrix} \begin{Bmatrix} \ddot{X} \\ \ddot{\varphi}_y \\ \ddot{Y} \\ \ddot{\varphi}_{x'} \end{Bmatrix} = \Omega \begin{bmatrix} 0 & 0 & 0 & 0 \\ 0 & 0 & 0 & 0 \\ 0 & 0 & 0 & -J_p \\ 0 & J_p & 0 & 0 \end{bmatrix} \begin{Bmatrix} \dot{X} \\ \dot{\varphi}_y \\ \dot{Y} \\ \dot{\varphi}_{x'} \end{Bmatrix} \\ + \begin{bmatrix} K_{11} & K_{12} & 0 & 0 \\ K_{21} & K_{22} & 0 & 0 \\ 0 & 0 & K_{11} & -K_{12} \\ 0 & J_p & -K_{21} & K_{22} \end{bmatrix} \begin{Bmatrix} X \\ \varphi_y \\ Y \\ \varphi_{x'} \end{Bmatrix} = \begin{Bmatrix} m\varepsilon\Omega^2 \cos(\Omega t + \alpha) \\ \chi\Omega^2(J_t - J_p)\cos(\Omega t + \beta) \\ m\varepsilon\Omega^2 \sin(\Omega t + \alpha) \\ -\chi\Omega^2(J_t - J_p)\sin(\Omega t + \beta) \end{Bmatrix}$$

To write these equations in a more compact form, complex coordinates are introduced, considering the coordinate $-\varphi_{x'}$ to obtain all positive terms and symmetric matrices:

$$\begin{cases} m\ddot{r} + K_{11}r + K_{12}\phi = m\varepsilon\Omega^2 e^{i(\Omega t + \alpha)} \\ J_t\ddot{\phi} - iJ_p\Omega\dot{\phi} + K_{12}r + K_{22}\phi = \chi\Omega^2(J_t - J_p)e^{i(\Omega t + \beta)} \end{cases}$$

where:

$$\begin{cases} r = X + iY \\ \phi = \varphi_y - i\varphi_{x'} \end{cases}$$

These equations can be written in matrix form to obtain an even compact equation as described in many works in literature [24,28,29]:

$$M\ddot{q} - i\Omega G\dot{q} + Kq = \Omega^2 f e^{i\Omega t}$$

Where all the matrices are symmetric:

$$q = \begin{Bmatrix} r \\ \phi \end{Bmatrix} \quad M = \begin{bmatrix} m & 0 \\ 0 & J_t \end{bmatrix} \quad G = \begin{bmatrix} 0 & 0 \\ 0 & J_p \end{bmatrix} \quad K = \begin{bmatrix} K_{11} & K_{12} \\ K_{21} & K_{22} \end{bmatrix} \quad f = \begin{Bmatrix} m\varepsilon e^{i\alpha} \\ \chi(J_t - J_p)e^{i\beta} \end{Bmatrix}$$

3.2.2 Forces generated by damping

Damping can be introduced in the equation as a generalized force on the right-hand side of the equation. It can be divided in rotating and non-rotating damping, both proportional to the speed of the centre of the rotor, seen respectively from the fixed frame XY , and from the rotational frame $\xi\eta$. The energy losses that reduce the spin speed, caused for example by aerodynamic drag or bearing drag, do not affect the behaviour of the rotor, indeed with the assumption of constant spin speed it is supplied from the driving system. In the case of viscous damping the equation of the system become:

$$M\ddot{q} + (C_n + C_r - i\Omega G)\dot{q} + (K - i\Omega C_r)q = \Omega^2 f e^{i\Omega t}$$

C_n is the non-rotating damping matrix which has the same shape of the stiffness matrix K and can be expressed as:

$$C_n = \begin{bmatrix} C_{11} & C_{12} \\ C_{21} & C_{22} \end{bmatrix}$$

The force produced is proportional to the speed of the rotor \dot{q} .

C_r is the rotating damping matrix that, in the equation, is multiplied by the displacement q and velocity \dot{q} . The force generated is proportional to the speed seen from the rotating reference frame, which written in the fixed frame is equal to:

$$V_p = \dot{r} - i\Omega r$$

Generally, in rotors, this force is produced by the deflection of the shaft combined with its rotation and acts when the whirl speed ω is different with respect to the spin speed Ω . This effect is produced by the energy dissipated by the hysteretic cycle of materials as shown in fig. 3.5(a), where it is represented the elliptical hysteresis cycle on the stress-strain plane. In fig. 3.5(c) and 3.5(d) are shown the points correspondent to the hysteresis cycle in two different configurations, depending on the spin speed of the rotor: if the spin speed is lower than the whirl speed, the force opposes the motion of the shaft, stabilizing the system; if the spin speed is higher, then it excites the whirl motion with a destabilizing effect [30].

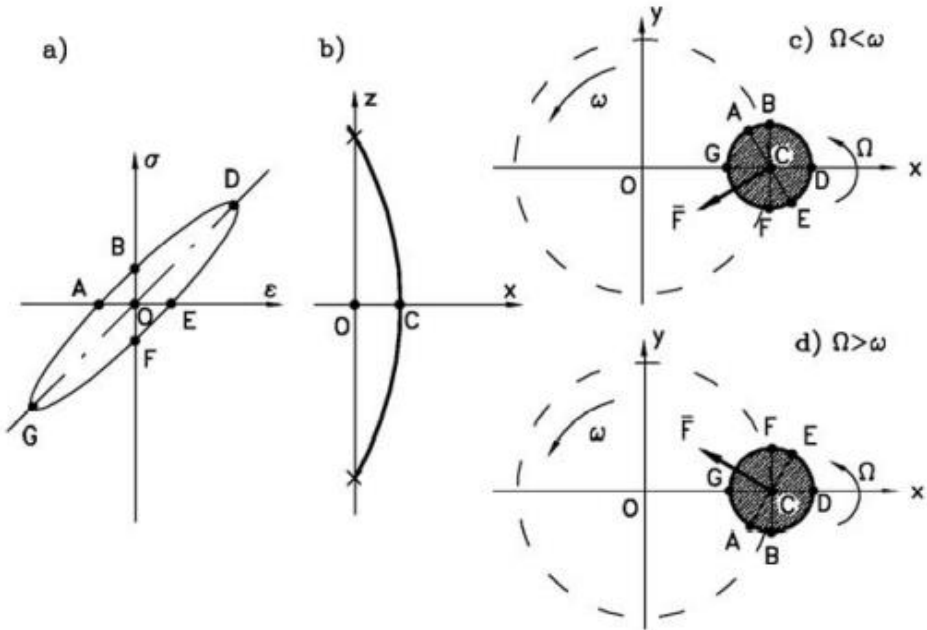


Figure 3.5: (a) Hysteresis cycle in stress-strain plane. (b) Scheme of a bent rotor during whirling. (c), (d) Trajectory of point C during whirling in the two configurations with whirling speed lower than spin speed and whirling speed higher than spin speed [24]

4. Vibration Condition Monitoring

Condition-Based Maintenance, CBM, is used to make maintenance actions thanks to the different signs present in many machines indicating that a failure is going to occur. This technique is adopted to predict the failure of a system through the information obtained monitoring its operating conditions, which can be of different type such as vibrations, noises, contaminants, or lubricating oil. Condition Monitoring collects the condition of the system and give a better knowledge of the failure causes and effects [31]. Machinery Condition Monitoring, MCM, can be considered as one of the best methods to perform monitoring activities and it is used in many industries to prevent the failure of the machines [32].

Preventive Maintenance was a first solution, according to which maintenance interventions must be carried out between time intervals such that the probability of a breakdown of the system is low probable. It is difficult to evaluate the optimal level of preventive maintenance such that the overall cost of manufacturing, or the cost of providing a certain customer service, is minimized. Furthermore, excessive maintenance involves work - and at the same time a cost - higher and unjustified. Condition-Based Maintenance, (CBM), is a better solution, with which the maintenance activities are carried on only when a functional failure is detected [33, 34, 35]. The vibration analysis is particularly interesting: each mechanical component in nominal operation has a certain vibration signature [35], the appearance of damage in the component modifies this signature and allows to recognize the warning signs of a defect. Such a technique is characterized also by the possibility of being applied remotely on the machine, without the need for direct observation of the component. In offline condition monitoring system, the analysis is carried out later in the laboratory or directly on site, while in online condition monitoring system the signal containing the information of the component of interest is acquired continuously and constantly analysed [32]. When applying the vibration analysis for the monitoring of rolling bearings, it is possible to adopt the lubricant analysis, indeed lubricant carries information from inside the machinery in the form typically of suspended particles due to possible wear of components and chemical contaminants. This system can only be of a periodic type, as many days pass between collection and analysis of the lubricant [32]. To identify the origin of the main operating defects of the bearings in time it is so necessary to collect vibration signals during operations.

4.1 Sources of vibration in a rotor-bearing system

Bearings are critical components of rotating machines and generate different vibrations both with and without the presence of defects. Identifying the possible defects and the associated vibrations under operating condition can avoid malfunctioning and breakdown of machines. The sources of vibrations that came from a bearing can be divided in [1, 2]:

- Variable compliance: these types of vibrations are present also in geometrically perfect bearings due to the discrete number of balls. It can be reduced increasing the number of rolling elements.
- Geometrical imperfections: the vibrations came from the geometrical error produced during the manufacturing process. Surface roughness produces vibrations at frequencies higher than about sixty times bearing rotational speed. They therefore appear in the high-frequency part of the frequency spectrum of the signal. Waviness instead produces vibrations that have the main frequencies below sixty times the rotation speed.
- Localised defects: these defects, already described in chapter 2.4.2 are generally caused by fatigue phenomenon, corrosion and by abrasive particles in the lubricant. The produced vibrations depend on the position of the crack. A defect in the inner race generates high-energy pulses at the frequency that rolling elements pass through the inner race, referred to, in literature, as BPFI (Ball Pass Frequency Inner Race). Defects indeed enter and exit the loaded area and produce vibrations. Defects on the outer race are produced with the same mechanism, but with a frequency equal to BPFO (Ball Pass Frequency Outer Race) because the outer ring is fixed. Defected rolling elements produce frequency values multiple of the BSF (Ball Spin Frequency spin), with a vibration signal energy that depend on the position of the ball with respect to the loading area. Cage can generate random vibrations instead, due to the sliding between cage and rolling body, with a wide range of frequencies.

Imbalance forces are the main source of vibration in rotating machines and their values may change in time due to depositions or wear. Obtaining a perfect balancing is almost impossible and expensive, so the most common way to solve the problem is to increase the damping, in order to dissipate greater dynamic energy [36]. The sources of vibrations that came from a rotor can be divided in [37, 38]:

- Unbalance: the presence of the eccentricity in a rotor already explained in chapter 3.2.1 produce a vibration due to the centrifugal force acting on the centre of mass of the shaft with a sinusoidal waveform in the time domain. In spectral data Frequency of the signal is equal to the rotational speed of the rotor 1xRPM (1x rotational speed).
- Angular and parallel misalignments: it is generated when the shaft and bearings are not aligned. The two types of misalignments are angular and parallel, or a combination of both. They occur when the shaft centrelines of two mating components meet at angles or are offset from one another. They typically produce high axial and radial amplitudes with a phase difference of 180-degree across the couplings. Dominant frequencies produced are at 1xRPM and/or 2xRPM, depending upon the degree of misalignment and on the type and design of the couplings.
- Mechanical looseness: possible causes can be that the machine has some components that came loose from the mounting process. This can generate random and unorganized vibrations that generate high running speed amplitude followed by multiples, in the spectrum analysis.

To analyse the raw vibration signal obtained monitoring the system in is necessary to process this information to obtain specific features, which can be used to categorize the status of operation of components. It is than possible to extrapolate the characteristics of the signal in time or frequency domain.

4.2 Characteristics of the signal in the time domain

Time domain parameters are usually adopted to recognise bearing damage [39]. This kind of analysis can estimate the conditions of the machine through temporal vibrational signal data. The following parameters will be used to analyse the signals in the time domain and are the same described in many works in literature [2, 23, 39, 40, 41]:

Range:

$$\text{Range} = \max(x_k) - \min(x_k)$$

where x_k is the generic value of the analysed variable x .

This parameter is than adopted to find out the peak value.

Peak Value:

$$Peak\ value = \frac{1}{2} \times Range$$

This statistic parameter is often adopted to recognise the damage level inside rolling elements bearings. It is evaluated with different formulation in literature, but in this work, it is decided to follow the definition of works [39, 42] as the half of the range value previously described.

Root Mean Square:

$$RMS = \sqrt{\frac{1}{N} \sum_{K=1}^N x_k^2}$$

Where N is the number of examined elements of the signal x within the considered time domain.

This parameter describes the intensity of the signal. If a component is damaged, it produces a higher variation of intensity increasing the RMS value [43, 44].

Standard deviation:

$$SD = \sqrt{\frac{1}{N} \sum_{K=1}^N (x_k - \bar{x})^2}$$

Where N is the number of examined elements of the signal x within the considered time domain, \bar{x} is the mean value of the signal equal to

$$\bar{x} = \frac{1}{N} \sum_{K=1}^N x_k$$

This parameter is equal to the root mean square (RMS) if the mean value \bar{x} is equal to 0. The standard deviation can be considered as the value of energy of the signal [41].

Skewness:

$$SK = \frac{\frac{1}{N} \sum_{k=1}^N (x_k - \bar{x})^3}{\sigma^3}$$

Where N is the number of examined elements of the signal x within the considered time domain, σ is the standard deviation of the signal.

The skewness is a statistical measure of lack of symmetry in the distribution of statistical data. Positive values indicates that the data present mostly higher values than the mean \bar{x} , while a negative value indicates that the data are mostly below the mean \bar{x} of the signal [45].

Kurtosis value:

$$KV = \frac{\frac{1}{N} \sum_{k=1}^N (x_k - \bar{x})^4}{\sigma^4}$$

Where N is the number of examined elements of the signal x within the considered time domain, σ is the standard deviation of the signal.

Kurtosis measure how the data are flat or peaked with respect to a normal distribution. It indicates the presence of defects inside bearings components. With the presence of defects inside bearings its value increases because of the peak generated by the damage. However, if the damage has wide dimensions, it generates a near flat signal that decreases the value of KV until it reaches the value of $KV = 3$, that typically characterise a healthy bearing [46].

Crest factor:

$$Crf = \frac{Peak\ value}{RMS}$$

The Crest factor links the two values *Peak value* and *RMS* and it is property linked to the peak value of the signal under examination. The Crest Factor can be a useful indicator for detecting damage at the beginning of their development. Indeed, it detect an instantaneous acceleration even if the RMS doesn't vary significantly [47].

Clearance factor:

$$Clf = \frac{\text{Peak value}}{\left(\frac{1}{N} \sum_{k=1}^N \sqrt{|x_k^2|}\right)^2}$$

Where N is the number of examined elements of the signal x within the considered time domain.

The clearance factor is an impulsive factor that is rarely used to analyse the wear of mechanical systems [48].

Shape factor

$$Shf = \frac{RMS}{\frac{1}{N} \sum_{k=1}^N |x|}$$

Where N is the number of examined elements of the signal x within the considered time domain.

The impulse factor links the RMS and the mean of the absolute values of the signal, and it is often adopted to detect the presence of defect in mechanical system.

Impulse factor:

$$Imf = \frac{\text{Peak value}}{\frac{1}{N} \sum_{k=1}^N |x|}$$

Where N is the number of examined elements of the signal x within the considered time domain.

The impulse factor links the Peak value and the mean of the absolute values of the signal, and it is an impulse indicator.

4.3 Characteristics of the signal in the frequency domain

The frequency domain refers to the analysis of signals with respect to frequency, rather than time [56]. This technique is widely adopted for predictive diagnostics of rolling bearing and take advantage of the Fast Fourier Transform FFT that can turn a signal from the time domain, as the one produced by an accelerometer sensor, to the frequency one [49, 50]. Fourier transform is found to be very useful and efficient tool to analyse vibration signals, able to detect most of the common vibration problems. The digital signature of a healthy bearing produces vibrations mainly caused by the variable compliance, due to the discrete number of balls present in the bearing, as it has been already described in chapter 4.1. The characteristic excited frequencies came from the passage of the rolling elements in the loaded area that generate peaks in the signal. If localized defects are present inside the components, particularly in the inner ring of the bearing, they excite the characteristic frequency of the bearing. Distributed defect, as surface roughness or waviness instead doesn't produce impulsive signal but, on the contrary, it has a randomly distributed phase, and the frequencies are no longer useful assuming more complicated characteristics with a high content of non-stationary contributions [51]. As described in [52] the raw signal describing the acceleration of the bearing doesn't contain many interesting information about the possible presence of defect inside its component. It is so often performed the study of the envelope of the acceleration (EA, "Envelope Analysis") which allows the individuation of the signal indicating the state of health of the bearing [2, 53]. The envelope may be defined as the outer shape of the signal and envelope detection is widely applied in roller bearing analyses. It is a method that intensify the repetitive components of a dynamic signal, and for bearing vibration envelope detection is adopted to identify the pulses intensity and finding the repetition rate of these pulses. Repetition rate is related to the bearing characteristics frequencies which will be described later as (BPFI, BPFO, BSP and FTF) and can be found by spectrum analysis of the demodulated signal. The analysis of the envelope of the signal is performed following the steps described in fig. 4.1.

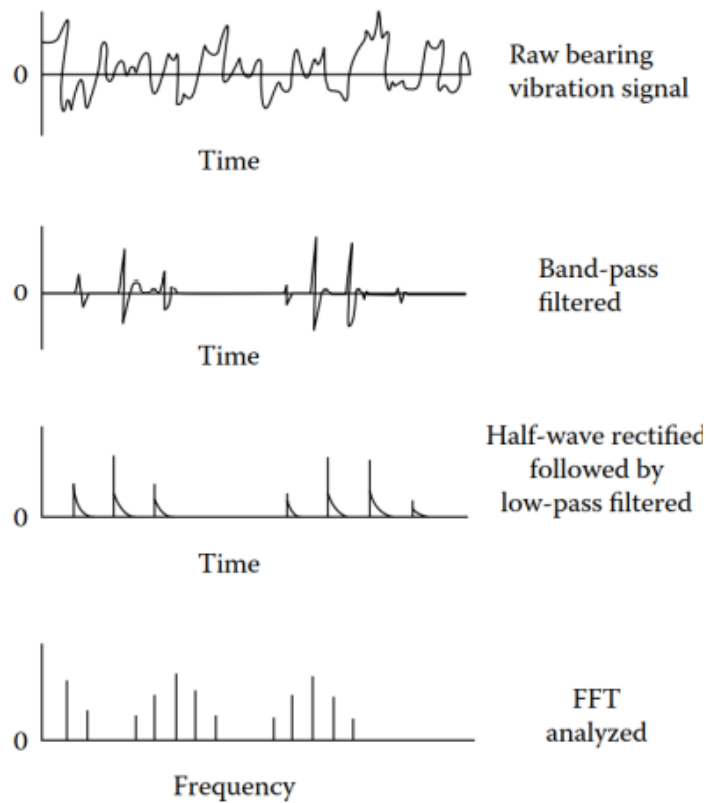
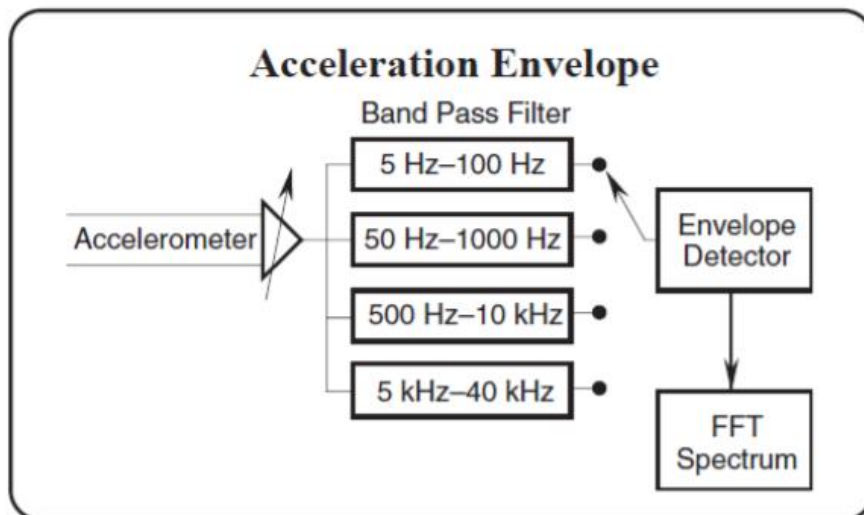


Figure 4.1: Scheme of the envelope analysis applied to a vibration signal [49].

- The acceleration signal can be obtained in the time domain, from accelerometer located on a real machine. The acceleration is so a typical parameter chosen to study the behaviour of a system containing bearings.
- The raw signal obtained from the accelerometer, appropriately amplified, is filtered by using a band-pass filter removing the low-frequency content usually related to common machinery problems. The typical frequencies adopted from the Band Pass Filter depends on the shaft rotational speed with the values described in the following table:

Table 4.1: Typical values for the band pass filter in the envelope analysis [49].

Angular velocity	Band Pass Filter	Range
0 – 50 RPM	5 – 100 Hz	0 – 10 Hz
25 – 500 RPM	50 – 1000 Hz	0 – 100 Hz
250 – 5000 RPM	500 – 10000 Hz	0 – 1000 Hz
2500 - ... RPM	5000 – 40000 Hz	0 – 10000 Hz

- The signal is demodulated through an envelope detector (envelope sensor), which can operate as described in fig. 4.2, rectifying the signal and obtaining the envelope through a low-pass filter.

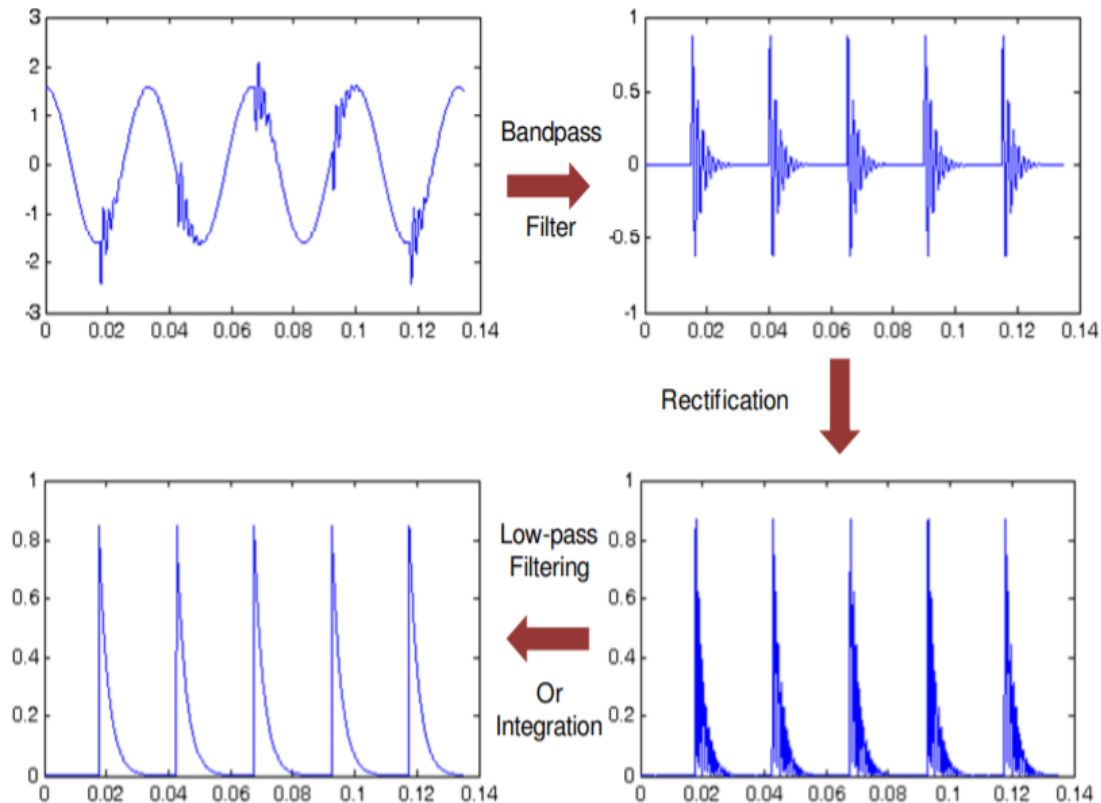


Figure 4.2: Envelope Analysis by Jaafar Alsalaet [49].

It is also possible to operate in a different way through the Hilbert transform of the filtered signal. After the signal is bandpass filtered, the FFT is performed, and the negative spectrum is cancelled doubling the positive spectrum. Finally, the inverse of the FFT is taken to obtain the Hilbert transform. It is then possible to evaluate the envelope evaluating the modulus of the “analytical signal” obtained, filtering the single-sided spectrum using a FIR (Finite Impulse Response) filter.

- The demodulated signal, which corresponds to the envelope of the raw signal, is finally analysed in the frequency domain through the application of the Fast Fourier Transform.

Some of the parameters useful for the study of the excited frequencies of a bearing are so reported afterwards, considering all the assumption already described in chapter 2 [51, 55].

Rotation frequency of the shaft

$$f_s = \frac{\omega}{60}$$

Where ω indicate the rotational speed of the shaft in RPM.

The Rotation frequency of the shaft indicate the rotational speed of the rotor. The eccentricity in a rotor already explained in chapter 3.2.1 produce a vibration due to the centrifugal force acting on the centre of mass of the shaft that. In spectral data frequency of the signal is equal to the f_s .

Fundamental Train Frequency

$$FTF = \frac{f_s}{2} \left(1 - \frac{d}{D} \cos \alpha \right)$$

where d is the diameter of the rolling element and D the mean diameter of the bearing, f_s is the frequency of rotation of the shaft and α is the contact angle of the bearing in the case of an angular bearing (for a radial bearing with balls or rollers is equal to $\alpha = 0^\circ$).

The Fundamental Train Frequency indicates the rotational speed of the centre of the rolling elements with respect to the centre of the shaft and is equal to the rotating speed of the cage of the bearing. A defect present in the cage can excite the FTF, though the presence of the FTF in the spectre of the signal usually indicate a bad mounting of the bearing system.

Ball Pass Frequency Outer Race

$$BPFO = N \frac{f_s}{2} \left(1 - \frac{d}{D} \cos \alpha \right)$$

Where N is the number of rolling elements in the bearing, d is the diameter of the rolling element and D the mean diameter of the bearing, f_s is the frequency of rotation of the shaft and α is the contact angle of the bearing in the case of an angular bearing (for a radial bearing with balls or rollers is equal to $\alpha = 0^\circ$).

The Ball Pass Frequency Outer Race indicate the frequency at which the rolling elements pass through a point located on the outer race. This frequency is usually excited by the vibrations produced with the Variable compliance of a healthy bearing due to the passage of the rolling bodies through the loading zone. Peaks will be much more accentuated with the presence of a defect on the outer ring.

Ball Pass Frequency Inner Race

$$BPFI = N \frac{f_s}{2} \left(1 + \frac{d}{D} \cos \alpha \right)$$

Where N is the number of rolling elements in the bearing, d is the diameter of the rolling element and D the mean diameter of the bearing, f_s is the frequency of rotation of the shaft and α is the contact angle of the bearing in the case of an angular bearing (for a radial bearing with balls or rollers is equal to $\alpha = 0^\circ$).

The Ball Pass Frequency Inner Race is a frequency excited especially with the presence of a defect on the inner ring of the bearing. Indeed, the passage of the rolling bodies on the defect generate an impulse at time laps equal to $1/BPFI$ when the defect is on the loading area. The defect rotates at a frequency equal to the Fundamental Train Frequency generating in the frequency domain side bands around the various harmonics of the BPFI due to the modulation process, which distance themselves from the peaks (BPFI) at the various harmonics of integer multiples of the rotation frequency of the shaft f_s .

Ball Spin Frequency

$$BSF = \frac{D}{2d} \left[\left(1 - \frac{d}{D} \cos \alpha \right)^2 \right]$$

Where N is the number of rolling elements in the bearing, d is the diameter of the rolling element and D the mean diameter of the bearing, f_s is the frequency of rotation of the shaft and α is the contact angle of the bearing in the case of an angular bearing (for a radial bearing with balls or rollers is equal to $\alpha = 0^\circ$).

The Ball Spin Frequency indicates the frequency at which each rolling element rotates around its centre. The presence of a defect on a rolling element generates an impulse when the defect encounter both the outer and the inner ring of the bearing at time laps equal to $1/2BSF$ when the defect is in the loading zone. The rotation of the defect with respect to the bearing centre also generate side bands around the various harmonics of the BSF due to the modulation process, which distance themselves from the peaks (BSF) at the various harmonics of integer multiples of the rotation frequency of the shaft f_s .

5. Rotor-Bearing model

Predictive maintenance is used to detect anomalies in operations and possible defects in the components to address them before they result in failure. Maintenance intervention in Predictive Maintenance can be scheduled periodically, monitoring mechanical operating parameters during the operating use of the system to identify typical signal characteristics of damaged component but not yet faulty; the machine can be stopped at a time that is most convenient and the damaged component replaced. [58, 59]

The analysis of the fracture conditions in the bearings is extremely important in industrial context to predict the rupture of the bearings and consequentially of the machinery [57]. As an early analysis, it is essential to predict and consequently avoid damage to the machinery. In this work, the acceleration signal produced by the vibration of the rotor-bearing system, is studied in different locations on the shaft, and it is used for the detection of defects in bearings. The detection and analysis of faults play a vital role in highly reliable operations. Using vibration analysis, the condition of a machine can be periodically monitored. In [58] there is an interesting analysis of the dynamic behaviour of a real coupled rotor-bearing system. Results show that excessive vibrations on the bearings have different sources such as mechanical looseness and misalignment. Tiwari et al. [60] studied the behaviours and the dynamic response of a balanced rotor supported by ball bearings that present radial internal clearance. Liew et al. [61] also introduce the effect of ball centrifugal force, analysing the effect on the resulting vibration of the bearing. In [62] are investigated contact force, displacement and vibration frequencies of the bearing also considering the gyroscopic moment of balls and the waviness of the rings, modelled by using sinusoidal function. Al-Bedoor [63] has considered a model with the coupled torsional and lateral vibrations of the simple Jeffcott rotor demonstrating the existence of inertial coupling and interaction between lateral and torsional vibrations.

5.1 Rotor-bearing system

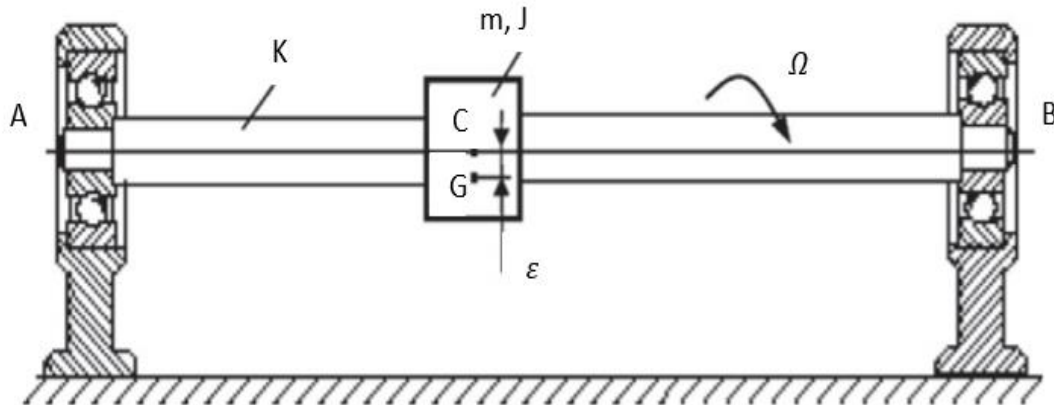


Figure 5.1: Rotor bearing system: Elastic rotor with stiffness K , mass m , inertia J , eccentricity ε rotating at constant spin speed Ω and supported by the two bearings at points A and B [58].

In this work the shaft of the rotor is supported at its ends by two, ball or roller bearings, that are modelled with the same assumption of Chapter 2. The bearings support radial forces, while rotational motion of the shaft ends is left free. In fig. 5.1, the shaft is modelled as massless and flexible with length L . The rotor is otherwise considered as a rigid disc rotating with a constant angular speed Ω and with mass m . The principal moments of inertia of the rigid body will be referred to as the polar moment of inertia J_p about the rotation axis and transversal moment of inertia J_t about any axis in the rotation plane. One of the principal axes of inertia coincides, in the undeformed position, with Z-axis and its ellipsoid of inertia has axial symmetry with respect to the same axis. Furthermore, the rotor is attached to the shaft at a distance a from the left bearing and the system is assumed axially symmetrical.

To analyse the motion of this system, it is introduced the inertial system of coordinate XYZ and the rotational frame $\xi\eta z$ already described in Chapter 3. Y-direction is parallel to the ground and perpendicular to the rotor axle, while X-axis is perpendicular to the ground as in fig. 5.2. The imperfection of the shaft considered in this model are the static and couple unbalance, while the shaft bow is neglected. It is also considered the moment generated by the Gyroscopic effect of the rotor, due to the change in direction of its angular speed as already described in Chapter 3.

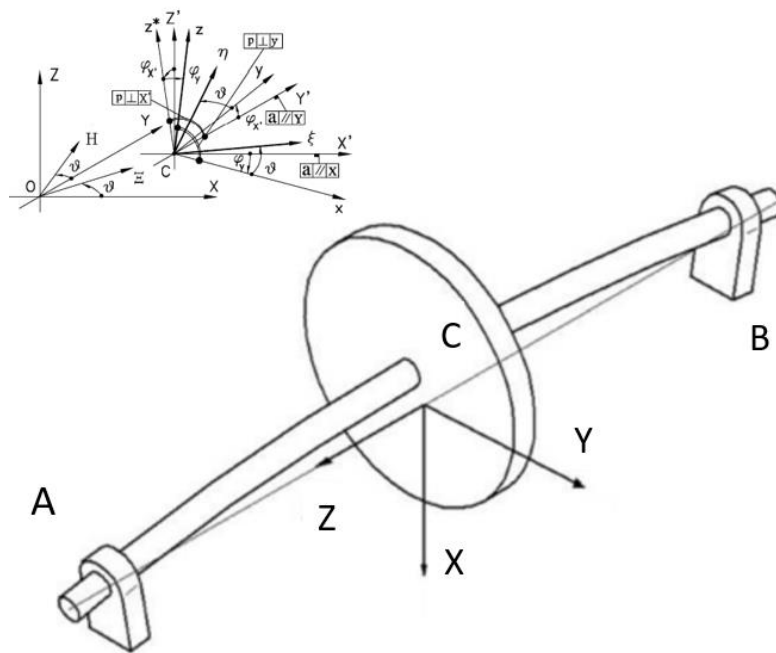


Figure 5.2: Rotor reference frame [64].

Coupling the model of the rotor with the one of the bearings, the degrees of freedom of the system increase. This is caused by the relative movement of the two ends of the shaft A, B with respect to the outer ring of the bearing. The shaft ends are indeed fixed to the inner rings of the bearings and can move with respect to the outer rings that are considered integral with the stator casing fixed to the XYZ -frame. The system has then 8 degrees of freedom, that include the translation (X, Y) and rotation (φ_x, φ_y) of the centre of the rotor C , and two degrees of freedom for each shaft end (X_A, Y_A, X_B, Y_B) [65].

5.2 Equations of the system

Forces generated by the rotor are the same already described in Chapter 3. Moreover, it is also considered the weight of the rotor, positive along the X coordinate. Equations of a rotor with 4 degrees of freedom, that have been described in Chapter 3 can be written for this model introducing the constant weight force f_w on the right-hand side of the equation, acting on the centre C of the disc. The damping force of the rotor is considered of the viscous type and depend on the velocity \dot{q} of the centre of the rotor

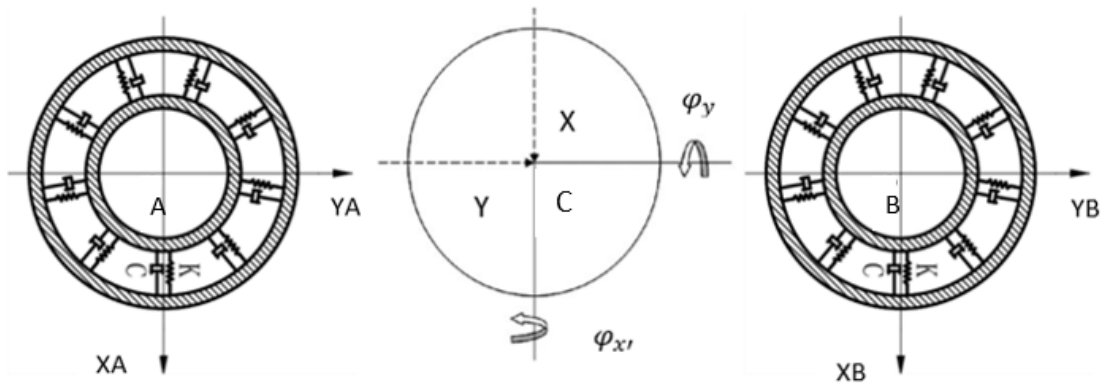


Figure 5.3: Degree of freedom of the system: on the sides bearing A and B with coordinates respectively X_A , Y_A and X_B , Y_B . In the middle the Centre of the shaft with coordinate X , Y , $\varphi_{x'}$, φ_y .

with respect to the fixed frame. The structural damping caused by the deflection of the shaft is neglected. Elastic forces of the shaft depend on the relative displacement between the centre of mass C and the shaft ends A and B . To obtain the value of the force the stiffness matrix K must be multiplied by the vector $(q - q_b)$ that indicates the deflection of the shaft [24, 65, 66].

$$M\ddot{q} + (C_n - i\Omega G)\dot{q} + K(q - q_b) = \Omega^2 f e^{i\Omega t} + f_w$$

The degree of freedom of the system increase with respect to the 4-dof model because of the motion of the shaft ends. The problem has now 8 degrees of freedom as was described previously in fig. 5.3:

- 4 describe the motion of the centre of mass C : $X, Y, \varphi_{x'}, \varphi_y$ which indicates respectively displacements and rotation of the centre of gravity of the shaft.
- 4 indicate the motion of the shaft ends that are fixed to the inner rings of the bearings and can translate with respect to the outer rings. Each inner ring has 2 degrees of freedom that indicate the translation of the ring perpendicular to the axle of the rotor along X and Y direction: X_A, Y_A, X_B, Y_B .

To solve the system, it is necessary to find the relation between the coordinate of the centre of mass and the shaft ends. Internal forces of bearings depend on the displacement and velocity of points A and B with respect to the fixed frame XYZ . Bearing forces act to the rotor centre through the shaft which has the following stiffness matrix, depending on the Young modulus of the material E :

$$K = \begin{bmatrix} K_{11} & K_{12} \\ K_{21} & K_{22} \end{bmatrix}$$

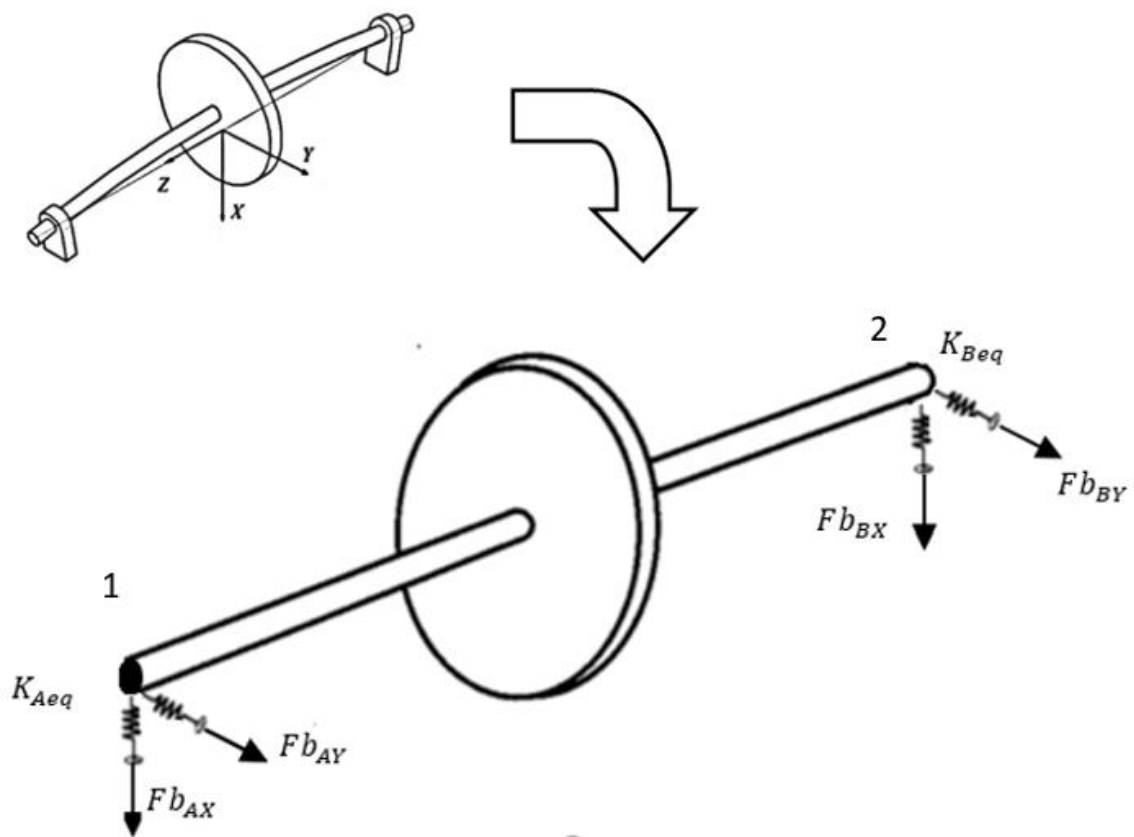


Figure 5.3: Scheme of the rotor-bearing system where Fb are the bearing forces and k_{eq} are the equivalent stiffness of the shaft represented as rigid supported by two springs [65, 68].

Consequently, the stiffness of the shaft can be seen as two springs, located between bearings and points 1 and 2 as in fig. 5.3.

The internal force of bearings is so transmitted through the shaft with the same modulus. Forces of the bearings (Fb_{Ax} , Fb_{Ay} , Fb_{Bx} , Fb_{By}) are directed along direction X and Y. They follow the relations of Section 2.4 and depends on the displacement and velocity of both the shaft ends (A, B). The equivalent vector of forces written in function of the coordinate of the centre of the rotor C is obtained through the transfer matrix T with the following operations [69, 70]:

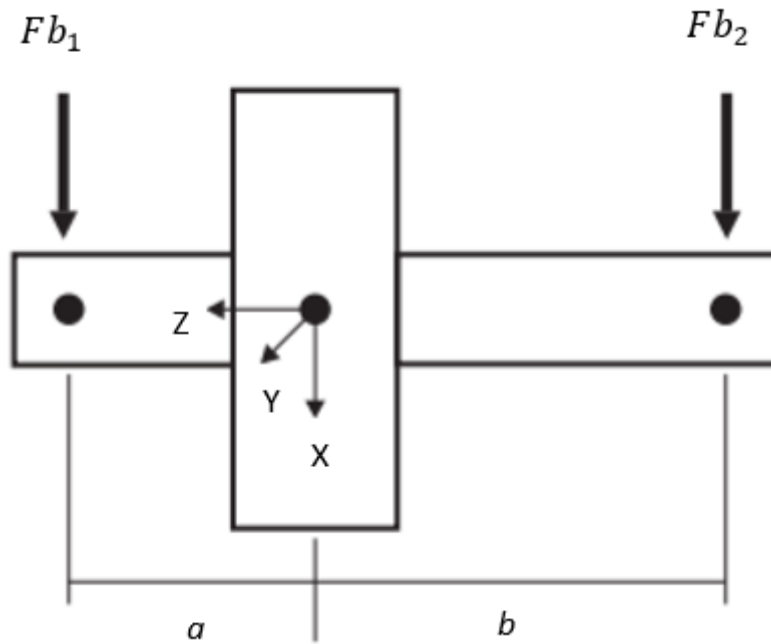


Figure 5.4: Bearing forces applied to the rotor ends.

$$Fb_x = Fb_{1x} + Fb_{2x}$$

$$Mb_x = -Fb_{1y}a + Fb_{2y}b$$

$$Fb_y = Fb_{1y} + Fb_{2y}$$

$$Mb_y = Fb_{1x}a - Fb_{2x}b$$

These equations can be written in matrix form:

$$\begin{bmatrix} Fb_x \\ Mb_y \\ Fb_y \\ Mb_x \end{bmatrix} = T \begin{bmatrix} Fb_{1x} \\ Fb_{1y} \\ Fb_{2x} \\ Fb_{2y} \end{bmatrix}$$

Where T indicates the transfer matrix that it is equal to:

$$T = \begin{bmatrix} 1 & 0 & 1 & 0 \\ a & 0 & -b & 0 \\ 0 & 1 & 0 & 1 \\ 0 & -a & 0 & +b \end{bmatrix}$$

It is also possible to write these equations with complex notation to obtain the complex force vector f_b . Forces and moments of bearings are written as:

$$\begin{aligned} Fb &= Fb_x + iFb_y \\ Mb &= Mb_y - iMb_{x'} \end{aligned}$$

Written in matrix form these equations became:

$$f_b = \begin{Bmatrix} Fb \\ Mb \end{Bmatrix} = T \begin{Bmatrix} Fb_1 \\ Fb_2 \end{Bmatrix}$$

Where the transfer matrix in complex notation became:

$$T = \begin{bmatrix} 1 & 1 \\ a & -b \end{bmatrix}$$

The external points 1 and 2 shown in fig. 5.3 are related to the centre of the rotor through the same transfer matrix already described and follows these formulas:

$$\begin{cases} X_1 = X_C + \varphi_y a \\ Y_1 = Y_C - \varphi_{x'} a \\ X_2 = X_C - \varphi_y b \\ Y_2 = Y_C + \varphi_{x'} b \end{cases}$$

Introducing the two complex vectors:

$$\begin{cases} r_1 = X_1 + iY_1 \\ r_2 = X_2 + iY_2 \end{cases}$$

It is possible to write the relation between points 1 and 2 in a compact form introducing the transpose of the transfer matrix T :

$$\begin{Bmatrix} r_1 \\ r_2 \end{Bmatrix} = T^T \begin{Bmatrix} r \\ \phi \end{Bmatrix}$$

Where T indicates the transfer matrix and the vectors r and ϕ are the same already described in Chapter 3:

$$\begin{cases} r = X + iY \\ \phi = \varphi_y - i\varphi_{x'} \end{cases}$$

With the introduction of the vector f_b , which indicates the forces of the bearing acting on the point C of the shaft, it is possible to write 4 additional equations that link the displacement of the bearings to the one of the centres of mass. Bearings forces depend on the displacements and velocity of the inner rings with respect to the fixed reference frame and they are transmitted through the shaft with the same modulus. In fig. 5.4 the scheme of the end of the shaft is represented with the displacement along X coordinate. X_A indicates the coordinate of the centre of the inner ring of the bearing

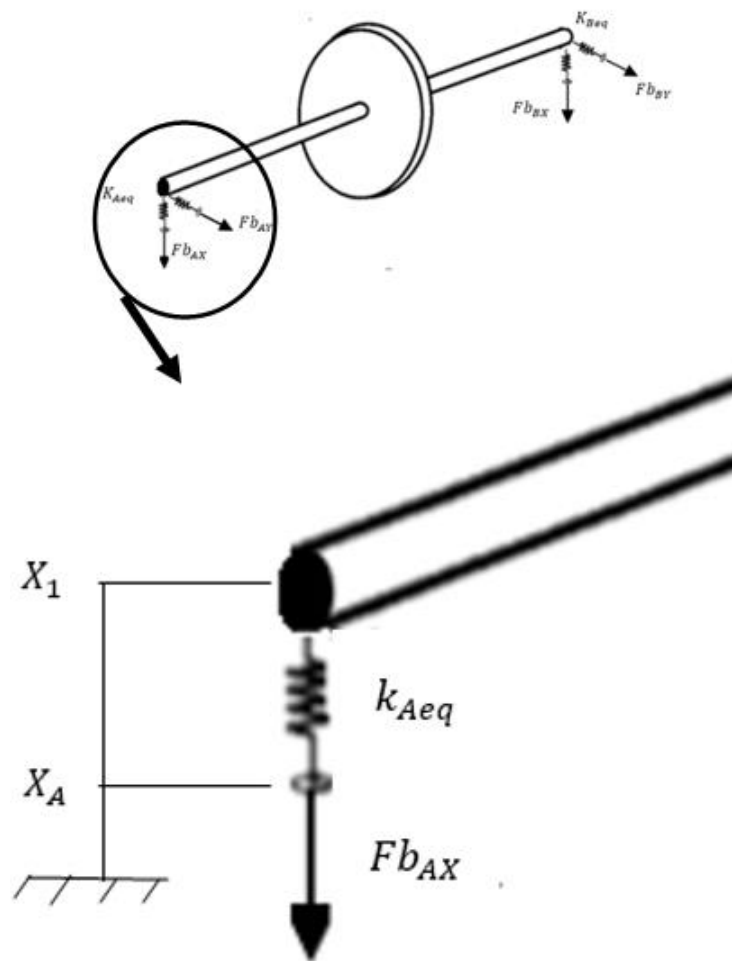


Figure 5.5: Scheme of the shaft end with the equivalent stiffness K_{Aeq} and the bearing force Fb_{AX} along X direction [68].

that is fixed to the shaft end. Displacement $(X_1 - X_A)$ instead indicates the deformation of the shaft represented as a spring with stiffness K_{Aeq} .

$$\begin{aligned} (X_1 - X_A) k_{Aeq} &= Fb_{AX} \\ (Y_1 - Y_A) k_{Aeq} &= Fb_{AY} \\ (X_2 - X_B) k_{Beq} &= Fb_{BX} \\ (Y_2 - Y_B) k_{Beq} &= Fb_{BY} \end{aligned}$$

Where values of forces Fb are obtained from displacement and velocity of points A and B, depending also on the configuration of the rolling elements inside the bearings as explained in Chapter 2.4. Values of k_{eq} are obtained with the following formula from matrix K :

$$\begin{cases} K_{Aeq} = K(2,2) \frac{1}{a^2 - b^2} - K(1,1) \frac{b^2}{a^2 - b^2} \\ K_{Beq} = K(2,2) \frac{1}{b^2 - a^2} - K(1,1) \frac{a^2}{b^2 - a^2} \end{cases}$$

The 4 equations that link the displacement of the bearings to the one of the centre of mass, written in matrix form and in complex coordinate with respect to the centre of mass, became:

$$K(q - q_b) = f_b$$

These equations, with the four equations of the rotor are so enough to solve the problem:

$$\begin{cases} M\ddot{q} + (C_n - i\Omega G)\dot{q} + K(q - q_b) = \Omega^2 f e^{i\Omega t} + f_w \\ K(q - q_b) = f_b \end{cases}$$

5.3 Implementation of the numerical model in MATLAB code

The equations of motions of the system are then solved through a MATLAB code. The code is divided in different scripts and functions that are recalled from the principal script “*Rotor_bearing_model.m*”. The code is divided in the following scripts and reported in fig. 5.6:

“Data” Script:

It contains all the inputs of the model. Regarding each bearing, the inputs are the same of the thesis of Giorio [2] and are summarized in tab. 5.1. It is introduced the possibility to change the initial configuration of the rolling elements inside the two bearings, as will be described in Chapter 6. In the script are present also the inputs containing the information about the geometry of the rotor (summarized in tab. 5.2) and the parameters to start the numerical integration, where the time step is chosen in order to allow each rolling bodies to lie inside the damaged area at least for one time step (summarized in tab. 5.3).

Inside this script it is possible to implement the size of defects present in the different component of the system:

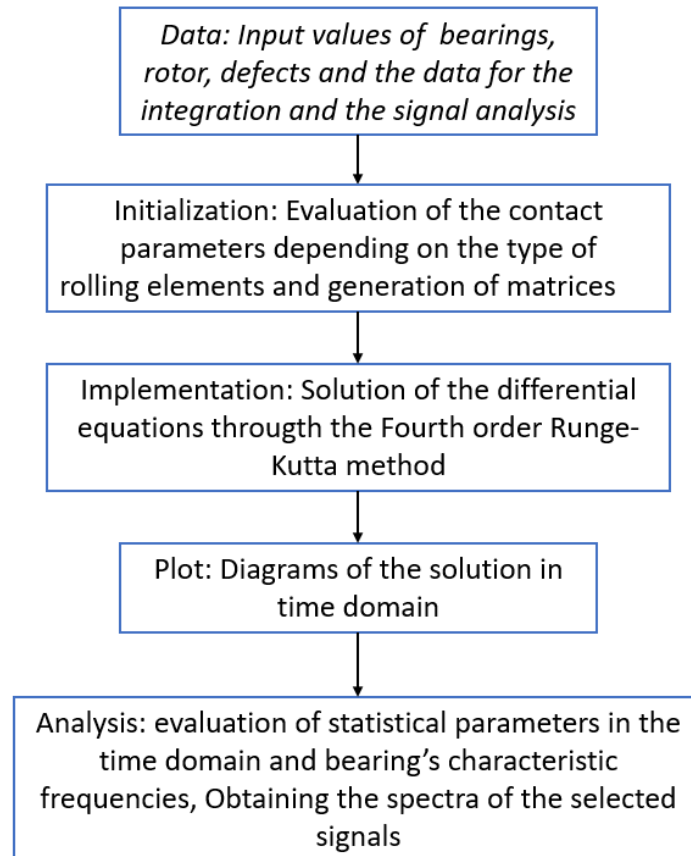


Figure 5.6: Flow chart of the implemented model.

- *Bearing rings*: both for bearing A and bearing B defects can be introduced in the model as a raw vector. The parameters that can be modified are the depth H , the initial angle θ_{init} , the form factor ff for each of the defects. There is than to choose the respective raceway.
- *Bearing rolling element*: both for bearing A and bearing B, defects can be introduced in the model as a raw vector. The parameters that can be modified are the depth H , the rolling element and the initial angle θ_{init} .
- *Rotor*: it is possible to choose the value of the eccentricity ε and the angle error χ of the rotor.

Table 5.1: Bearings Data

Bearings A and B

Inner ring diameter d_1	32.1 mm
Outer ring diameter D_2	54.67 mm
Bore diameter d	25 mm
Type of rolling element	Sphere
Length of rolling elements (if cylinder)	/
Ratio between race and sphere diameters	1.08
Diameter of rolling element d_r	11.274 mm
Number of rolling element N	7
Contact angle (assumed)	0°
Clearance g	22.57×10^{-3} mm
Poisson coeff. ν	0.3
Young modulus E	2×10^5 MPa
Linear stiffness K_{lin}	10^5 N/mm
Local damping coeff. c_b	$K_{lin} \times 10^{-5}$
Initial configuration bearing A	25.7 deg
Initial configuration bearing B	0 deg

Table 5.2: Rotor data

Rotor

Mass m	5×10^{-3} ton
Polar moment of inertia J_p	2×10^3 ton mm ²
transversal moment of inertia J_t	1.2×10^3 ton mm ²
Length L	0.8×10^3 mm
Distance between disc and left bearing	0.4×10^3 mm
Diameter D	25 mm
Viscous damping coeff. c_n	$200 \times 10^{-3} \frac{Ns}{mm}$
Rotor spin speed Ω	1000 RPM
Young modulus E	2×10^5
Weight force along X dir. W	100 N

Table 5.3: Integration input

Integration	
Initial time t_1	0 s
Final time t_2	2 s
Angular increment $d\theta$	0.05\0.1 deg
Cage rotation before stationary signal	1

Table 5.3: Initial conditions

Initial conditions			
$X_0 = g/2$	$\dot{X}_0 = 0$	$X_A = g/2$	$\dot{X}_A = 0$
$\varphi_{y_0} = 0$	$\dot{\varphi}_{y_0} = 0$	$Y_A = 0$	$\dot{Y}_A = 0$
$Y_0 = 0$	$\dot{Y}_0 = 0$	$X_B = g/2$	$\dot{X}_B = 0$
$\varphi_{x'_0} = 0$	$\dot{\varphi}_{x'_0} = 0$	$Y_B = 0$	$\dot{Y}_B = 0$

Furthermore, the input data for the analysis of the signal are the name of the variable to analyse, the maximum frequency to be represented in the frequency spectra, the width of the window for the envelope detector and the band of the band-pass filter.

Initializations scripts:

After the definition of data, the program evaluates the contact parameters depending on the type of rolling elements and define the lengths of the selected defects following the theory described in Chapter 2. From the input it generates all the matrices needed to write the equations of the system previously described: the mass matrix M , the damping matrix D , the stiffness matrix K , the gyroscopic matrix G and the unbalance force vector f_e .

“Implementation” script:

The integration of the differential equations of the rotor is performed through the fourth order Runge-Kutta method with respect to point C (fig. 5.6). The equations are written in matrix form adopting the complex notation already described. As a first step matrix A is defined as [71, 72]:

$$A = \begin{bmatrix} 0 & I \\ -M^{-1}K & -M^{-1}C \end{bmatrix}$$

Where I indicates the identity matrix.

Then the Z_0 vector is introduced defined as:

$$Z_0 = \begin{Bmatrix} q_{t_1} \\ \dot{q}_{t_1} \end{Bmatrix}$$

Where q_{t_1} is the complex vector already defined in Chapter 3 at the initial time t_1 .

The external forces evaluated at the initial time t_1 are concentrated in the P_0 vector that is defined as the sum of the external forces F_e , representing the weight force and the unbalance force in the model, and the nonlinear forces which in the model is represented by the bearing force f_b :

$$P_0(Z_0) = \begin{Bmatrix} 0 \\ M^{-1}(F_{E,0} + F_{b,0}(Z_0)) \end{Bmatrix}$$

Four coefficients K_i are obtained from these matrices, following the scheme in fig. 5.7 and are adopted to find the displacement and velocity vector q, \dot{q} at the next time step $t = t_1 + dt$. It is then possible to evaluate vector Z_1 at time $(t_1 + dt)$ repeating the cycle until the final time $t = t_2$ defined in the input.

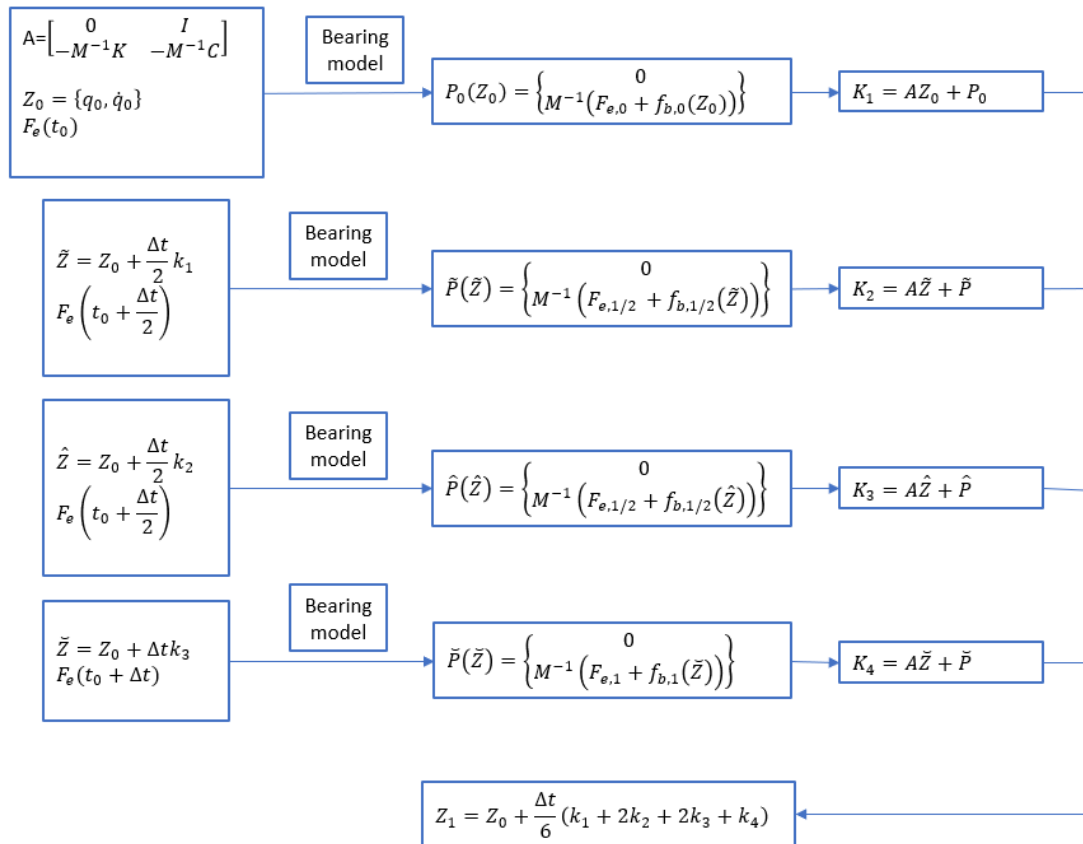


Figure 5.7: Fourth order Runge-Kutta method.

The bearing force F_b is obtained from the function called “*Bearing_force.m*” that presents as inputs the displacement and the velocity of the inner ring of a bearing and the time. The output is the force due to the deformation of the rolling elements, along X and Y directions. The values of the displacements of points A and B can be found iteratively following the flowchart in fig. 5.8: knowing the coordinate of point C, position 1 and 2 are obtained through the transfer matrix T . Then the value of the bearing force is obtained through the “*fsolve*” MATLAB function which numerically solve the following equations:

$$(X_1 - X_A) k_{Aeq} - Fb_{AX} = 0$$

$$(Y_1 - Y_A) k_{Aeq} - Fb_{AY} = 0$$

$$(X_2 - X_B) k_{Beq} - Fb_{BX} = 0$$

$$(Y_2 - Y_B) k_{Beq} - Fb_{BY} = 0$$

The “*Bearing_force*” function evaluate the reaction forces of bearings due to the deformation and velocity deformation of the rolling elements. It considers the presence of defects inside bearings which can be defined in the “*Data*” script. It follows the flow chart in fig. 5.9.

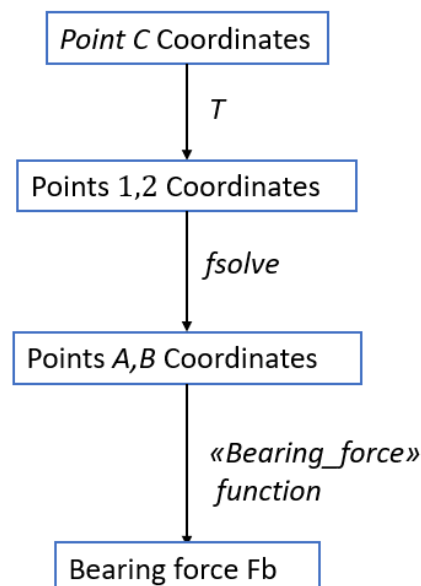


Figure 5.8: Evaluation of the Bearing force from the coordinate of the centre C.

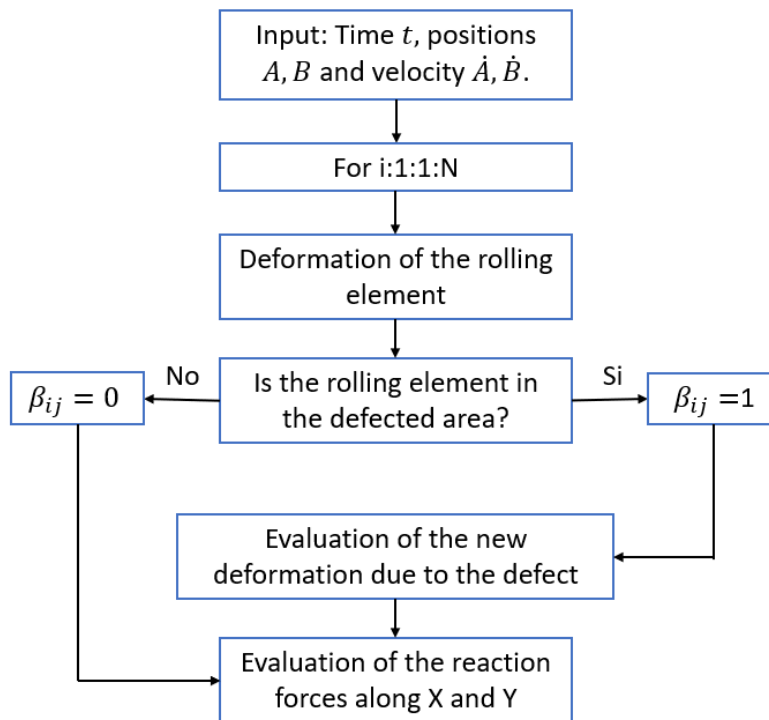


Figure 5.9: Bearing function of the code.

“Plot” script:

The initial transient equal to a multiple of the cage rotation, which can be chosen by the user as input data for the analysis is eliminated. Then the results in time domain are plotted: the displacement, trajectory, velocity, and acceleration of the rotor in the centre C and at its ends A, B.

“Analysis” script:

The script that performs the signal analysis calculates the statistical parameters in the domain of time useful for the analysis, evaluates the characteristic frequencies of the bearings, obtains the spectrum of the amplitude of the raw vibration signal and the spectrum in frequency of the amplitude of the envelope of the vibration signal chosen in the “Data” script for the analysis.

6. Numerical simulation and analysis of the system

The numerical simulations of the model are performed in the following cases:

- Model with healthy bearings.
- Model with a bearing damaged in the internal ring.
- Model with a bearing damaged in the external ring.
- Model with damaged rolling element of the bearing.
- Model with eccentricity on the rotor.

The considered bearings are radial ball bearings SKF 6305, with the input data selected from the catalogue [17]. The data of the rotor are the same described in Chapter 5 as all the other input of the simulations. The output of the code gives the displacement, velocity, and acceleration of the shaft in point C (translations and rotations) and of the external points of the shaft A, B (translations). The values of acceleration are then analysed after a complete rotation of the bearing cage, to eliminate the initial transient. The output of the analysis are the frequency spectrum, the envelope, and the frequency spectrum of the envelope of the vibration signal, and it is performed for the acceleration signal of all the three points A, B, C of the rotor because the acquisition of the signals in real machines is usually performed through accelerometer.

6.1 Healthy bearings

Firstly, the rotor is considered rigid, imposing a high value of the young's modulus E . The rotor's eccentricity is considered equal to 0 and the centre of mass is in the middle of the shaft length. Furthermore, balls position of both the bearings, at the initial condition are considered equal. This condition is not general but can be compared to a single bearing model that appears in many works in literature. Results in term of acceleration of centre of mass C along X and Y directions are shown in fig. 6.1.

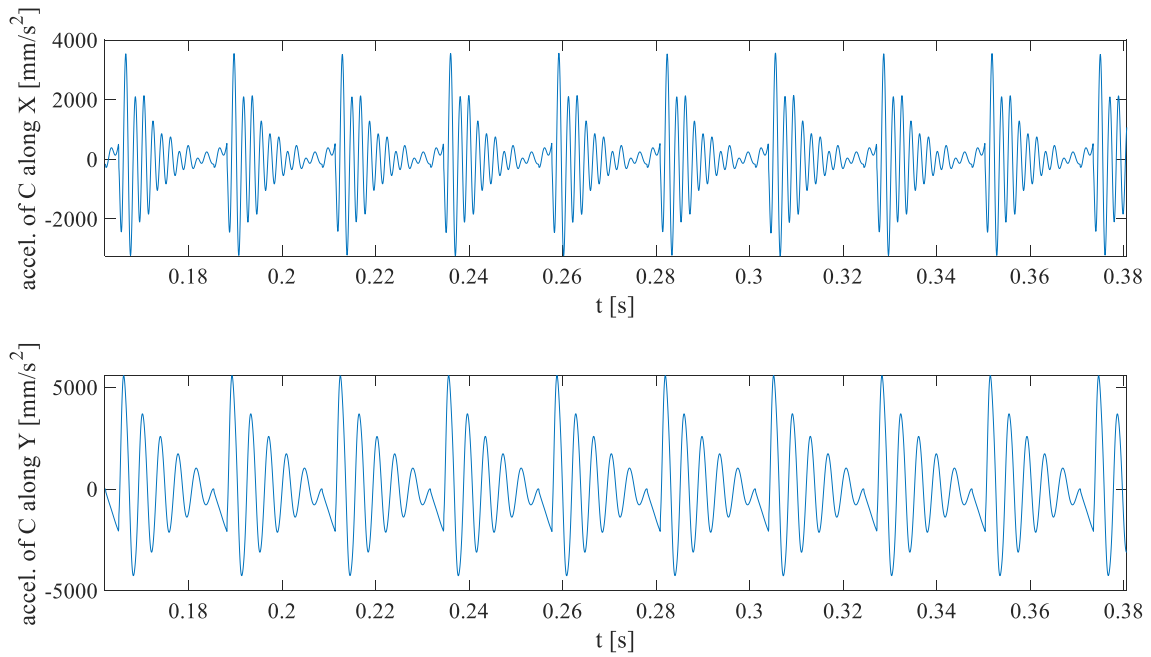


Figure 6.1: Acceleration of point C along X and Y direction

Accelerations of points A and B are the same of point C both in X and Y directions while the shaft never rotates along ϕ_x and ϕ_y . It is clearly visible in fig. 6.1 that in case of non-defective bearing it is in any case present one vibration due to the periodic variation of the contact stiffness between tracks and rolling elements. This phenomenon is called Varying Compliance Vibration and it is confirmed also in other works in literature [73]. In the X direction, the acceleration signal presents a peak value equal to $PV = 1857 \frac{mm}{s^2}$ that is quite near to $RMS = 604 \frac{mm}{s^2}$ confirming the integrity of the bearing. The two signals (acceleration on X and Y) are comparable in terms of range of amplitude and therefore can be used to obtain the survey features to be used. The one in the direction of the applied load (X direction) is used as reference vibration signal:

with the application of the FFT to the raw signal it is obtained the frequency spectrum of the acceleration of C along X coordinate fig. 6.2.

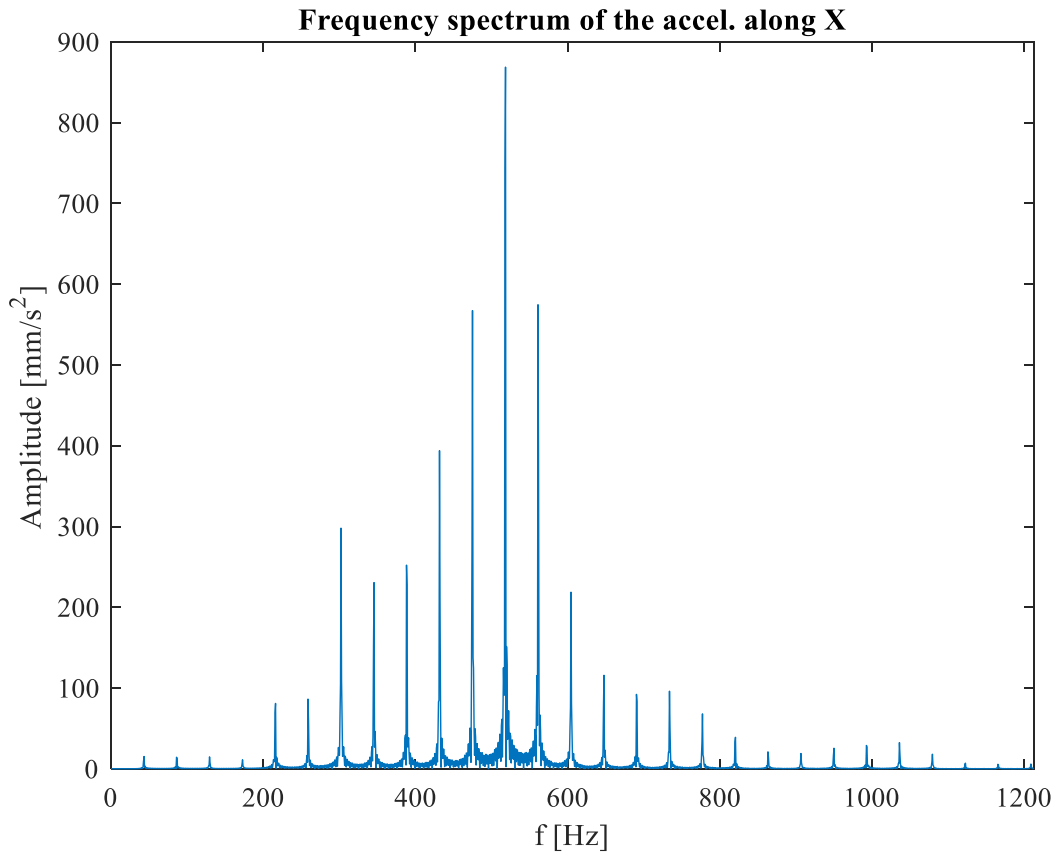


Figure 6.2: Frequency spectrum of the acceleration of C along X coordinate

With this type of frequency analysis harmonics are excited at higher frequencies with respect to the characteristic frequencies of the bearing, which makes this type of display not particularly suitable for recognition of defects within rolling bearings. It is so adopted the acceleration envelope analysis in direction X whose proceedings were presented in Chapter 3. In fig 6.3 it is shown the acceleration signal in X direction after being filtered by applying a band-pass filter with:

$$[f_{min}, f_{max}] = [500, 10000] \text{ Hz}$$

according to the indications reported in the literature in [49] for the subsequent extraction of the signal envelope.

The envelope of the signal is shown in red, obtained by means of the Hilbert transform, following the application of a generated FIR filter starting from an ideal “brick-wall” filter through a Kaiser window of amplitude 200 Hz and shape parameter $\beta=8$.

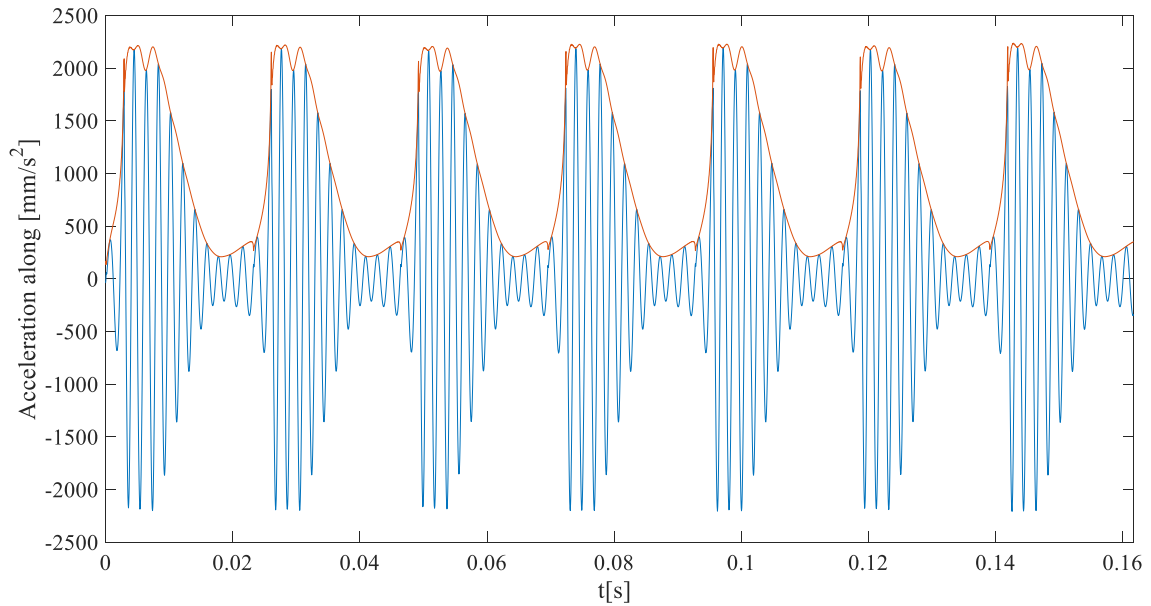


Figure 6.3: Acceleration of C filtered by band-pass filter in (blue) and envelop in (red).

The frequency spectrum of the envelope of the vibration signal, fig. 6.4, is useful for monitoring through the technique of the *EA*, in which the average value of the signal is subtracted to eliminate the amplitude of oscillation corresponding to a zero frequency. In fig. 6.4 is shown how the peak of greater amplitude correspond to the frequency of 43.3676 Hz. This value is quite equal to the $BPFO = 43,1749$ Hz that indicates the frequency at which the rolling elements go through the loading area. It differs of 0.1157 Hz that is a value lower than the resolution of the frequency spectrum used: 0.939 Hz.

This means that the peak lies within the uncertainty interval. The harmonics of higher order are also present in the results with smaller amplitude. In the following chapters signals are analysed with the same procedure and only the frequency spectrum of the envelope of the vibration signal is shown because it gives much information about the system condition.

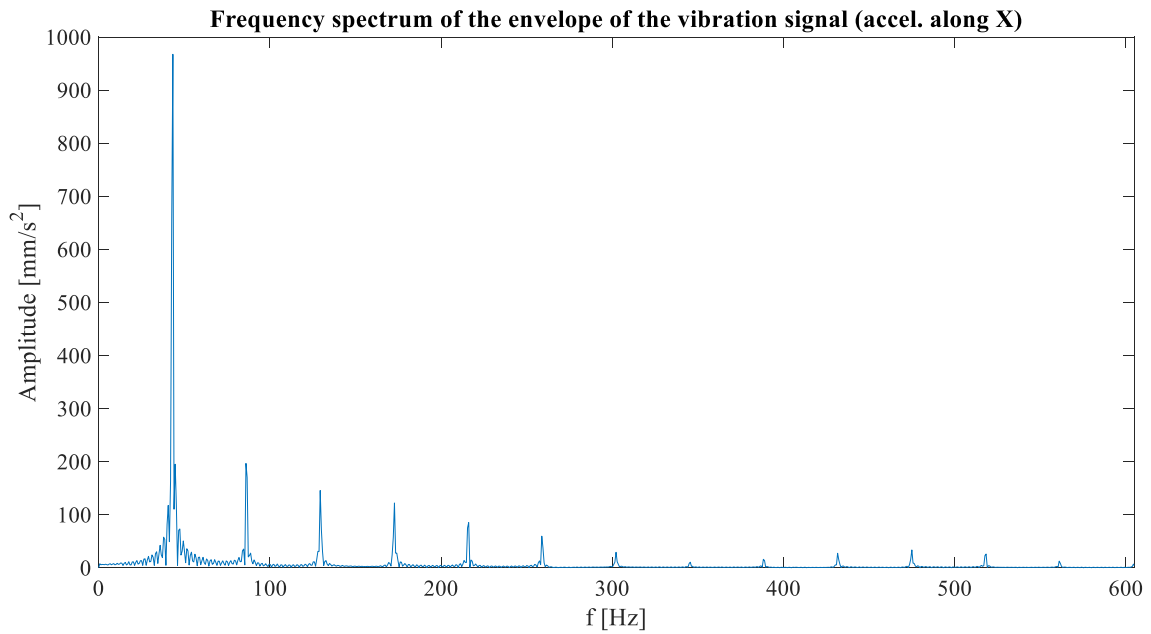


Figure 6.4: Frequency spectrum of the envelope of the vibration signal (accel. along X).

6.1.1 Case with rigid shaft

To produce a more realistic simulation, the initial positions of balls, in the two bearings are considered different as in fig. 6.5.

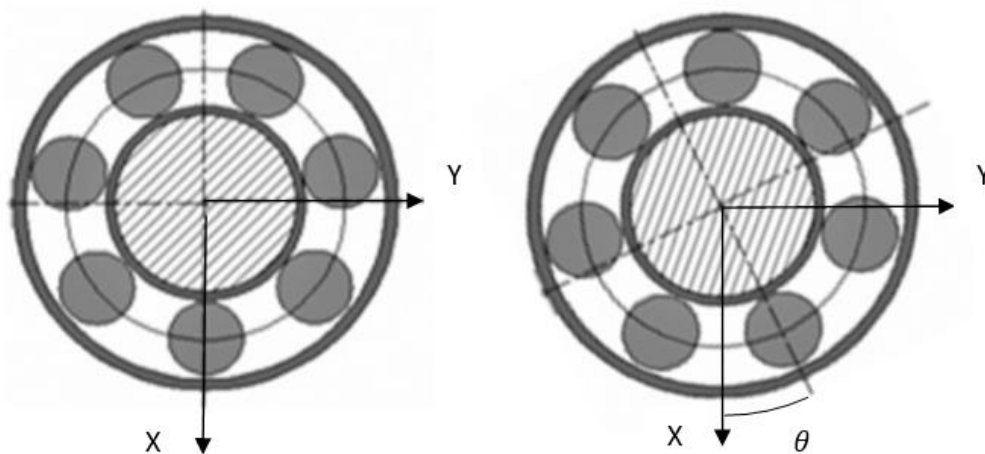


Figure 6.5: Initial configuration of a bearing with $\theta = 0$ (left) and with variable θ (right) [49].

In particular, in the following simulations, at time $t = 0$ in bearing B at the initial time there is always a ball at the angle $\theta = 0$ from the vertical position as in fig. 6.5 (left). The initial position of balls in bearing A is chosen in different configurations fig. 6.5 (right). The angle $\Delta\theta$ between two balls of the selected bearings is obtained as:

$$\Delta\theta = \frac{360^\circ}{7} = 51.4^\circ$$

Where 7 is the number of balls in the bearing.

The considered initial angles θ_{init} for bearing A are $\theta_{init,A} = \frac{\Delta\theta}{4} = 12.85 \text{ deg}$ and $\theta_{init,A} = \frac{\Delta\theta}{2} = 25.7 \text{ deg}$. The resultant signal of the acceleration of the three points A , B and C have the same order of magnitude in both cases, so it is reported only the signal of C :

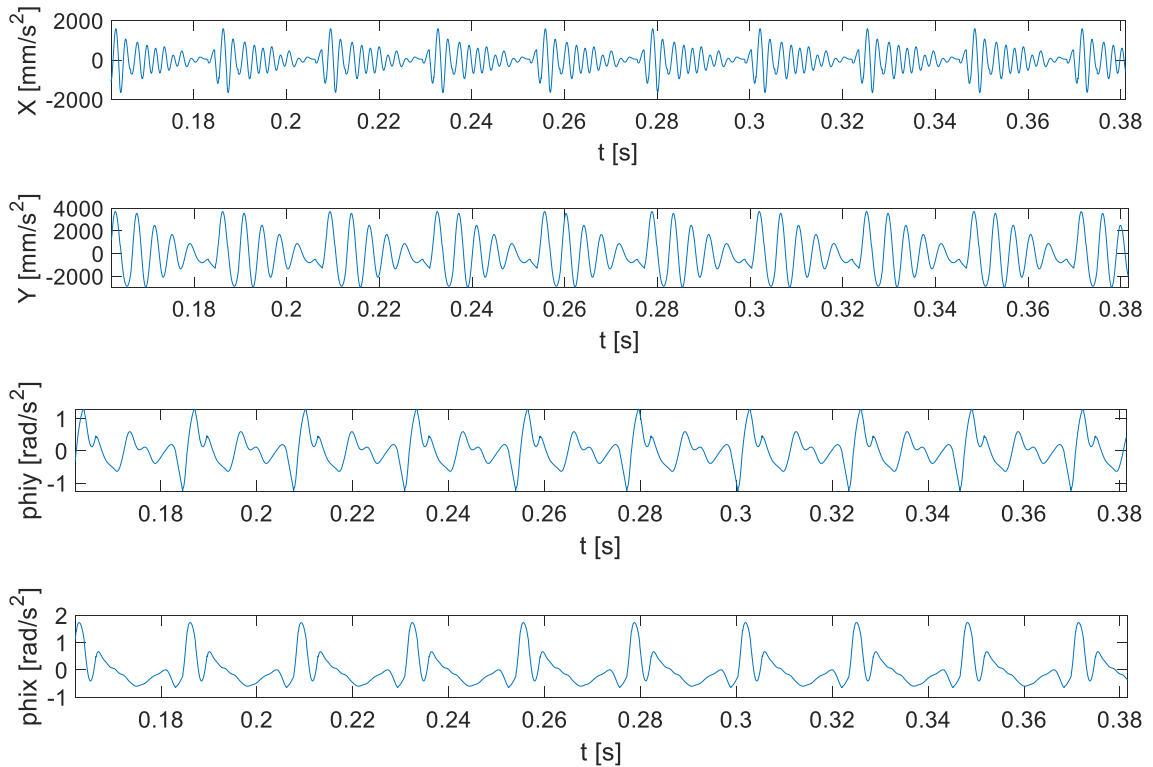


Figure 6.6: Acceleration of point C along the four coordinates X , Y , $\text{Phi}Y$ and $\text{Phi}X$ with initial angle equal to $\theta_{init,A} = \frac{\Delta\theta}{4} = 12.85 \text{ deg}$.

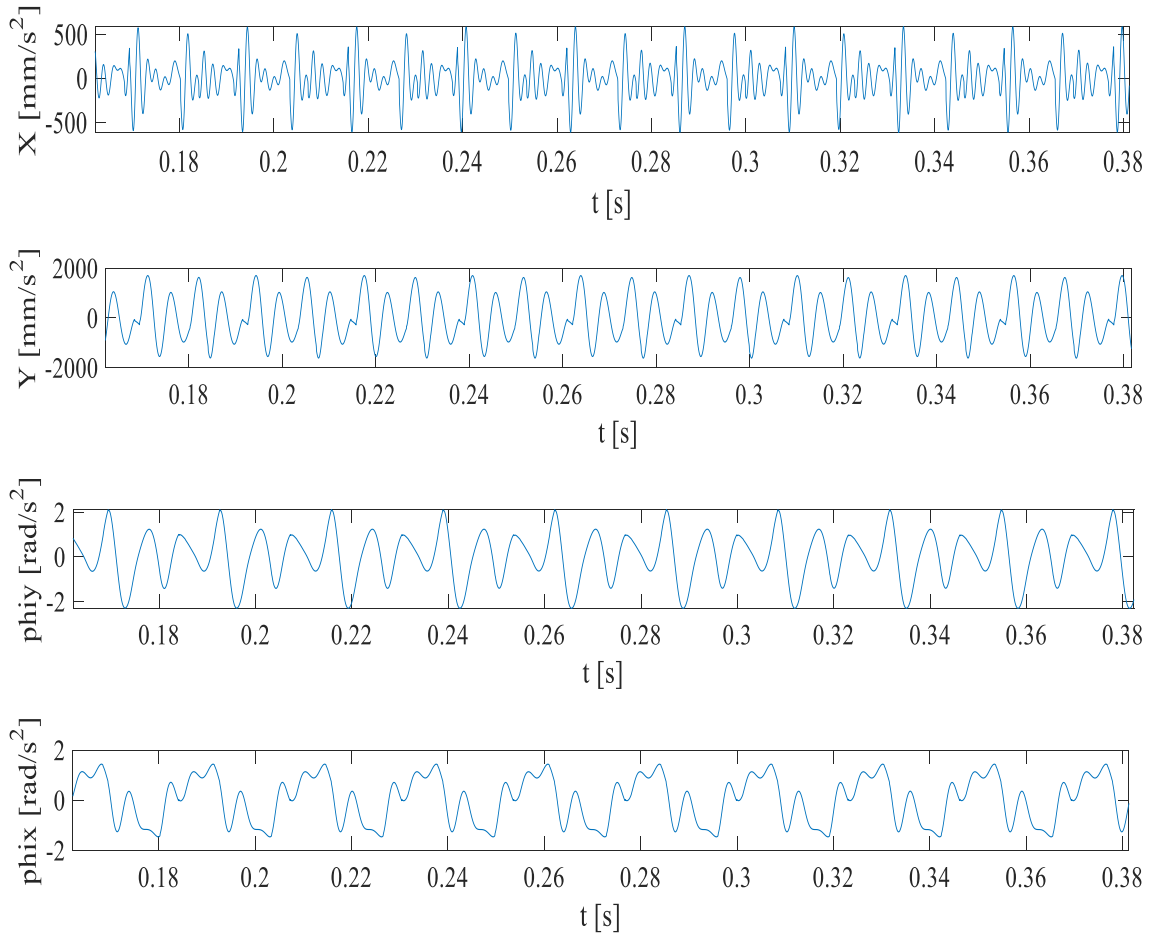


Figure 6.7: Acceleration of point C along the four coordinates X , Y , $\text{Phi}Y$ and $\text{Phi}X$ with initial angle equal to $\theta_{init,A} = 25.7 \text{ deg}$.

In fig. 6.6 and fig. 6.7 it is also shown the value of angular acceleration that in the condition of $\theta_{init,A} = 0$ is equal to 0, while with $\theta_{init,A} = 12.85 \text{ deg}$ and $\theta_{init,A} = 25.7 \text{ deg}$ increases. The Peak Value of the acceleration signal along X , instead decreases from $3403.9 \frac{\text{mm}}{\text{s}^2}$ with $\theta_{init,A} = 0$, to $1856.5 \frac{\text{mm}}{\text{s}^2}$ with $\theta_{init,A} = 12.85 \text{ deg}$ until $648.9111 \frac{\text{mm}}{\text{s}^2}$ with $\theta_{init,A} = 25.7 \text{ deg}$.

In fig 6.8 is represented the frequency spectrum of the envelope of the vibration signal of the acceleration of point C along X , obtained with the same procedure of Chapter 5.1. It is visible that the peak of greater amplitude corresponds to frequencies of $2BPFO = 86,3498 \text{ Hz}$. The other peaks have lower amplitude values and are at frequencies multiple of $BPFO$. Furthermore, the amplitude of each peak is decreased from the case of fig. 6.4. When the rotor is supported by the two bearings with the same balls position, their signal is equal, with the same sign and is summed up obtaining an equivalent signal like that of a single bearing already studied in work [2]. present one vibration due to the periodic variation of the contact stiffness between tracks and rolling elements. These peaks demonstrate the presence of the so-called

Varying Compliance Vibration that is a vibration due to the periodic variation of the contact stiffness between races and rolling elements which is present also in the case of a healthy bearing. The same considerations also apply in the case with the frequency spectrum of the envelope of the vibration signal of points A and B.

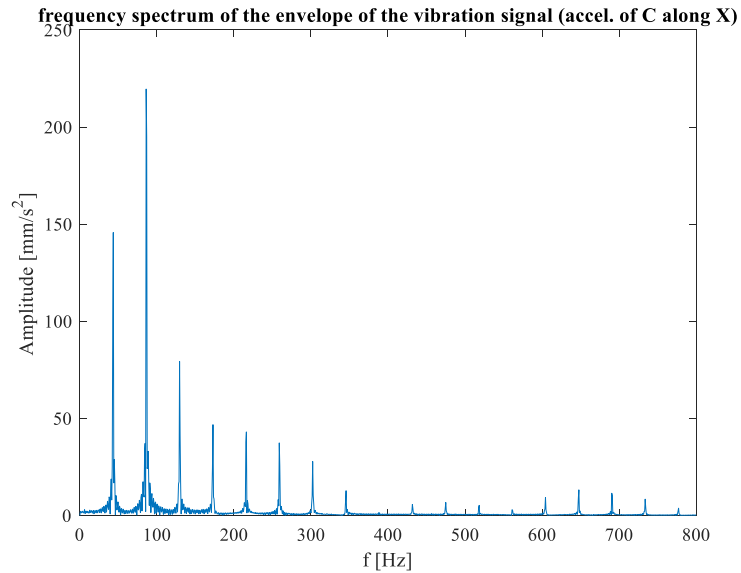


Figure 6.8: Frequency spectrum of the envelope of the vibration signal of the acceleration of point C along X with $\theta_{init,A} = 12.85 \text{ deg}$

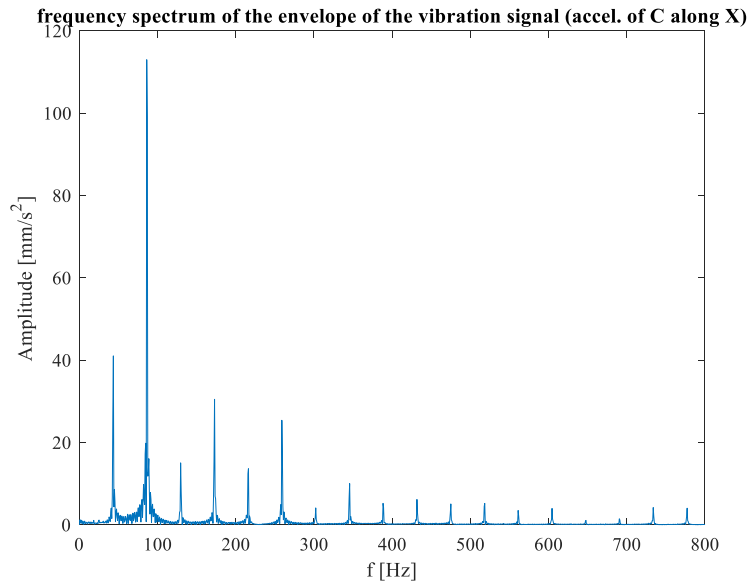


Figure 6.9: Frequency spectrum of the envelope of the vibration signal of the acceleration of point C along X with $\theta_{init,A} = 25.7 \text{ deg}$

6.1.2 Case with elastic shaft.

The stiffness of the shaft is now considered assuming a young modulus equal to $E = 2^5 \text{ MPa}$. To obtain a more realistic simulation the balls position in the two bearings differs of $\frac{\Delta\theta}{2} = 25.7 \text{ deg}$. The rotor is still considered balanced with null eccentricity and symmetric with respect to the two bearings. acceleration's signal of points A, B and C are analysed along X direction because it gives more information about the presence of defects. In fig. 6.10 are shown the result of the three accelerations and it is possible to observe that with respect to the case with the rigid shaft, signal of point C has lower amplitude with a lower Peak Value $PV = 291.4 \frac{\text{mm}}{\text{s}^2}$ while points A and B present higher peaks of accelerations. In this configuration the shaft act as a spring that attenuate vibrations coming from bearings as it can be observed also looking at the trajectory, without the initial transient, of the three points in fig 6.11.

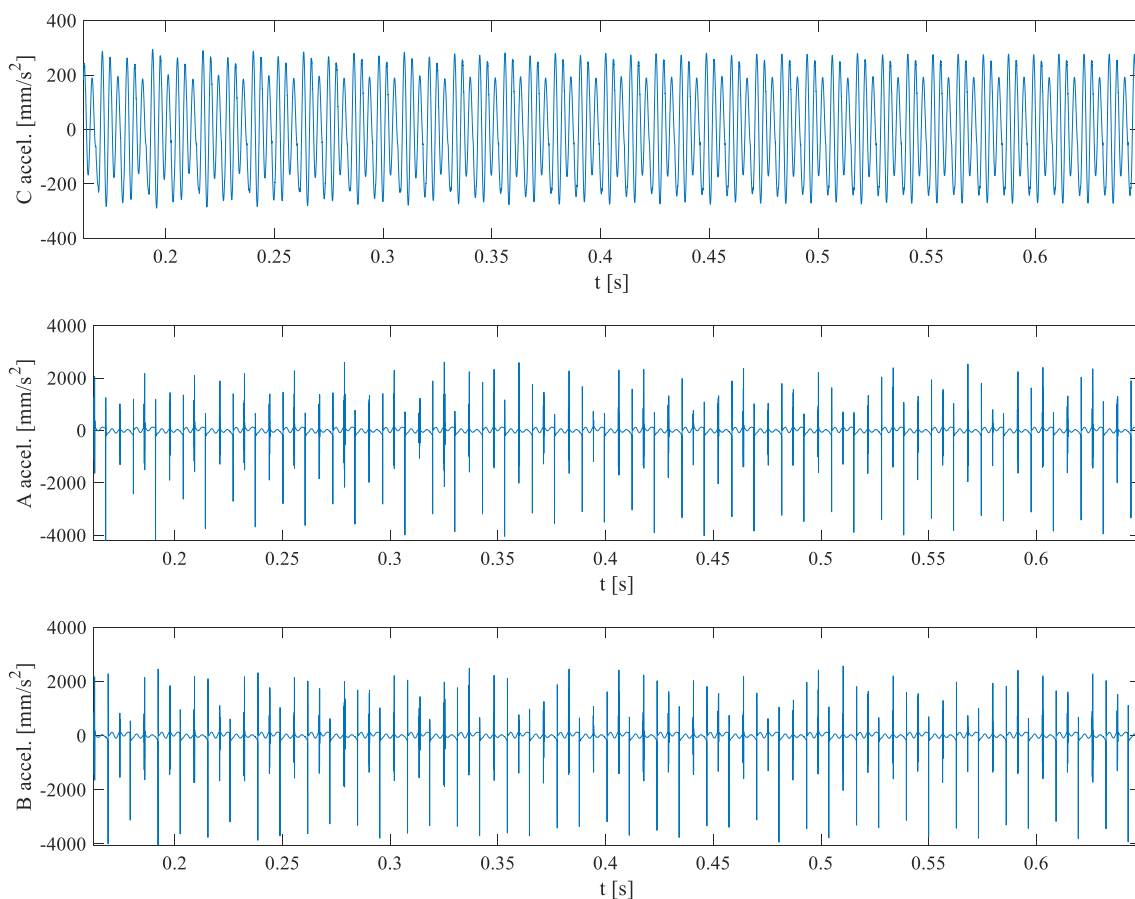


Figure 6.10: Acceleration of points C, A and B along X direction of an elastic shaft with young modulus $E = 2^5 \text{ MPa}$.

6. Numerical simulation and analysis of the system

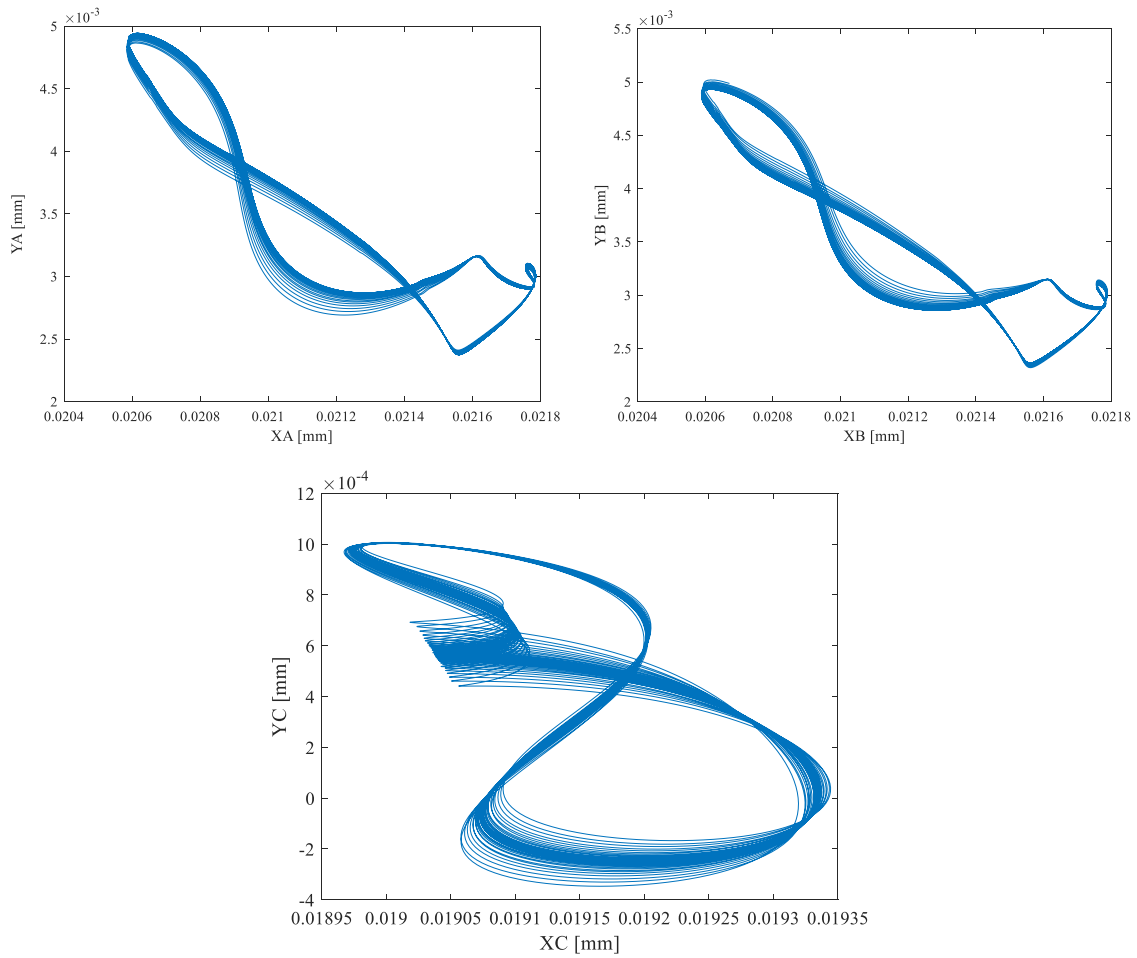


Figure 6.11: Trajectory of points A, B and C of an elastic shaft with young modulus $E = 2^5 \text{ MPa}$.

Also, from the frequency spectrum of the envelope of the vibration signals fig. 6.12 it is observable that the amplitude of the peaks with respect to point C are lower than point B. The spectrum of point A is not reported because it has a behaviour like point B. Furthermore, peaks in both signals are in correspondence to frequencies values that are multiple of $BPFO = 43.17\text{Hz}$ equal to $n \times BPFO$ (with $n = 1, 2, \dots$) confirming the presence of Varying Compliance Vibration as in the case of rigid shaft.

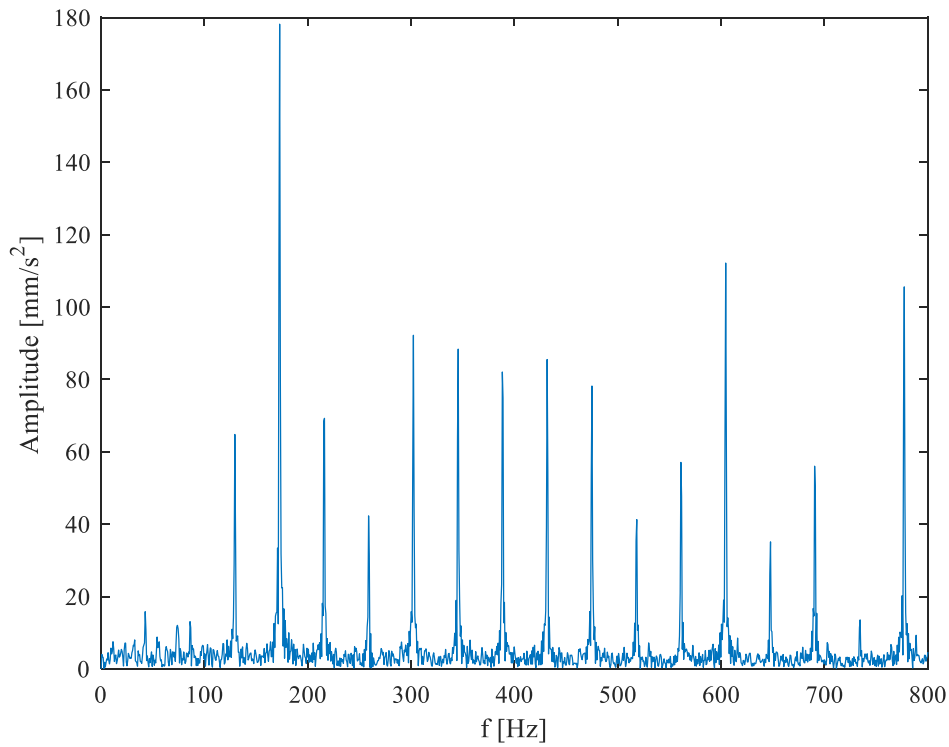
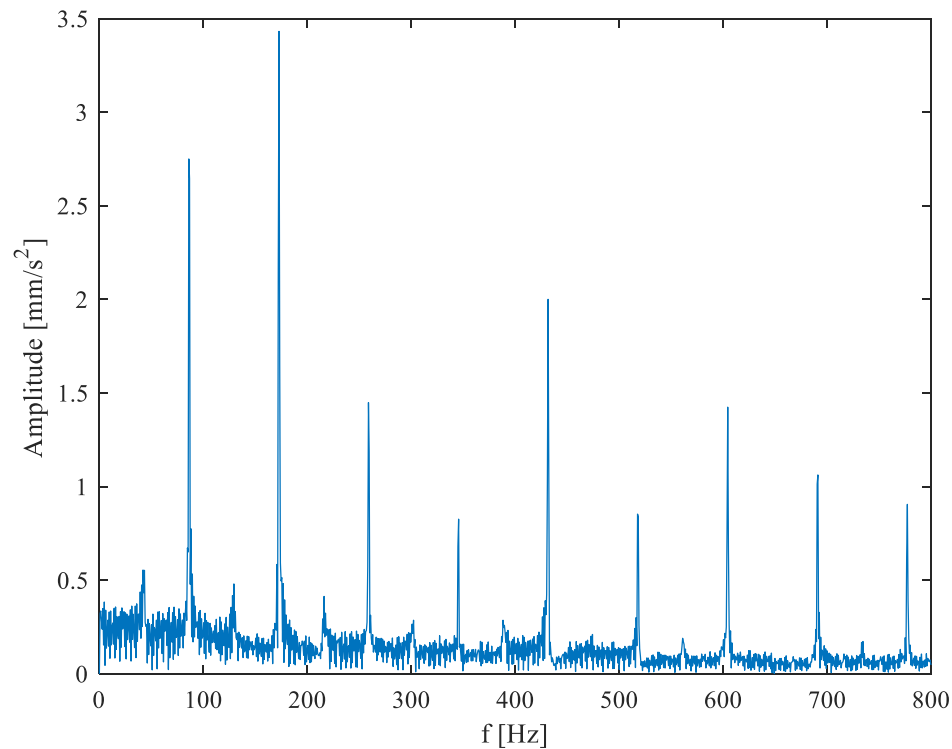
Frequency spectrum of the envelope of the vibration signal on signal (accel. B along X)**Frequency spectrum of the envelope of the vibration signal on signal (accel. C along X)**

Figure 6.12: Frequency spectra of the envelope of the vibration signals of the acceleration of points B and C along X of an elastic shaft with young modulus $E = 2^5 \text{ MPa}$.

6.2 Bearing damaged in the external ring.

Bearing A is now considered with a localized defect on the outer race, of maximum depth $H = 0.1 \text{ mm}$ with the form factor $ff=1$ and positioned at $\theta_{init} = 0^\circ$. The position of the balls in the two bearings is always considered different of the angle $\frac{\Delta\theta}{2} = 25.7 \text{ deg}$ and are analysed the case of rigid and elastic shaft.

6.2.1 Case with rigid shaft.

In fig 6.13 is shown the acceleration signal with the defect located in bearing A in the case of a rigid rotor:

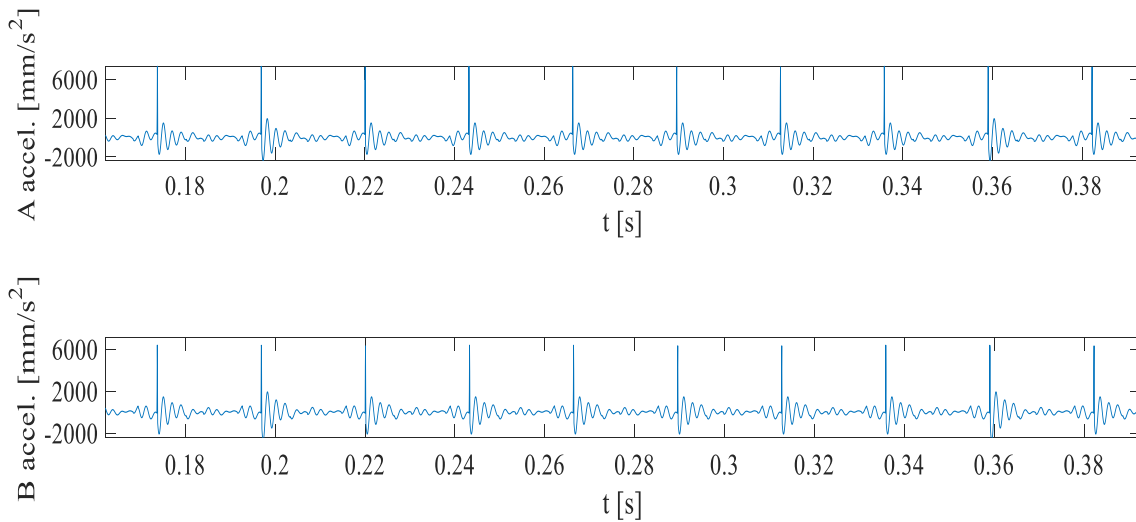


Figure 6.13: Acceleration of point A and B along X direction with a defect on the external ring. (Rotor length $L = 0.2 \times 10^3 \text{ mm}$)

It is possible to observe that the peaks of the acceleration signal are a bit lower in bearing B if the defect is on the outer ring of bearing A. To underline this behaviour, it is decided to increase the length of the rotor to $L = 0.8 \times 10^3 \text{ mm}$.

Compared to the case of a healthy bearing, the acceleration along Y is practically unchanged. Along X direction instead it is possible to observe the periodic peaks caused by the defect (fig. 6.14). The peak value is higher on bearing A with the value $PV_A = 13360 \frac{\text{mm}}{\text{s}^2}$ that is about 10 times higher than the *RMS value* $= 1437.1 \frac{\text{mm}}{\text{s}}$ indicating an impulsive nature of the time-domain signal at work the presence of the localized defect. It decreases moving away from it: $PV_C = 7.0201 \times 10^3 \frac{\text{mm}}{\text{s}^2}$ and $PV_B = 2.0937 \times 10^3 \frac{\text{mm}}{\text{s}^2}$. The defect localized in bearing A induce a shock in the

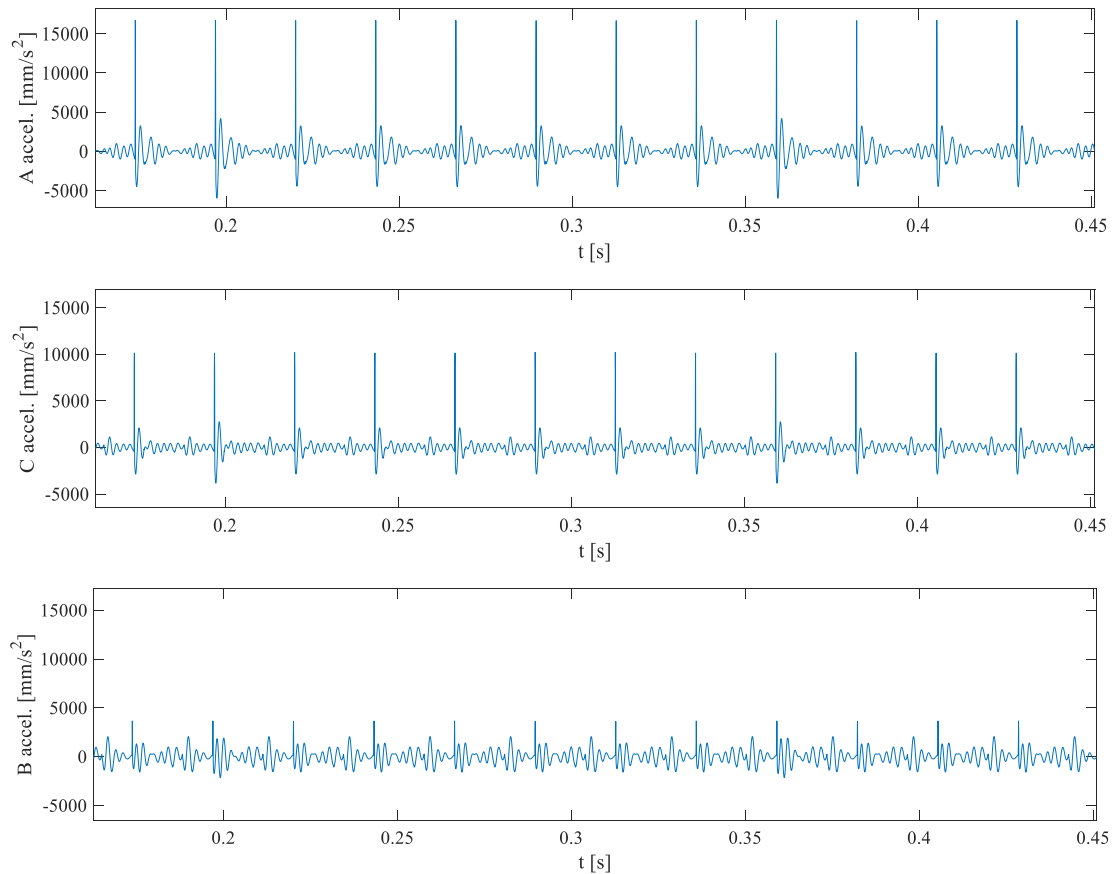
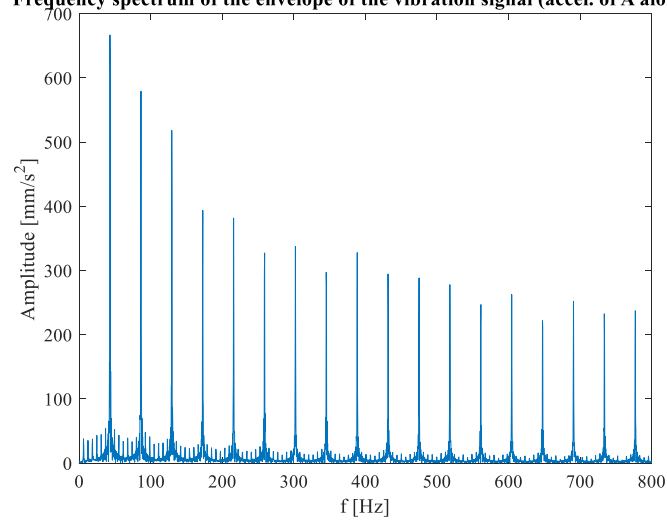


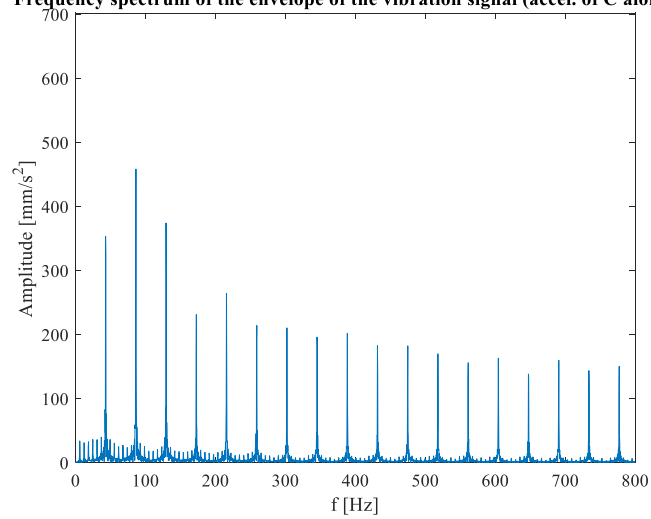
Figure 6.14: Acceleration of point A, C and B along X direction with a defect on the external ring. (Rotor length $L = 0.8 \times 10^3 mm$)

system that moves from it to the other end of the shaft decreasing its intensity. This behaviour can be shown also from the spectrum of the envelope of the vibration signal (fig 6.15). Peaks on point A have higher amplitude than on points C and B confirming the presence of a defect on the bearing in that position. The effect is however visible on the spectra of all the three points considering that the peaks present amplitude evidently higher than the case of a system with both healthy bearings. A localized defect in the outer race of the bearing generates pulses in the acceleration's signals with a frequency equal to the passing frequency of rolling elements on the outer race. The excited frequencies are multiple of the BPF0=43.1749 Hz and the amplitude values are higher than the case of not defected bearing on chapter 6.1.2. Also, the amplitude of the successive harmonics is increased, and the amplitude decay is delayed, indicating a greater impulsive nature of the signal in the time domain.

Frequency spectrum of the envelope of the vibration signal (accel. of A along X)



Frequency spectrum of the envelope of the vibration signal (accel. of C along X)



Frequency spectrum of the envelope of the vibration signal (accel. of B along X)

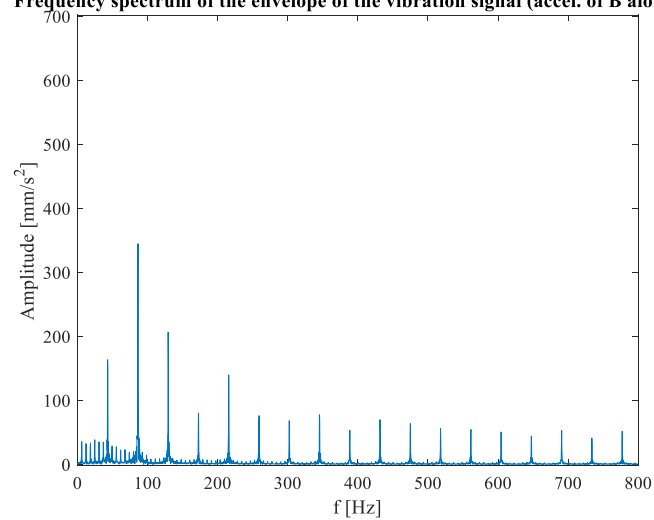


Figure 6.15: Frequency spectra of the envelope of the vibration signals of the acceleration of point A, C and B along X direction with a defect on the external ring of bearing A.

6.1.2 Case with elastic shaft

The stiffness of the shaft is now considered assuming a young modulus equal to $E = 2^5$ MPa. To obtain a more realistic simulation the balls position in the two bearings differs of $\frac{\Delta\theta}{2} = 25.7$ deg. The rotor is still considered balanced with null eccentricity and symmetric with respect to the two bearings. Acceleration's signal of points A, B and C are analysed along X direction because it gives more information about the presence of defects. In fig. 6.16 are shown the three acceleration signals of points A, C and B and it is possible to observe that peaks on bearing A, which defected, have a greater amplitude than the case of healthy bearing. As in the case of rigid rotor bearing A induce a shock in the system that propagate until bearing B each time that a sphere enters in the defected area. Compared to the rigid rotor bearing B is hardly affected by each shock in this configuration because the elasticity of the shaft absorbs the impulse generated by the defect and decrease its effect on the other end of the rotor B. So, to also underline the effect on bearing B the length of the shaft is reduced to $L = 0.1 \times 10^3$ mm as in fig. 6.17 and it is possible to observe that decreasing the length of the rotor, despite the elasticity of the shaft, the effect of the defect is visible also on point B. In this configuration it is evaluated the frequency spectrum of the envelope of the vibration signal for each of the three points in fig. 6.18. It is possible to observe peaks at the same frequencies of the case with rigid shaft equal to $n \times BPF0$ (with $n=1, 2, \dots$) with decreasing amplitude from point A to point C until point B.

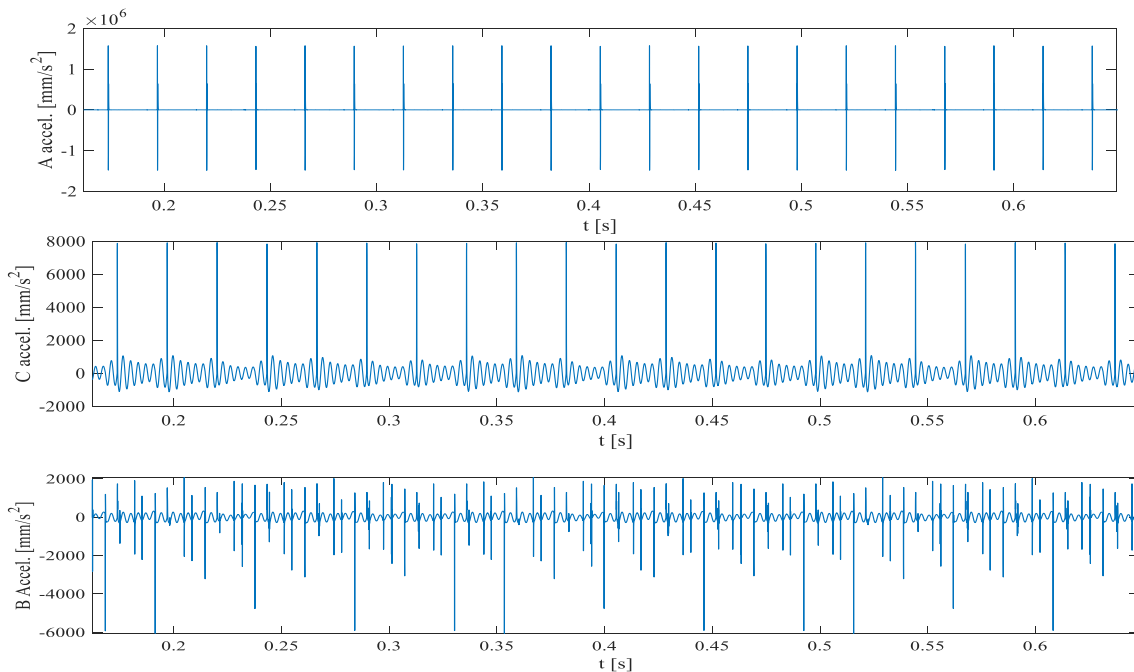


Figure 6.16: Acceleration of point A, C and B along X direction with a defect on the external ring. (Rotor length $L = 0.2 \times 10^3$ mm).

6. Numerical simulation and analysis of the system

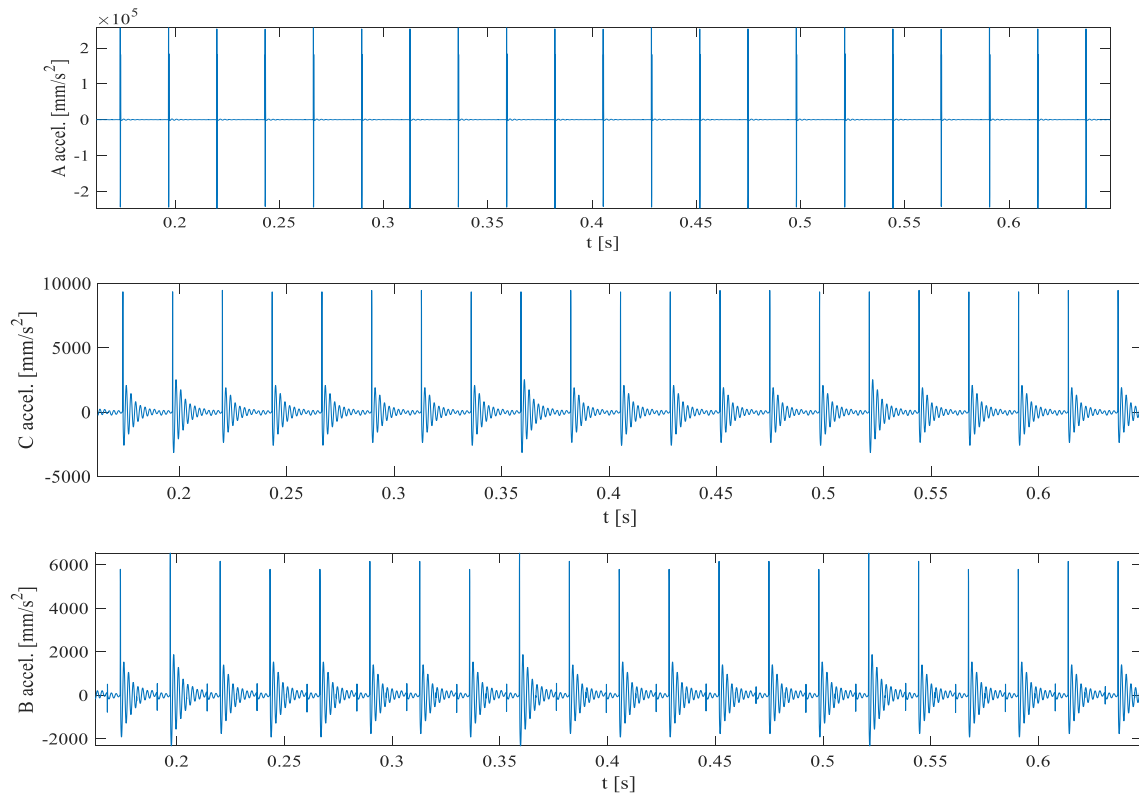
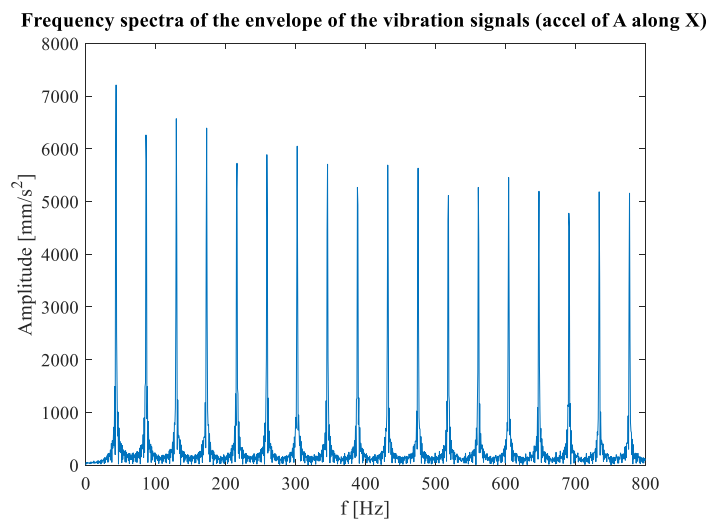
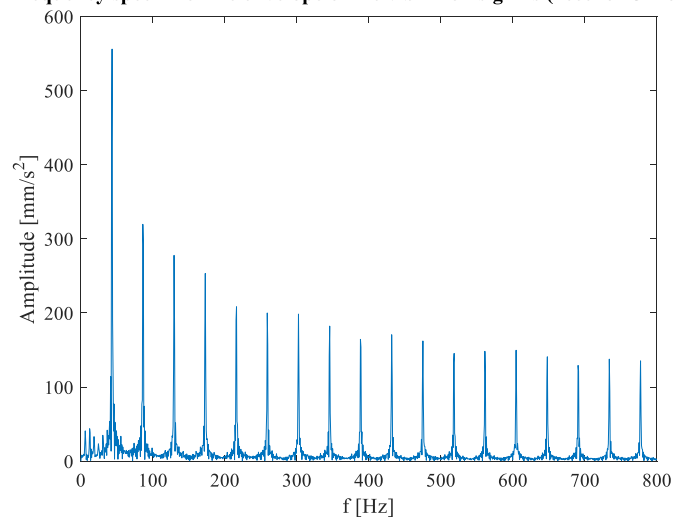


Figure 6.17: Acceleration of points A, C and B along X direction with a defect on the outer ring. (Rotor length $L = 0.1 \times 10^3 \text{ mm}$).



Frequency spectra of the envelope of the vibration signals (accel of C along X)



Frequency spectra of the envelope of the vibration signals (accel of B along X)

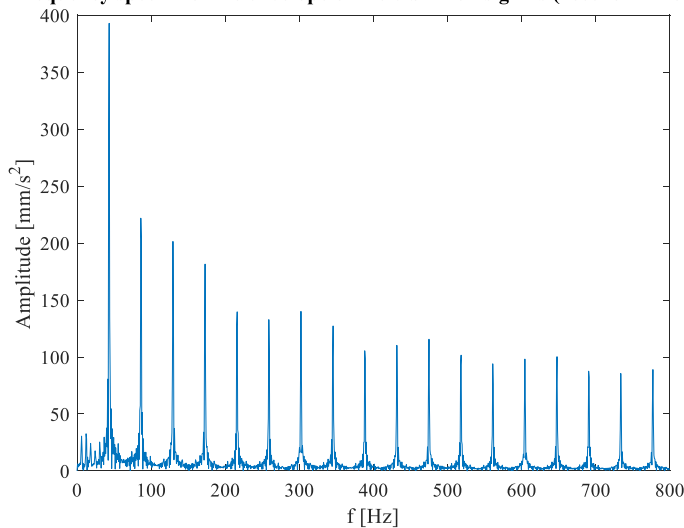


Figure 6.18: Frequency spectra of the envelope of the vibration signals of the acceleration of points A, C and B along X direction with a defect on the outer ring of bearing A.

6.3 Bearing damaged in the inner ring

Bearing A is now considered with a localized defect on the inner race, of maximum depth $H = 0.1$ mm with the form factor $ff=1$ and positioned at $\theta_{init} = 0^\circ$. The position of the balls in the two bearings is always considered different of the angle $\frac{\Delta\theta}{2} = 25.7$ deg and are analysed the case of rigid and elastic shaft.

6.3.1 Case with rigid shaft

In fig 6.19 is shown the acceleration signal with the defect located in bearing A in the case of a rigid rotor considering the length of the rotor equal to $L = 0.8 \times 10^3$ mm to underline the differences between the results.

Compared to the case of a healthy bearing, the acceleration along Y doesn't change relevantly. The amplitude of the acceleration peaks along the X direction, is modulated in amplitude because the inner race rotates integrally with the shaft, and consequently the defect-rolling element interactions occur in different positions with respect to the load area. Peak value is higher on bearing A with the value $PV_A = 13627 \frac{\text{mm}}{\text{s}^2}$. It decreases moving away from it: $PV_C = 8425.6 \frac{\text{mm}}{\text{s}^2}$ and $PV_B = 4065.6 \frac{\text{mm}}{\text{s}^2}$. The defect localized in bearing A induce a shock in the system that move from it to the other end of the shaft decreasing its intensity. This can be shown also from the spectrum of the envelope of the vibration signal in fig 6.20 where the excited frequencies are more than the case with the defect on the outer ring. The interaction between a rolling element and the defected area generates peaks on the spectra in correspondence of the pass frequency of the rolling elements with respect to a determined point of the inner race BPF_I. The defect rotates with the same frequency of the shaft f_s and the resulting vibration signal is modulated in amplitude generating side bands around the various harmonics of the BPF_I, distanced from the peaks of integer multiples of the rotation frequency of the shaft f_s . In the spectrum regarding point A the highest peak corresponds to the frequency equal to the rotational frequency of the shaft $f_s = 16.6$ Hz which is also the frequency of the inner ring of the bearing with the defect. Peaks are present also at values of frequencies multiple of the f_s with decreasing amplitude. The second highest peak correspond to the $BPF_I = 73.49$ Hz and the lateral band are also present with values of $BPF_I + f_s = 90.16$ Hz, $BPF_I - f_s = 56.82$ Hz and with decreasing amplitude $BPF_I - 2f_s$, $BPF_I + 2f_s$. In point C are present the same peaks all with lower amplitude. Point B, instead, present as higher peak the $BPF_O = 43.17$ Hz, but are also evident all the peaks described for point A with amplitude lower than the two points A and C. In this configuration It is so possible to detect the presence of the defect also monitoring the other end of the shaft.

6. Numerical simulation and analysis of the system

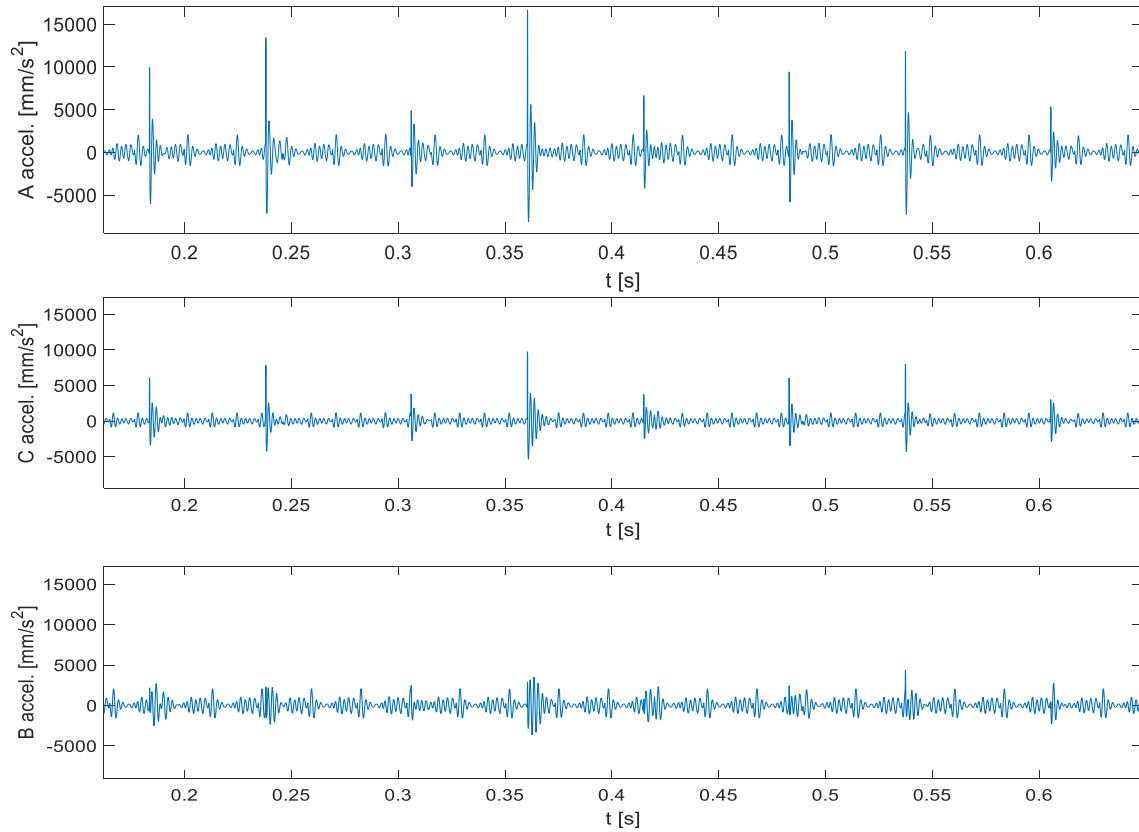
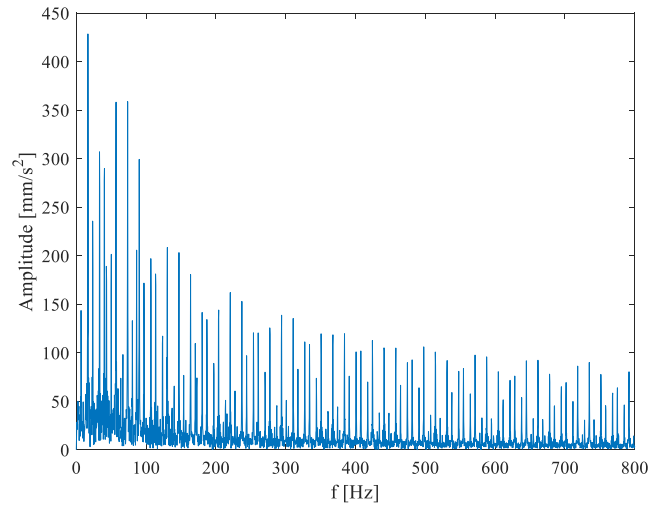


Figure 6.19: Acceleration of point A, C and B along X direction with a defect on the inner ring of bearing A. (Rotor length $L = 0.8 \times 10^3 \text{mm}$).

Frequency spectrum of the envelope of the vibration signal (accel. of A along X)



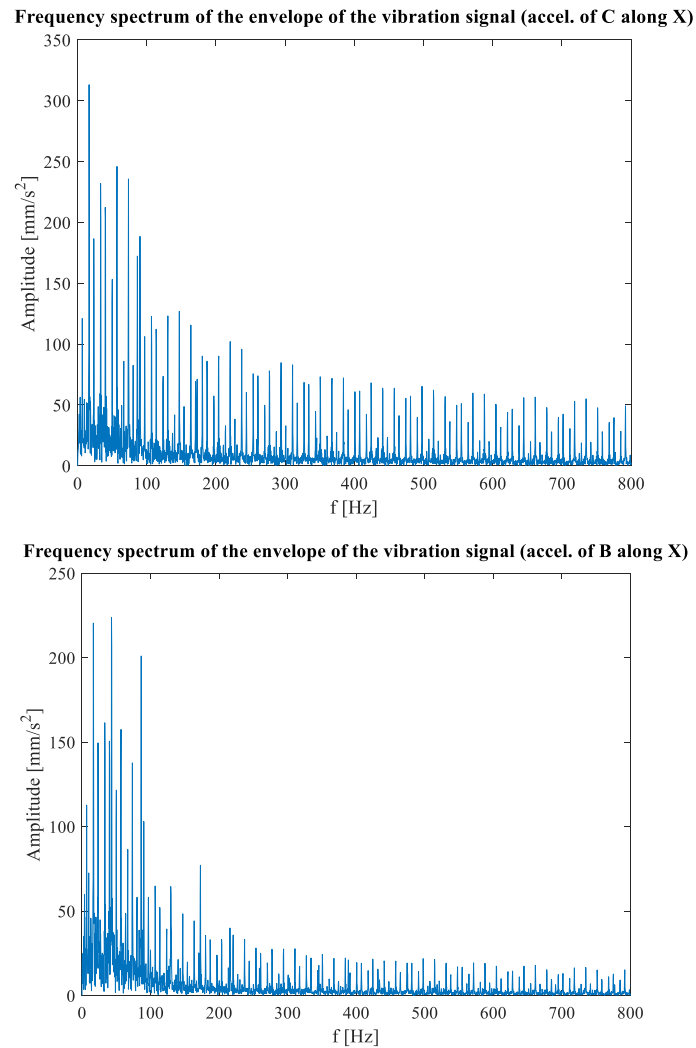


Figure 6.20: Frequency spectra of the envelope of the vibration signals of the acceleration of points A, C and B along X with a defect on the inner ring of bearing A.

6.3.2 Case with elastic shaft

The stiffness of the shaft is now considered assuming a young modulus equal to $E = 2^5$ MPa. To obtain a more realistic simulation the balls position in the two bearings differs of $\frac{\Delta\theta}{2} = 25.7$ deg. The rotor is still considered balanced with null eccentricity and symmetric with respect to the two bearings. acceleration's signal of points A, B and C are analysed along X direction because it gives more information about the presence of defects. The length of the shaft is considered as in the case of defected outer ring $L = 0.1 \times 10^3$ mm to underline the effect of the defect on all the three points. In fig. 6.21 are shown the three acceleration signals of points A, C and B. Also, in this case, the presence of the defect creates a shock in the system that propagate

until bearing B each time that the inner ring enters in the defected area in contact with a sphere. As for the rigid case the amplitude of the acceleration peaks along the X direction, is modulated in amplitude because the inner race rotates with the shaft, and consequently the defect-rolling element interactions occur in different positions with respect to the load area.

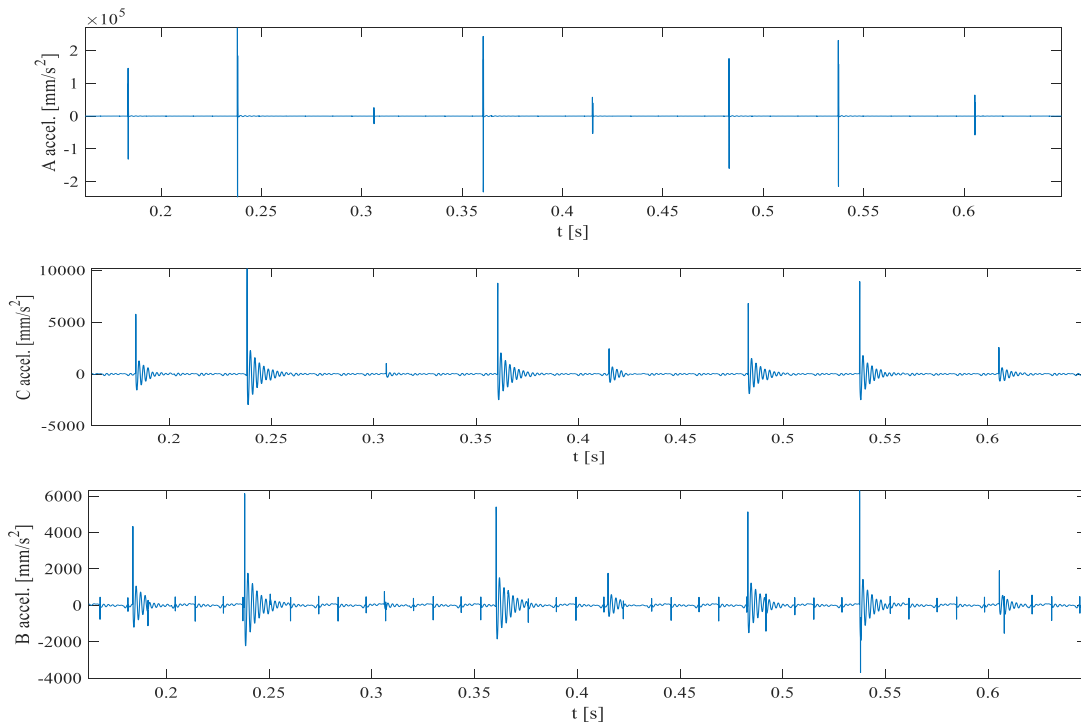


Figure 6.21: Acceleration of point A, C and B along X direction with a defect on the internal ring. (Rotor length $L = 0.1 \times 10^3 mm$).

In fig. 6.22 are represented the frequency spectra of the envelope of the vibration signals of the acceleration of points A, C and B along X direction. Point A present many peaks at high amplitude confirming the presence of a localized defect. The first peak on the left correspond to the shaft frequency equal to $f_s = 16.6$ Hz which is also the rotational frequency of the defect. They are present also the frequency multiple of the shaft frequency equal to $n \times f_s$ with $(n=1, 2, \dots)$ with decreasing amplitude. The other two peaks on the left that have similar amplitude correspond to $BPFI = 73.49$ Hz and his lateral band $BPFI - f_s = 56.82$ Hz. They are also present with lower amplitude, the peaks with frequencies equal to $BPFI + f_s = 90.16$ Hz and $BPFI - 2f_s$, $BPFI + 2f_s$. In points C and B, the highest peak corresponds to the shaft frequency $f_s = 16.6$ Hz. They are then present the same peaks of point A all with lower amplitude. Furthermore, on point B, peaks at frequencies multiple than $BPFO$ became relevant with respect to the other peaks, but it is also possible to detect the presence of the characteristic frequency of the defect.

6. Numerical simulation and analysis of the system

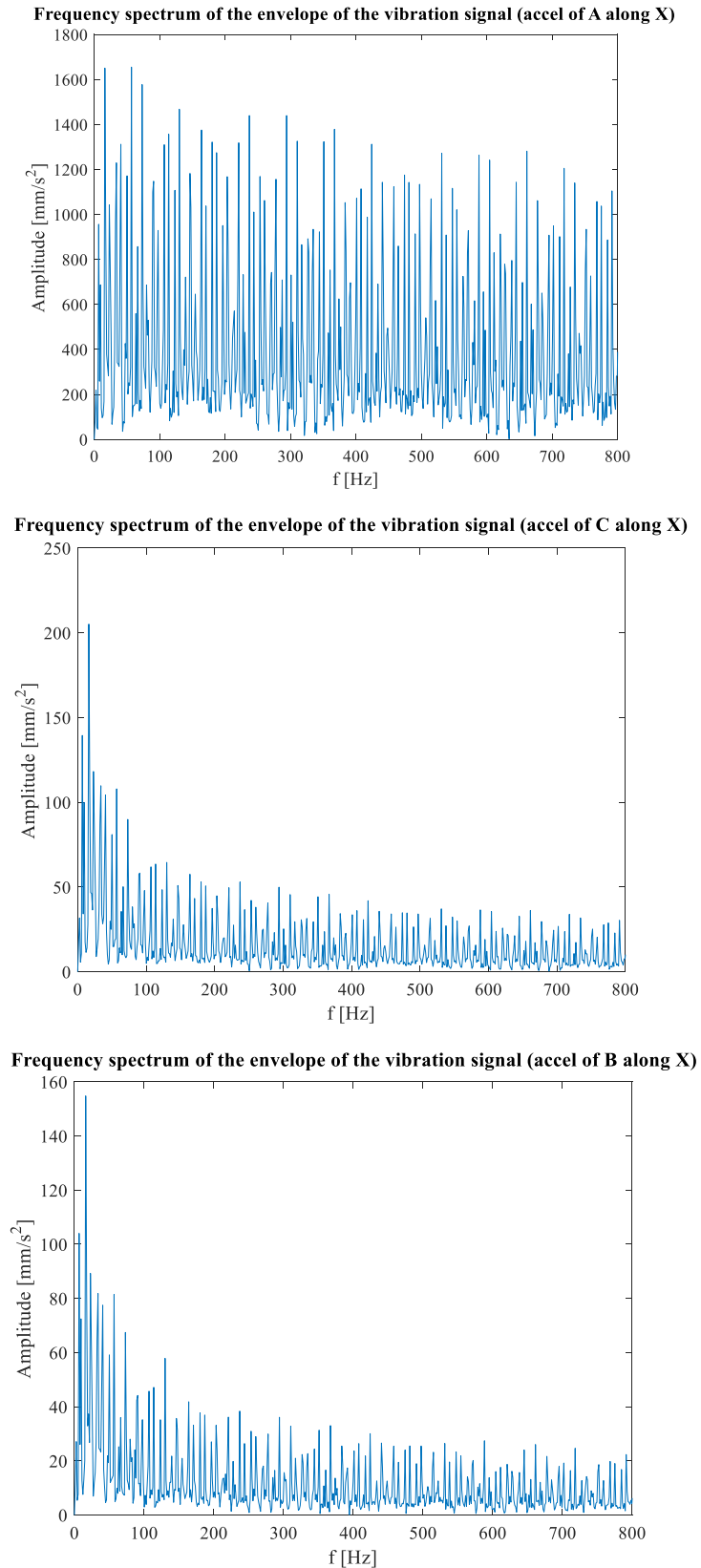


Figure 6.22: Frequency spectra of the envelope of the vibration signals of the acceleration of points A, C and B along X direction with a defect on the internal ring of bearing A.

6.4 Bearing with damaged rolling element

Bearing A is now considered with a localized defect on the first rolling element from the vertical line, of maximum depth $H = 0.05$ mm with the form factor equal to 1. The position of the balls in the two bearings is always considered different of the angle $\frac{\Delta\theta}{2} = 25.7$ deg and are analysed the case of rigid and elastic shaft.

6.4.1 Case with rigid shaft

In fig. 6.23. is shown the acceleration signal with the defect located in the rolling element of bearing A in the case of a rigid rotor considering the length of the rotor equal to $L = 0.8 \times 10^3$ mm to underline the differences between the results.

In this condition the amplitude of the acceleration peaks in the direction of the external load is modulated, as the interaction between the defect on the rolling element and each of the two raceways occurs in different angular positions due to the precession of the balls around the axis of rotation of the shaft. Peaks in the direction of the load X are of greater amplitude than those in the perpendicular direction. Peak value is higher on bearing A with the value $PV_A = 7905.2 \frac{\text{mm}}{\text{s}^2}$. It decreases moving away from it: $PV_C = 5312.8 \frac{\text{mm}}{\text{s}^2}$ and $PV_B = 2814.8 \frac{\text{mm}}{\text{s}^2}$ underlining also in this configuration that the defect localized in bearing A induce a shock in the system that move from it to the other end of the shaft decreasing its intensity. In the spectrum of the envelope of the vibration signal in fig 6.24 it is possible to observe that for the three accelerations signals the highest peaks correspond to the BPF0 or values multiple of it ($n \times BPF0$ with $n= 1, 2 \dots$). They are also present peaks at frequency equal to $2n \times BSF$ (with $n=1, 2 \dots$) indicating the presence of defects in rolling elements. Indeed, the BSF indicates the Ball Spin Frequency and represents the rotation frequency of each rolling element with respect to its axis and so also of the defect. Each ball rotation the defect interacts with the outer and inner race generating an impulse each $2 \times BSF$ when the defect is in the loaded area of the bearing. Furthermore, the rolling element rotate around the bearing axis with the same speed of the cage. FTF indicate the rotation frequency of the cage and so of the defect in the loaded area, with the effect of modulating the vibration signal. The lateral bands of the peaks, present in the in the spectra in the domain of the frequency of the vibration signal, are so visible with values integers of the cage rotation frequency FTF. They are evident in the spectra of bearing A and bearing C while they have much lower amplitude in the spectra of bearing B because of the distance from the defect.

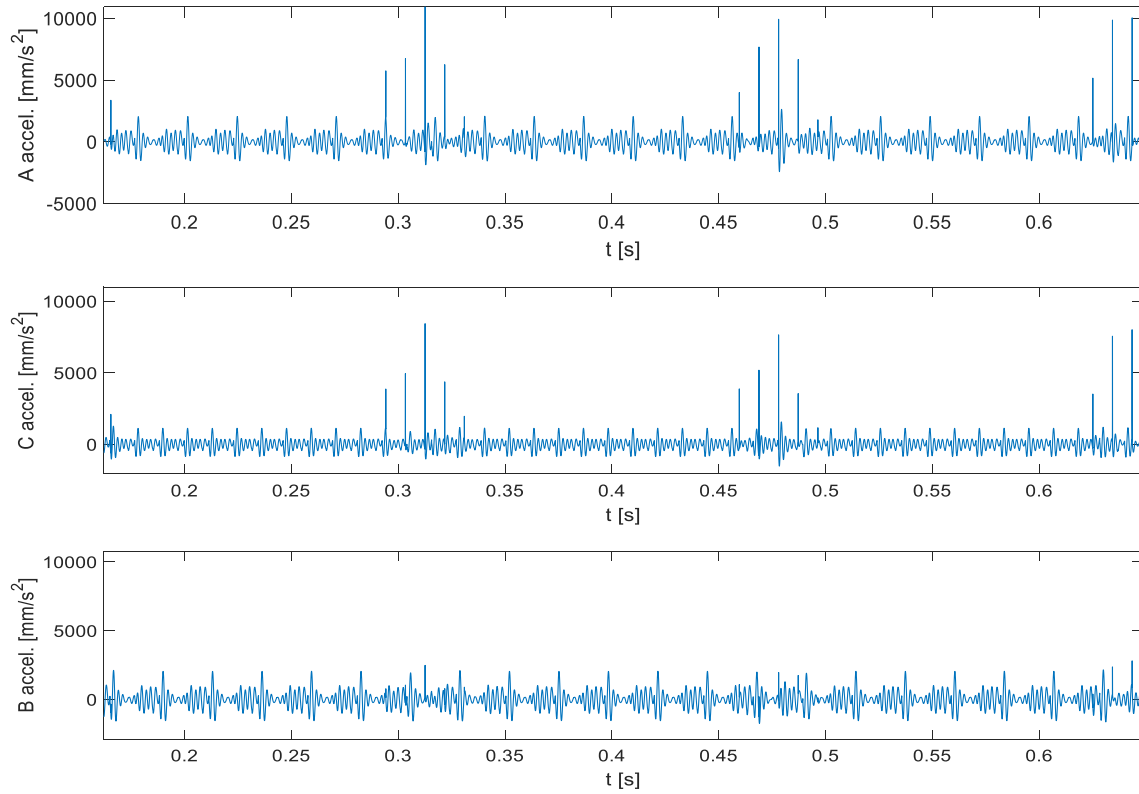
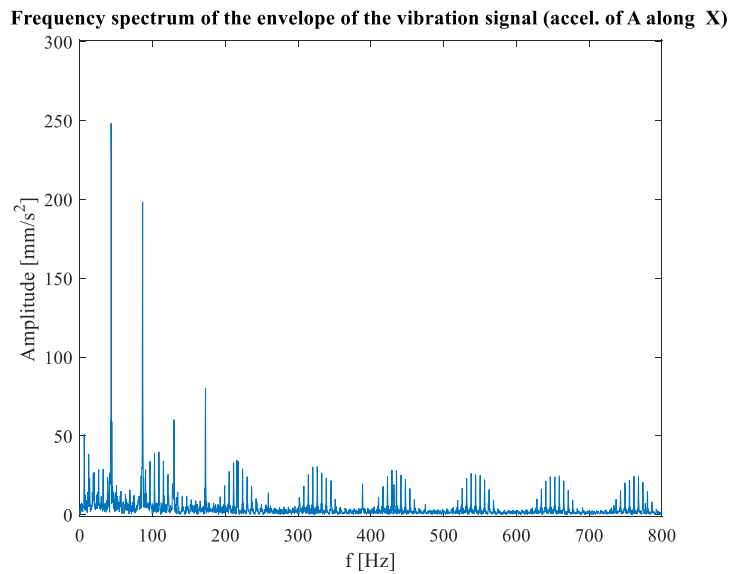


Figure 6.23: Acceleration of point A, C and B along X direction with a defect on a rolling element. (Rotor length $L = 0.8 \times 10^3 \text{mm}$).



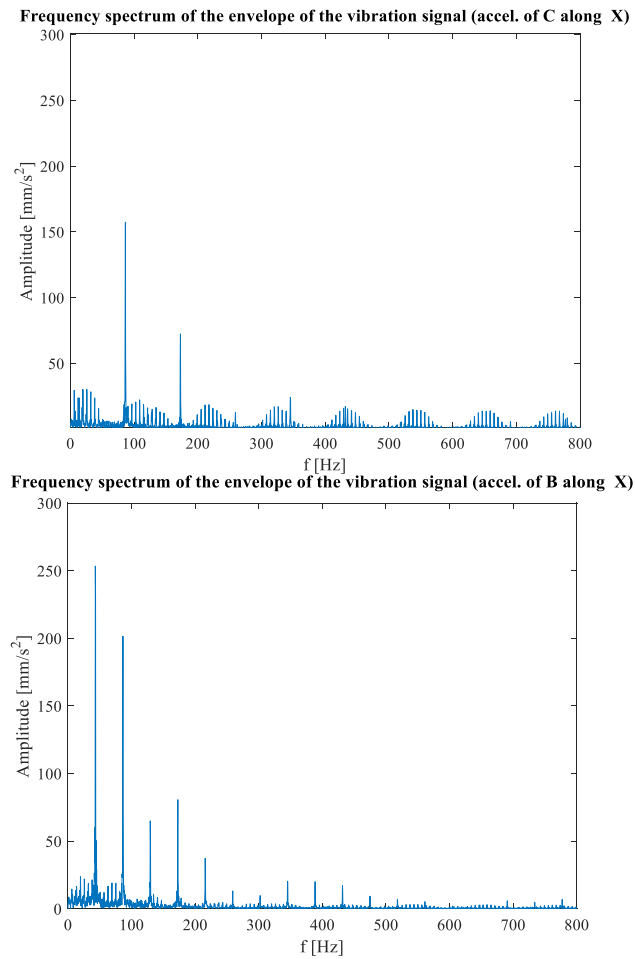


Figure 6.24: Frequency spectra of the envelope of the vibration signals of the acceleration of points A, C and B along X with a defect on a rolling element of bearing A.

6.4.2 Case with elastic shaft

The stiffness of the shaft is now considered assuming a young modulus equal to $E = 2^5$ MPa. To obtain a more realistic simulation the balls position in the two bearings differs of $\frac{\Delta\theta}{2} = 25.7$ deg. The rotor is still considered balanced with null eccentricity and symmetric with respect to the two bearings. acceleration's signal of points A, B and C are analysed along X direction because it gives more information about the presence of defects. The length of the shaft is considered as in the case of defected rings $L = 0.1 \times 10^3$ mm. In fig. 6.25 are shown the three acceleration signals of points A, C and B. As for the rigid case the amplitude of the acceleration peaks along the X direction, is modulated in amplitude as the interaction between the defect on the rolling element and each of the two raceways occurs in different angular positions due

to the precession of the balls around the axis of rotation of the shaft. The defect on the ball of bearing A produces a shock in the system that move from it to the other end of the shaft decreasing its intensity as it is possible to observe both in the acceleration signal and in the frequency spectra of the envelope of the vibration signals of fig. 6.26. Defect affects a lot the shape of the spectrum of points A and C where present peaks are at frequency equal to $2n \times BSF$ (with $n=1, 2 \dots$) as in the case of rigid rotor with the respective lateral band with values integers of the cage rotation frequency FTF. In point B instead, it is possible to observe peaks at $2n \times BSF$ (with $n=1, 2 \dots$) with amplitude much decreased with respect to point A, and also peaks corresponding to the BPFO or values multiple of it ($n \times BPFO$ with $n=1, 2 \dots$).

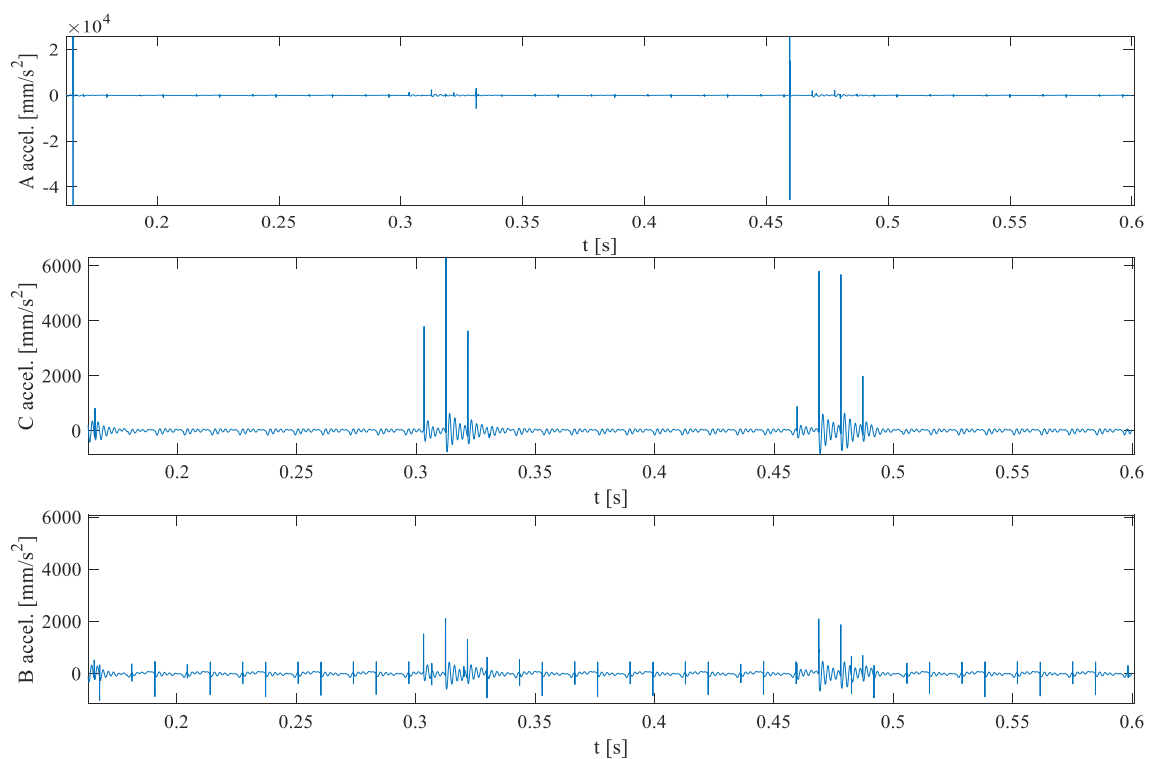


Figure 6.25: Acceleration of point A, C and B along X direction with a defect on a rolling element. (Rotor length $L = 0.8 \times 10^3 \text{ mm}$).

6. Numerical simulation and analysis of the system

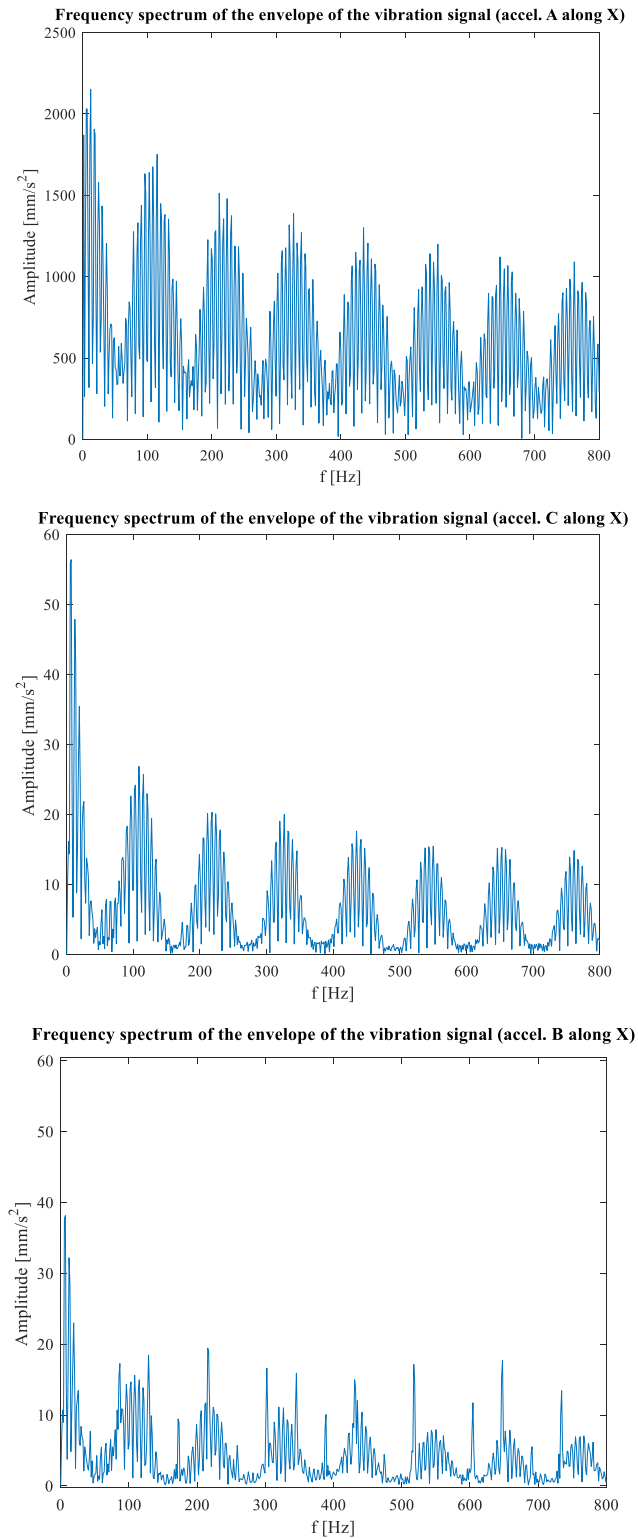


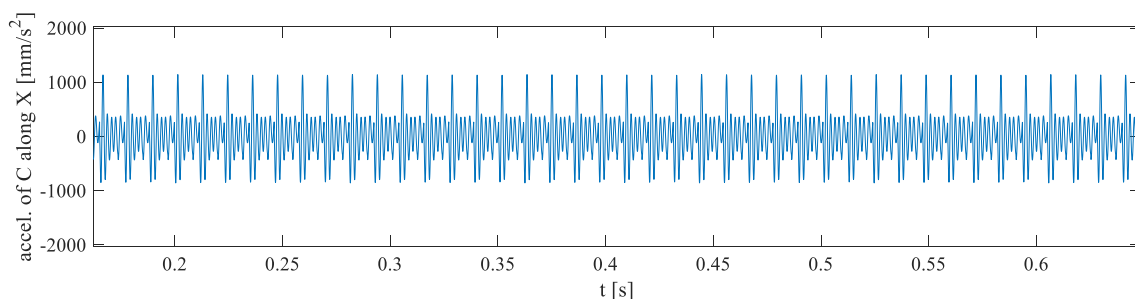
Figure 6.26: Frequency spectra of the envelope of the vibration signals of the acceleration of points A, C and B along X with a defect on a rolling element of bearing A.

6.5 Eccentricity on the rotor

In practice, it never occurs that centre of mass P in which mass is located exactly coincides with the elastic centre C of the cross section, point at which the elastic reaction of the shaft acts. The distance between the two points C and P is the eccentricity ε of the shaft and causes a static unbalance $m\varepsilon$. The position of the balls in the two bearings is always considered different of the angle $\frac{\Delta\theta}{2} = 25.7$ deg and are analysed the case of rigid and elastic shaft. Only the effect of unbalance on the acceleration of point C is reported because it has the same effect in point B and A.

6.5.1 Case with rigid shaft

Considering the shaft with three different values of unbalance: (0, 0.01, 0.1) fig. 6.27 is obtained, and observing the accelerations the peak values increase increasing the value of eccentricity: with $\varepsilon = 0$ mm, 0.01 mm, 0.1 mm peak values became $PV_C = 999.5 \frac{\text{mm}}{\text{s}^2}$, $1055.7 \frac{\text{mm}}{\text{s}^2}$ and $1613.4 \frac{\text{mm}}{\text{s}^2}$. Point C, with the presence of unbalance, oscillate on its trajectory as shown in fig. 6.28. In the frequency spectrum of the envelope of the vibration signal of the acceleration of point C are present the frequency equal to $n \times BPF0$ (with $n=1, 2, \dots$) caused by Varying Compliance Vibration of both the bearings. The low value of eccentricity produces smaller amplitudes of vibrations, while increasing the eccentricity they increase. In the vertical vibration along X is showed clearer the effect of the shaft unbalance as compared to the vibrations in horizontal direction. Indeed, in the frequency spectrum of the envelope of the vibration signal of the acceleration of point C along X, Increasing the value of eccentricity, the peak correspondent to the frequency of the shaft $f_s = 16.6$ Hz increases its amplitude. Fig. 6.29 The low rotational speed produces smaller amplitudes of vibrations, with the increase in rotational speed the amplitude of vibration also increases. The vertical vibrations showed clearer picture of shaft unbalance as compared to the vibrations in horizontal direction. The vibrations spectrum of the unbalance shaft revealed that it strongly depends upon the operating conditions.



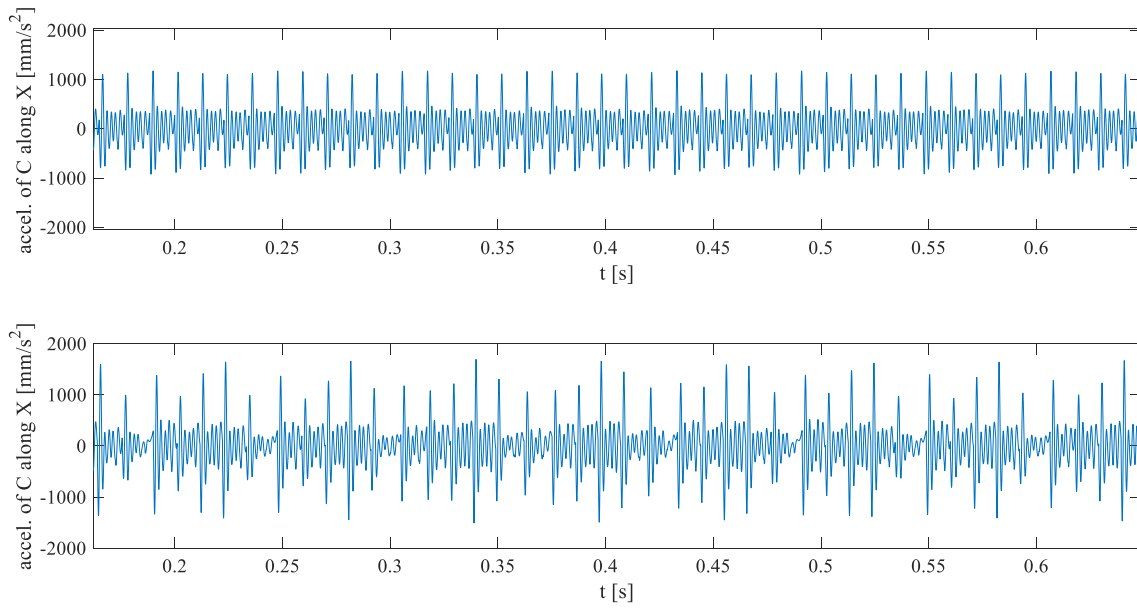


Figure 6.27: Acceleration of point C along X direction with increasing unbalance of the rotor equal to $\varepsilon = 0 \text{ mm}$ (top image), $\varepsilon = 0.01 \text{ mm}$ (middle image), $\varepsilon = 0.1 \text{ mm}$ (bottom image)

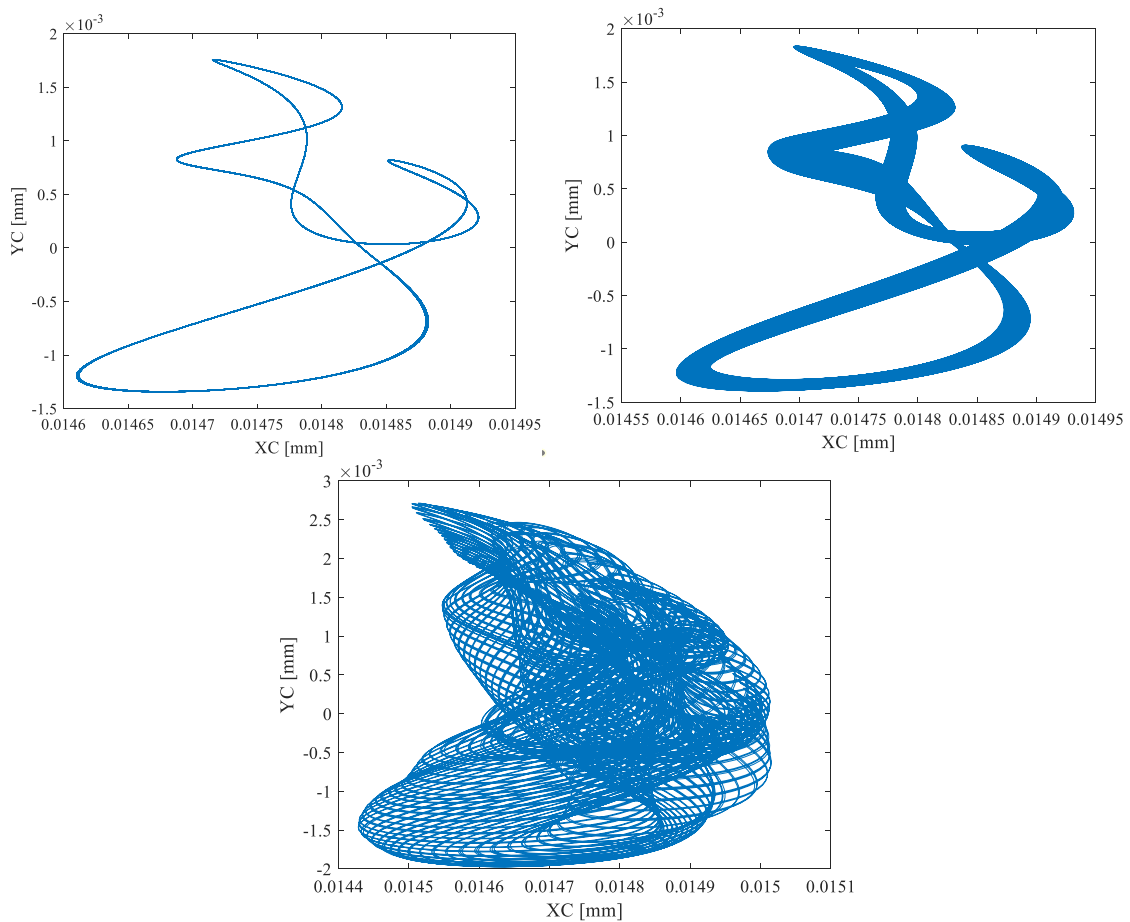


Figure 6.28: Trajectory of point C increasing the value of unbalance $\varepsilon = 0 \text{ mm}$, 0.01 mm , 0.1 mm

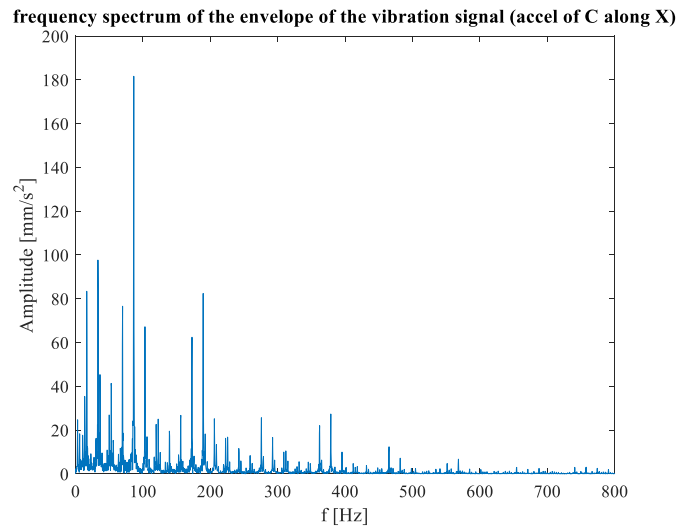
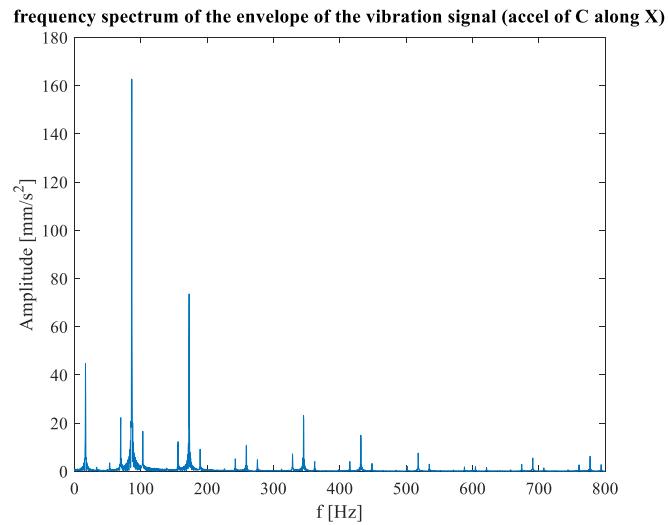


Figure 6.29: Frequency spectra of the envelope of the vibration signal of the acceleration of point C with eccentricity $\varepsilon = 0.01 \text{ mm}$ and $\varepsilon = 0.1 \text{ mm}$, respectively.

6.5.2 Case with elastic shaft

The position of the balls in the two bearings is always considered different of the angle $\frac{\Delta\theta}{2} = 25.7 \text{ deg}$ and are analysed the case of elastic shaft with Young modulus $E = 2^5 \text{ MPa}$. In tab. 6.1 are reported the Peak value of the three points C, A and B with three different values of eccentricity from 0 mm to 0.1 mm . As it is possible to observe also from the relative accelerations in fig. 6.30 the eccentricity value of 0.01 mm generates a small amplitude variation, while with $\varepsilon = 0.1 \text{ mm}$ it peak values increase

significantly. The values increase with higher eccentricity for all the three points. The trajectory in fig. 6.31 behave similarly to the case of rigid rotor, increasing oscillation with the increase of eccentricity.

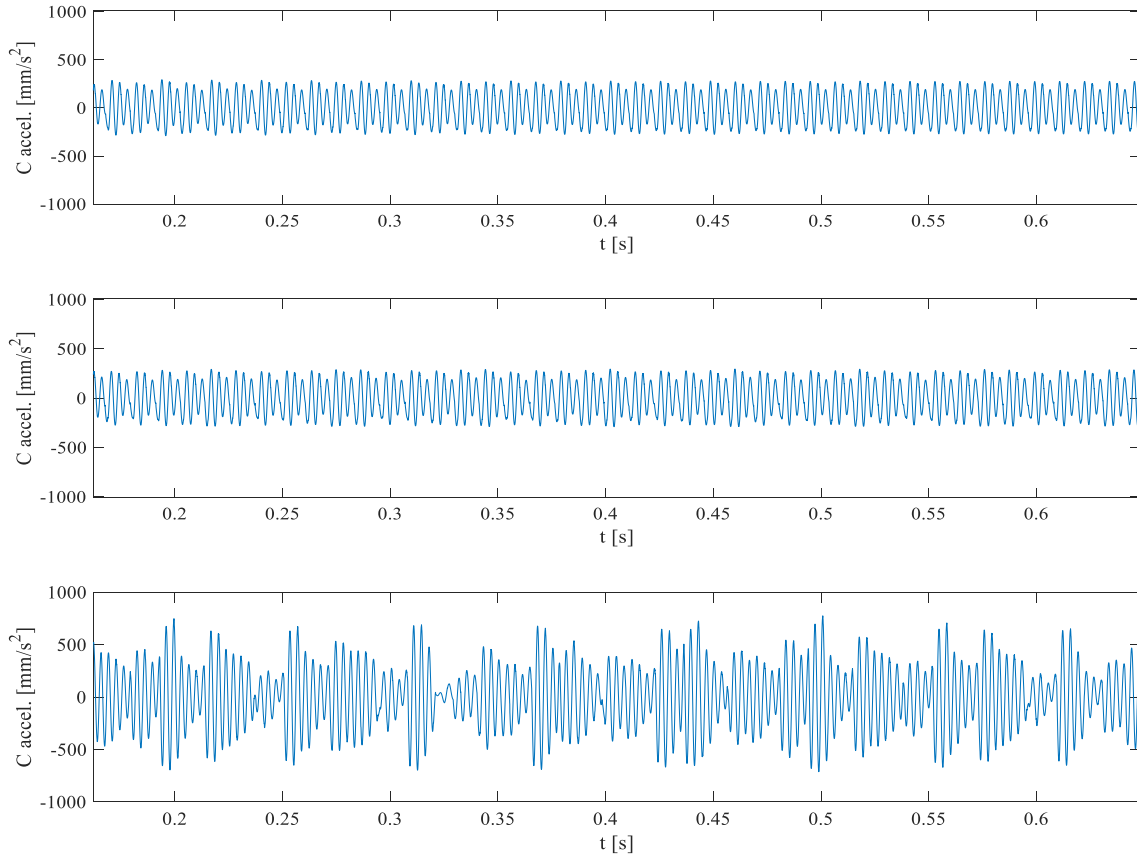


Figure 6.30: Acceleration of point C along X direction with increasing unbalance of the rotor equal to $\varepsilon = 0$ mm (top image), $\varepsilon = 0.01$ mm (middle image), $\varepsilon = 0.1$ mm (bottom image).

Table 6.1: Peak values of the three points C, A, B considering the eccentricity of the shaft $\varepsilon = 0$ mm, 0.01 mm and 0.1 mm.

Eccentricity [mm]	Peak value(C) $\left[\frac{mm}{s^2}\right]$	Peak value(A) $\left[\frac{mm}{s^2}\right]$	Peak value(B) $\left[\frac{mm}{s^2}\right]$
0	291.4	3433	3312
0.01	292.7	3561	3556
0.1	745.8	6018	5878

6. Numerical simulation and analysis of the system

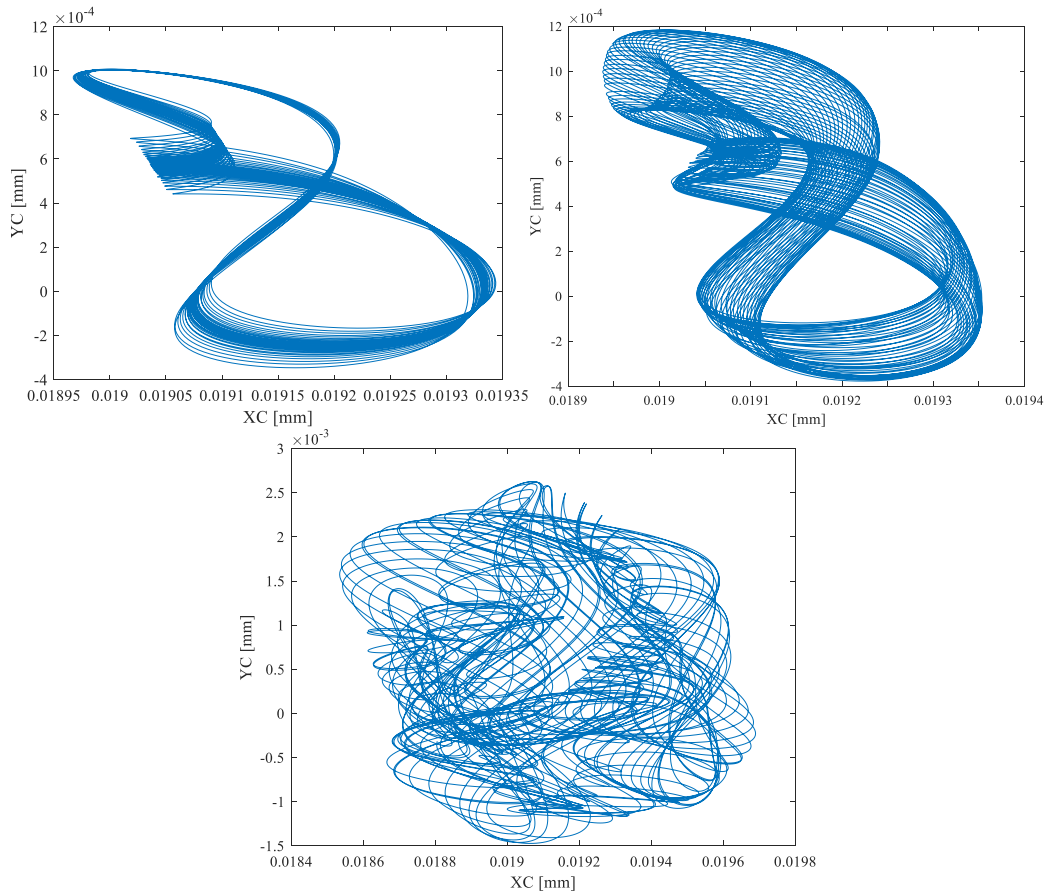
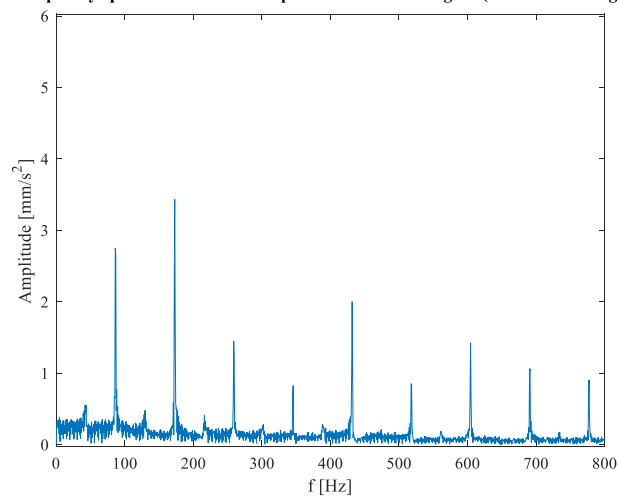


Figure 6.31: Trajectory of point C increasing the value of unbalance $\varepsilon = 0\text{mm}, 0.01\text{mm}, 0.1\text{mm}$.

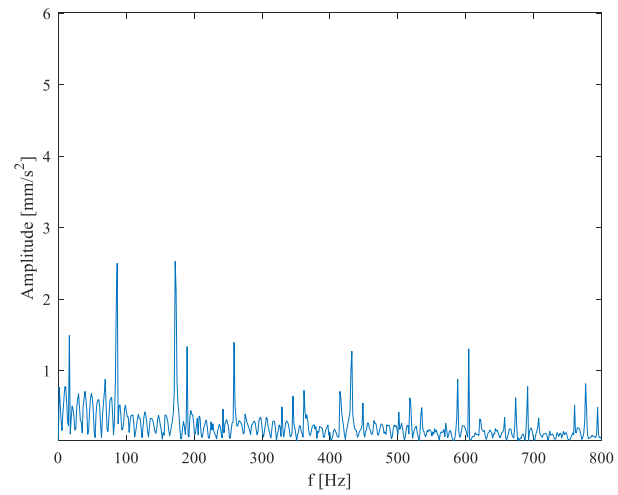
The frequency spectrum of the envelope of the vibration signal also changes from the previous case. The peak at frequencies multiple of BFO are still present indicating the effect of the Varying Compliance Vibration of the two bearings. With the presence of the eccentricity, it is also observable the frequency of the shaft $f_s = 16.67\text{ Hz}$ and its multiple values with amplitude increasing with higher values of eccentricity.

6. Numerical simulation and analysis of the system

Frequency spectrum of the envelope of the vibration signal (accel. of C along X)



Frequency spectrum of the envelope of the vibration signal (accel. of C along X)



Frequency spectrum of the envelope of the vibration signal (accel. of C along X)

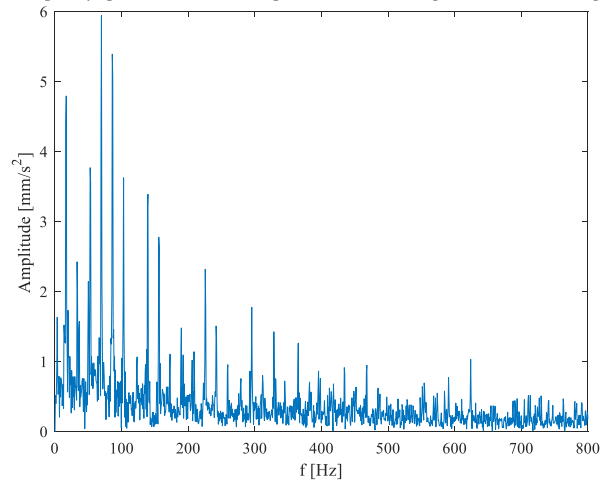


Figure 6.32: Frequency spectra of the envelope of the vibration signals of the acceleration of point C with increasing unbalance of the rotor equal to $\varepsilon = 0$ mm (top image), $\varepsilon = 0.01$ mm (middle image), $\varepsilon = 0.1$ mm (bottom image)

7. Conclusion and future development

In this master's degree thesis, the numerical model of a rotor-bearing system has been developed to be used as a tool for Virtual Condition Monitoring of real systems. The work starts from the thesis of Giorio [2] where it is described an analytical-numerical model of a radial bearing with 2 degrees of freedom. The bearing model is so included in a rotor-bearing system composed by a flexible rotor supported at its ends by rolling elements bearings. The analysis of the dynamic of the rotor is performed to detect the presence of defects on the system and the study is carried on through a search for information already available in the scientific literature. The simulation returns the time response of the rotor in three different points which are the centre of the rotor and the positions of bearings. It is possible to give as input any geometry of the rotor and bearings (only ball or roller radial bearing type) also considering the presence of possible defects on the different components. The signal of the accelerations of the three points is then analysed and the frequency spectra is obtained through the envelop analysis. The study of the spectra of the three different points is useful to detect the condition of the system giving information regarding the possible presence of defects. Each studied defect returns peculiar characteristics of the frequency spectra showing peaks with different intensity depending on the position of the defect and on the point of the rotor from which the signal is studied. The resultant spectra depend on the geometry of the defect and from its location and can be used for the Predictive Monitoring of the system observing and monitoring the behaviour of data points over time. The monitoring activity of the system in correspondence of a chosen point can then be adopted to determine the conditions of the entire system (out-monitoring).

A future development of the presented work regards a possible improvement of the model: it is possible to increase the degrees of freedom of the system adding the analysis of the signal along the axial coordinate. It can be introduced the possibility to study also different type of bearings such as angular contact bearings. Furthermore, the effect on the system of different kind of defects, for example distributed defects, can be simulated. It will be useful to decrease the simulation time to speed up the analysis of the case studied and to adopt this model with real systems it will be necessary to analyse the requirement of real sensors that applied on the rotor will

carry on the Vibration Condition Monitoring. Finally, it will be necessary to determine the positioning of sensors within the real system to optimize the acquired signal.

Bibliography

- [1] Pankaj Gupta e M.K Pradhan. "Fault detection analysis in rolling element bearing: A review". In: *Materials Today: Proceedings* 4.2 (2017), pp. 2085– 2094. doi: 10.1016/j.matpr.2017.02.054.
- [2] Lorenzo Giorio. "Modellazione numerica del sistema cuscinetto per 'Machinery Condition Monitoring'" 2020
- [3] Cambridge University Press "Vibration Monitoring of Inductions Motors" pp. 75 – 89 DOI: <https://doi.org/10.1017/9781108784887.005>, Print publication year: 2020
- [4] C.S. Sunnersjö. "Varying compliance vibrations of rolling bearings". In: *Journal of Sound and Vibration* 58.3 (1978). cited By 107, pp. 363–373. doi: 10.1016/S0022-460X(78)80044-3.
- [5] C.S. Sunnersjö. "Rolling bearing vibrations-The effects of geometrical imperfections and wear". In: *Journal of Sound and Vibration* 98.4 (1985). cited By 82, pp. 455–474. doi: 10.1016/0022-460X(85)90256-1.
- [6] M.S. Patil, Jose Mathew, P.K. Rajendrakumar e Sandeep Desai. "A theoretical model to predict the effect of localized defect on vibrations associated with ball bearing". In: *International Journal of Mechanical Sciences* 52.9 (set. 2010), pp. 1193–1201. doi: 10.1016/j.ijmecsci.2010.05.005.
- [7] Dick Petersen, Carl Howard, Nader Sawalhi, Alireza Moazen Ahmadi e Sarabjeet Singh. "Analysis of bearing stiffness variations, contact forces and vibrations in radially loaded double row rolling element bearings with raceway defects". In: *Mechanical Systems and Signal Processing* 50-51 (gen. 2015), pp. 139–160. doi: 10.1016/j.ymsp.2014.04.014.
- [8] J. Brändlein, U. Merkle-Eschmann, P. Eschmann, L. Hasbargen e K. Weigand. "Ball and Roller Bearings: Theory, Design and Application." Wiley, 1999. isbn: 9780471984528.
- [9] Erwin Krämer. "Dynamics of Rotors and Foundations." Springer Berlin Heidelberg, 1993. doi: 10.1007/978-3-662-02798-1.
- [10] Henghai Zhang, Wenku Shi, Guozheng Liu e Zhiyong Chen. "A Method to Solve the Stiffness of Double-Row Tapered Roller Bearing". In: *Mathematical Problems in Engineering* 2019 (lug. 2019), pp. 1–13. doi: 10.1155/2019/1857931.

[11] Tedric A. Harris e Michael N. Kotzalas. "Essential Concepts of Bearing Technology." Taylor & Francis Inc, 9 ott. 2006. 392 pp. isbn: 084937183X

[12] Bernard J. Hamrock e William J. Anderson. "Rolling-element bearings". In: NASA Reference Publication 1105 (giu. 1983).

[13] E.J. Hearn. "Chapter 10 - Contact Stress, Residual Stress and Stress Concentrations". In: Mechanics of Materials 2 (Third Edition). A cura di E.J. Hearn. Third Edition. Oxford: Butterworth-Heinemann, 1997, pp. 381–442. isbn: 978-0-7506-3266-9. doi: 10.1016/B978-075063266-9/50011-1.

[14] A. Palmgren e G. Palmgren. Ball and Roller Bearing Engineering. A cura di SKF Industries Inc. SKF Industries, 1959.

[15] L. Houpert. "A Uniform Analytical Approach for Ball and Roller Bearings Calculations". In: Journal of Tribology 119.4 (ott. 1997), pp. 851–858. doi: 10.1115/1.2833896.

[16] Fred B. Oswald, Erwin V. Zaretsky e Joseph V. Poplawski. "Effect of Internal Clearance on Load Distribution and Life of Radially Loaded Ball and Roller Bearings". In: Tribology Transactions 55.2 (mar. 2012), pp. 245–265. doi: 10.1080/10402004.2011.639050.

[17] SKF. 6305 Ball Bearing - Technical Specifications. url: <https://www.skf.com/it/products/rolling-bearings/ball-bearings/deep-groove-ball-bearings/productid-6305>.

[18] M.S. Patil, Jose Mathew, P.K. Rajendrakumar e Sandeep Desai. "A theoretical model to predict the effect of localized defect on vibrations associated with ball bearing". In: International Journal of Mechanical Sciences 52.9 (set. 2010), pp. 1193–1201. doi: 10.1016/j.ijmecsci.2010.05.005.

[19] Fanzhao Kong, Wentao Huang, Yunchuan Jiang, Weijie Wang e Xuezheng Zhao. "A Vibration Model of Ball Bearings with a Localized Defect Based on the Hertzian Contact Stress Distribution". In: Shock and Vibration 2018 (2018), pp. 1–14. doi: 10.1155/2018/5424875.

[20] Sham Kulkarni e S.B. Wadkar. "Experimental Investigation for Distributed Defects in Ball Bearing Using Vibration Signature Analysis". In: Procedia Engineering 144 (2016), pp. 781–789. doi: 10.1016/j.proeng.2016.05.086.

[21] Pankaj Gupta e M.K Pradhan. "Fault detection analysis in rolling element bearing: A review". In: Materials Today: Proceedings 4.2 (2017), pp. 2085–2094. doi: 10.1016/j.matpr.2017.02.054.

- [22] Sarabjeet Singh, Carl Q. Howard e Colin H. Hansen. "An extensive review of vibration modelling of rolling element bearings with localised and extended defects". In: *Journal of Sound and Vibration* 357 (nov. 2015), pp. 300–330. doi: 10.1016/j.jsv.2015.04.037.
- [23] Prashant P. Kharche, Dr. Sharad V. Kshirsagar e K. B. Muchandani. "Review of Fault Detection in Rolling Element Bearing". In: *International Journal of Innovative Research in Advanced Engineering (IJIRAE)*. Vol. 1. Giu. 2014, pp. 169–174.
- [24] Giancarlo Genta. "Vibration Dynamics and Control." Springer US, (2009). doi: 10.1007/978-0-387-79580-5
- [25] Bishop, R E D; Gladwell, G M L. "The vibration and balancing of an unbalanced flexible rotor." ARCHIVE: "Journal of Mechanical Engineering Science" doi:10.1243/JMES_JOUR_1959_001_010_02
- [26] A.K. Samantaray, A. Mukherjee, R. Bhattacharyya. "Some studies on rotors with polynomial type non-linear external and internal damping ", (2006) doi: 10.1016/j.ijnonlinmec.2006.10.011
- [27] Edgar J. Gunter, Ph.D., "The INFLUENCE of BEARING ASYMMETRY on ROTOR STABILITY", URL: https://dyrobes.com/wp-content/uploads/2015/09/InfluenceOfBearingAsymmetryOnStability_linked.pdf
- [28] Wang Liqin, Cui Li, Zheng Dezhi; Gu Le, "Nonlinear Dynamics Behaviors of a Rotor Roller Bearing System with Radial Clearances and Waviness Considered. (2008). doi:10.1016/s1000-9361(08)60012-6
- [29] Agnieszka Muszynska, "Rotordynamics", Taylor and Francis, 2005.
- [30] Giancarlo Genta; Nicola Amati, "Hysteretic damping in rotordynamics: An equivalent formulation", (2010), doi: 10.1016/j.jsv.2010.04.036
- [31] Rosmaini Ahmad, Shahrul Kamaruddin, "An overview of time-based and condition-based maintenance in industrial application (2012) doi: 10.1016/j.cie.2012.02.002
- [32] Robert Bond Randall, "Vibration-based Condition Monitoring." John Wiley & Sons, Ltd, gen. 2011. doi: 10.1002/9780470977668.
- [33] C. Scheffer e P. Girdhar. "Practical Machinery Vibration Analysis and Predictive Maintenance. Practical Machinery Vibration Analysis and Predictive Maintenance." Elsevier Science, 2004. isbn: 9780080480220.
- [34] J. Levitt. "Complete Guide to Preventive and Predictive Maintenance." Industrial Press, 2003. isbn: 9780831131548.

- [35] A. Davies, cur. "Handbook of Condition Monitoring." Springer Netherlands, 1998. doi: 10.1007/978-94-011-4924-2.
- [36] C. Carmignani, P. Forte, E. Rustighi. "CONTROLLO ATTIVO DELLA DINAMICA DEI ROTORI MEDIANTE ATTUATORI PIEZOELETTRICI" URL: https://eprints.soton.ac.uk/355253/1/__soton.ac.uk_ude_personalfiles_users_erustigh_h_mydesktop_Temp%2520for%2520ePrints_AIAS2000_DINAMICAROTORI.PDF
- [37] Rahman, Md. Mizanur, Uddin, Mohammad Nasir. "Online Unbalanced Rotor Fault Detection of an IM Drive Based on Both Time and Frequency Domain Analyse." IEEE Transactions on Industry Applications, (2017). doi:10.1109/TIA.2017.2691736
- [38] Jason Mais. "Spectrum Analysis The key features of analyzing spectra" SKF USA. URL: https://www.skf.com/binaries/pub12/Images/0901d1968024acef-CM5118-EN-Spectrum-Analysis_tcm_12-113997.pdf
- [39] Sreejith, B. Verma, A.K. Srividya, A. "Fault diagnosis of rolling element bearing using time-domain features and neural networks" In: IEEE Region 10 and the Third international Conference on Industrial and Information Systems. 2008, pp. 1–6. doi:10.1109/iciinfs.2008.4798444
- [40] Gupta, Pankaj, Pradhan, M.K. "Fault detection analysis in rolling element bearing: A review." In: Materials Today: Proceedings 4.2 (2017), pp. 2085– 2094. doi: 10.1016/j.matpr.2017.02.054
- [41] P.K. Kankar, Satish C. Sharma e S.P. Harsha. "Fault diagnosis of ball bearings using machine learning methods". In: Expert Systems with Applications 38.3 (mar. 2011), pp. 1876–1886. doi: 10.1016/j.eswa.2010.07.119.
- [42] Jalel Chebil, Meftah Hrairi, N. M. Abu-Shikhah. "Signal Analysis of Vibration Measurements for Condition Monitoring of Bearings". In: Australian Journal of Basic and Applied Sciences. 2011. URL: https://www.researchgate.net/publication/274375367_Signal_Analysis_of_Vibration_Measurements_for_Condition_Monitoring_of_Bearings
- [43] S. Bagnoli, P. Citti, P. Rissone. "Note su alcune tecniche di diagnostica dei sistemi meccanici". In: Paolo Citti, Sergio Curioni e Michele Gasparetto. Scritti sulla Diagnostica del Macchinario e dei Materiali. 1989, pp. 23–39.
- [44] R.B.W. Heng, M.J.M. Nor. "Statistical analysis of sound and vibration signals for monitoring rolling element bearing condition". In: Applied Acoustics 53.1-3. 1998. doi: 10.1016/s0003-682x(97)00018-2.

- [45] Aditya Sharma, M Amarnath, PK Kankar. "Feature extraction and fault severity classification in ball bearings". In: *Journal of Vibration and Control* 22.1. 2014. doi: 10.1177/1077546314528021.
- [46] Dipen S. Shah, Vinod N. Patel. "A Review of Dynamic Modeling and Fault Identifications Methods for Rolling Element Bearing". In: *Procedia Technology* 14. 2014. doi: 10.1016/j.protcy.2014.08.057.
- [47] Zeki Kiral, Hira Karagülle. "Vibration analysis of rolling element bearings with various defects under the action of an unbalanced force". In: *Mechanical Systems and Signal Processing*. 2006. doi: 10.1016/j.ymssp.2005.05.001.
- [48] Tian Ran Lin, Kun Yu e Jiwen Tan. "Condition Monitoring and Fault Diagnosis of Roller Element Bearing". In: *Bearing Technology*. InTech, mag. 2017. doi: 10.5772/67143.
- [49] Jaafar Alsalaet. "Vibration Analysis and Diagnostic Guide". 2012.
- [50] Meinard Müller. "The Fourier Transform in a Nutshell". 2015. isbn: 978-3-319-21944-8.
- [51] Sham Kulkarni e S.B. Wadkar. "Experimental Investigation for Distributed Defects in Ball Bearing Using Vibration Signature Analysis". In: *Procedia Engineering* 144 (2016), pp. 781–789. doi: 10.1016/j.proeng.2016.05.086.
- [52] Robert B. Randall, Jérôme Antoni. "Rolling element bearing diagnostics—A tutorial". In: "Mechanical Systems and Signal Processing". 2011. pp. 485–520. doi: 10.1016/j.ymssp.2010.07.017.
- [53] Maurice L. Adams. *Bearings. Basic Concepts and Design Applications*. Machinery Vibration Inc., Cleveland and Ohio, USA. Taylor & Francis Ltd, 23 apr. 2018. 293 pp. isbn: 1138049085.
- [54] Jalel Chebil, Meftah Hrairi, N. M. Abu-Shikhah. "Signal Analysis of Vibration Measurements for Condition Monitoring of Bearings". In: *Australian Journal of Basic and Applied Sciences*. 2011. URL: https://www.researchgate.net/publication/274375367_Signal_Analysis_of_Vibration_Measurements_for_Condition_Monitoring_of_Bearings
- [55] Akhand Rai e S.H. Upadhyay. "A review on signal processing techniques utilized in the fault diagnosis of rolling element bearings". In: *Tribology International* 96 (apr. 2016), pp. 289–306. doi: 10.1016/j.triboint.2015.12.
- [56] Broughton, S. A., Bryan, K. "Discrete Fourier Analysis and Wavelets: Applications to Signal and Image Processing." New York: Wiley. 2008.

- [57] N. Tandon. "A comparison of some vibration parameters for the condition monitoring of rolling element bearings". In: *Measurement* 12 (1994) 285–289. doi: 10.1016/0263-2241(94)90033-7.
- [58] Hamdi Taplak, Selçuk Erkaya, Ibrahim Uzman. "Experimental analysis on fault detection for a direct coupled rotor-bearing system". In: *Measurement* 46 (2013) 366–344. doi: org/10.1016/j.measurement.2012.07.005
- [59] J. Levitt. "Complete Guide to Preventive and Predictive Maintenance." Industrial Press, 2003. isbn: 9780831131548.
- [60] M. Tiwari, K. Gupta, O. Prakash, Effect of radial internal clearance of a ball bearing on the dynamics of a balanced horizontal rotor, *J. Sound Vib.* 238 (2000) 723–756.
- [61] A. Liew, N. Feng, E.J. Hahn. "Transient rotor dynamic modelling of rolling element bearing systems." *ASME J. Eng. Gas Turb. Power* 124 (2002) 984–991.
- [62] G.H. Jang, S.W. Jeong, "Analysis of a ball bearing with waviness considering the centrifugal force and gyroscopic moment of the ball." *ASME J. Tribol.* 125 (2003) 487–498.
- [63] B.O. Al-Bedoor, "Modeling the coupled torsional and lateral vibrations of unbalanced rotors." *Comput. Methods Appl. Mech. Eng.* 190 (2001) 5999–6008.
- [64] Lourdes Rubio, José Fernández-Sáez "A new efficient procedure to solve nonlinear dynamics of a cracked rotor." In: "Nonlinear Dynamics." November 2012. DOI:10.1007/s11071-012-0569-x
- [65] Dede, Ekin and Wu, Helen. "A Lateral Vibration Analysis of a Flexible Rotor-Bearing System". *Proceedings of the 2nd International Conference on Mechanical Engineering and Mechatronics Toronto, Ontario, Canada, August 8–9 2013 Paper No. 149.* SSRN: <https://ssrn.com/abstract=3125881>
- [66] Cao, Hongrui, Niu, Linkai, Xi, Songtao, Chen, Xuefeng. "Mechanical model development of rolling bearing-rotor systems: A review." In: "Mechanical Systems and Signal Processing", 102(), 37–58. (2018). doi: 10.1016/j.ymssp.2017.09.023
- [67] Cheng, H., Zhang, Y., Lu, W. et al. "Research on ball bearing model based on local defects." In: *SN Appl. Sci.* 1, 1219. 2019. URL: <https://doi.org/10.1007/s42452-019-1251-4>

- [68] Olivier A. Bauchau, Yuri G. Nikishkov. "An Implicit Transition Matrix Approach to Stability Analysis of Flexible Multi-Body Systems." (2001). doi:10.1023/a:1011488504973
- [69] Amati, N.; Brusa, E. "Vibration condition monitoring of rotors on AMB fed by induction motors." (2001). doi: 10.1109/aim.2001.936760
- [70] G. Detoni, Fabrizio Impinna, Nicola Amati, Andrea Tonoli, Pina Piccolo, Giancarlo Genta. "Stability of a 4 degree of freedom rotor on electrodynamic passive magnetic bearings". August 2014.
- [71] Chiara Gastaldi, Teresa M. Berruti. "Competitive Time Marching Solution Methods for Systems with Friction-Induced Nonlinearities." In: "Applied Sciences", 8(2), 291– (2018). doi:10.3390/app8020291
- [72] Lai Tao, Yi Ting-Hua, Li Hong-Nan, Fu Xing. "An Explicit Fourth-Order Runge–Kutta Method for Dynamic Force Identification." In: "International Journal of Structural Stability and Dynamics", (), 1750120– (2017). doi:10.1142/S0219455417501206
- [73] Yang Rui, Hou Lei, Jin Yulin, Chen Yushu, Zhang, Zhiyong. "The VC resonance in a ball bearing rotor system affected by different ball numbers and rotor eccentricities." In: Journal of Tribology. (2018). doi:10.1115/1.4039566